Surface Modification of Lean Duplex Stainless Steels by Low Temperature Plasma Nitriding

A thesis submitted for the degree of

Master of Research (MRes)

By

Wenbo Dou

School of Metallurgy and Materials
College of Engineering and Physical Science
University of Birmingham
2014-11

Synopsis

Duplex stainless steels (DSSs) are materials of choice for the offshore gas and oil, petrochemical and chemical industries mainly due to their good combination of high strength, excellent corrosion-resistance in chloridic environment and relatively low cost. However, DSSs are characterised by low hardness, poor wear resistance and undesirable corrosion-wear in sea water.

In this work, two lean duplex stainless steels LDX2101 and LDX 2404 were plasma nitrided (PN) for 10 hours at temperatures ranging from 390℃ to 480℃ in a gas mixture of 25%N_2 + 75%H_2 in order to improve their surface hardness, load bearing capacity (LBC), dry wear resistance and corrosion-wear properties.

The results have demonstrated that a hardened case can be generated by PN on both LDX2101 and LDX 2404 steels. The original austenite and ferrite grains in the surface of these two steels were transferred respectively into S-phase and ε-Fe_3N needles embed in nitrogen saturated ferrite (α_N). The surface hardness of these two steels can be improved by about 6 times and the thickness increased with the treatment temperature ranging from 5 to 28 μm. In comparison, the plasma nitrided LDX2404 showed a higher surface hardness but a thinner hardened case than LDX2404.

The LBC and dry wear resistance of both steels can be effectively improved by the plasma nitriding treatments developed and the PN480 treated samples improved dry wear resistance by 8.1 x 10^3 and 3.7 x 10^2 times for LDX 2101 and LDX2404 respectively when tested under 70N. Unlike dry wear, the corrosion-wear resistance of both LDX 2101 and LDX2404 materials can be effectively improved only by low temperature PN390 and

PN420 treatment. The PN420 treatment showed the best improvement in corrosion-wear resistance by 7.4 and 8.1 times for LDX 2101 and LDX2404, respectively.

Based on the experimental results, the response of austenite and ferrite in the DSSs to plasma nitriding is discussed, the differences in microstructure and surface properties of these two lean duplex stainless steels LDX2101 and LDX 2404 are compared and the optimal treatment conditions for different applications are identified.

ACKNOWLEDGEMENTS

I would like to express my very great gratitude to my supervisors: Professor Hanshan Dong and Dr. Xiaoying Li, for their selfless dedications, supreme help and guidance throughout my research project.

Meanwhile, I would also like to extend my many thanks to all members of the Surface Engineering Group within the School of Metallurgy and Materials, Kaijie Lin, Qiongxi Liu and Qi Chen, for their selfless help during my research works.

Finally, I would really like to express my whole gratitude to my parents; Moreover, I should strongly give gratitude to my uncle Shujun Zhang and my aunt Tieru Wang for their support and inspiration during my MRes study in UK.

Publication

X. Y. Li; R. Roberts; W. B. Dou; H. S. Dong: Low temperature plasma surface alloying and characterisation of a superduplex stainless steel, International Heat Treatment & Surface Engineering, 8(2013), 61-64, DOI: 10.1179/1749514813Z.00000000090.

HONOUR

Certificate of Postgraduate Researchers
Materials Research Forum & Competition 2013

This is to certify that
Wenbo Dou

was runner-up in the poster presentation competition
Organised by the School of Metallurgy and Materials of
the University of Birmingham on 4th April 2014

UNIVERSITY OF
BIRMINGHAM

Prof. H. Dong
Director of Postgraduate studies

Contents

CHAPTER 1 INTRODUCTION

Duplex stainless steels (DSSs) are attractive for the offshore gas and oil, petrochemical and chemical industries mainly due to their good combination of high strength, excellent corrosion-resistance in chloridic environment and relatively low cost. For example, they have been successfully used for natural gas pipelines [1] and DSS is a possible collector in Li-ion batteries [2]. However, DSSs are characterised by low hardness and poor wear resistance and their severe wear in sea water (i.e. corrosion-wear) is a major concern for some demanding applications. Therefore, how to improve the surface hardness and corrosion-wear resistance of DSSs is a timely task for the surface engineering industry.

Recently, a new low-temperature plasma surface alloying technique has been developed to achieve combined improvements in hardness, wear resistance and fatigue properties for austenitic stainless steels without reducing their corrosion properties due to the formation of S-phase [3]. Although many papers have been published on S-phase surface engineering of austenite stainless steels during the past two decades, limited research has been conducted on the formation of S-phase in duplex stainless steels; indeed, it is still in debate if a single S-phase layer can be formed during a low-temperature thermo-chemical treatment of DSSs. Hence, the aim of this project was to study the response of lean duplex stainless steels to low-temperature plasma nitriding, thus advancing scientific understanding and promoting the application of S-phase surface engineering technology.

In this project, a lean duplex stainless steel was DC plasma nitrided under a range of treatment conditions. Energy dispersive X-ray spectroscopy (EDX), glow discharge spectrometry (GDS), X-ray diffraction (XRD) and scanning electron microscopy (SEM) were used to characterise the microstructure of plasma treated smaples. Their mechanical

properties were assessed by microhardness, electrochemical corrosion, dry wear and corrosion-wear tests.

The experimental results have shown that a dense, super-hard surface layer can be produced uniformly by low-temperature plasma treatments. The original austenitic phase became S-phase and the ferritic phase was transferred into ε-M_3N. Compared to the untreated sample, the surface hardness of the lean DSS was increased by up to six times, which is consistent with the load bearing capacity. The dry wear results were improved by increasing the treatment temperature. In contrast, the low-temperature treated exhibited the best resistance to electrochemical corrosion and corrosion-wear and the samples treated at higher temperatures performed significantly worse than the untreated material.

CHAPTER 2 LITERATURE REVIEW

2.1 Stainless Steels

2.1.1 Historical Notes

Stainless steels have more than 110 years of history since their discovery by Harry Brearley, a self-taught metallurgist, in 1911 [4, 5]. Even though they may remain unnoticed to the average person, stainless steels are all around us in a wide range of applications [5-7], from simple utensils to advanced engineering components [8]. The origins of stainless steels date back to the 18th century, with the identification chromium and nickel as alloying elements. The Fe-Cr and Fe-Cr-Ni alloys were experimentally investigated during the 19th century.

Stainless steels can be classified in austenitic, martensitic, and ferritic types, depending on their crystalline structure. The alloys developed between 1911 and 1914 were mainly ferritic, and martensitic stainless steels were produced in 1919. An austenitic stainless steel, containing 18% chromium and 8% nickel, was developed in 1926 [9]. Four years later, duplex stainless steel, with a ferritic-austenitic structure, was firstly produced at the Avesta Ironworks [10]. In the last 50 years, stainless steels have been used in famous buildings and civil structures, such as 452-metre-high Pentronas Towers and the Thames Barrier [5].

Figure 2.1 shows the total world production of austenitic stainless steels between 2003 and 2012 [11]; with the exception of the world financial crisis in 2009, the production of stainless steels remained stable in the developed countries and increased quickly in the developing countries. This trend reflects the special properties of these alloys and their value to society.

Stainless steels are iron-based alloys typically containing more than 10.5 wt% Chromium and less than 1.2 wt% Carbon, which exhibit high resistance to corrosion and oxidation. Figure 2.2 illustrates the basic principle behind their corrosion resistance. A protective layer of chromium oxide is formed on the surface of stainless steels, when they are exposed to any oxidising environment. If this layer is scratched or damaged, the exposed material oxidises and the protective oxide layer is quickly regenerated. Other alloying elements are added to these steels in order to address specific applications. For instance, molybdenum and nitrogen increase the pitting and crevice corrosion resistance, and nickel is responsible for the high toughness [12]. Therefore, the chemical composition and microstructure of stainless steels are tailored for each specific application and operating environment.

2.1.2 Categories and Properties

Depending on their crystallographic structure, stainless steels are classified in austenitic, martensitic, ferritic and duplex types [12]. Austenitic stainless steels (ASSs) are the largest group accounting for up to 70% of the world production of stainless steels [13]. These alloys a have face-centred cubic (fcc) structure, also called gamma phase (γ-Fe) [14] and they typically contain 0.02 wt% to 0.08 wt% carbon, 16 wt% to 26 wt% chromium and at least 8 wt% nickel. Other elements such as nitrogen and manganese are added to stabilise the FCC structure and enhance the mechanical properties, mainly strength and toughness. Because of their excellent corrosion resistance, good biocompatibility, and adequate strength, austenitic stainless steels are used in nuclear and biomedical applications [3];

Martensitic stainless steels are used in applications requiring high strength and toughness. They normally contain up to 1.2 wt% carbon, 12 wt% to 18 wt% chromium and 0.2 wt% to

1 wt% molybdenum. When fast cooled from high temperature, the diffusion of carbon is restricted and the lattice stretches along one crystallographic direction, to make enough room for the carbon atoms resulting in a body centred tetragonal (bct) structure, or martensitic structure. The lattice distortion imparts high hardness and strength to these steels [15, 16].

Ferritic stainless steels have a chromium content between 11 wt% and 27 wt% and a carbon content below 0.2 wt%, which produces a body-centred cubic (bcc) structure. Ferritic stainless steels are cheaper than austenitic or duplex stainless steels, but they exhibit poor corrosion resistance and weldability, which limits their applications. As a result, ferritic stainless steels are normally used in domestic appliances and utensils [17, 18]. Further developments of these alloys resulted in the so called duplex stainless steels, which have a mixed ferritic-austenitic structure and combine the properties of both alloys. Being the subject of this study, duplex stainless steels will be discussed in more detail in the next section.

Finally, a fifth kind of stainless steel, called precipitation-hardenable or PH steel, should be mentioned [19]. PH steels were developed during World War II, and they rely on heat treatments to produce certain properties, through changes in solid solubility and precipitation mechanisms at different temperatures.

2.2 Duplex Stainless Steels

2.2.1 Development of Duplex Stainless Steels

Duplex stainless steels, which combine the high strength of ferritic alloys and the good corrosion resistance of austenitic alloys, have been developed for nearly 80 years [20]. The first duplex stainless steels were iron alloys with chromium and nickel developed in the 1930s to improve intergranular corrosion properties. These steels exhibited good mechanical properties and corrosion resistance, but had limitations in the as-welded condition. A second generation of duplex stainless steels was developed in the 1970s with additions of nitrogen. These steels showed high strength, good toughness and excellent corrosion resistance in chloride environments, which made them appropriate for applications in offshore gas and oil fields in the North Sea and other demanding environments [20, 21].

2.2.2 Properties and Categories of Duplex Stainless Steels

The mechanical and corrosion properties of duplex stainless steels depend strongly on their phase composition, which typically involves equal amounts of ferrite and austenite. However, this stable balance in the phase composition is hard to achieve in production environments. Four alloying elements, namely chromium, molybdenum, nitrogen and nickel, are used to obtain a stable phase composition and to avoid the formation of detrimental intermetallic phases [8, 21]. The former two elements, i.e. chromium and molybdenum, are ferrite formers and they increase the corrosion resistance and the oxidation resistance. On the other hand, the latter elements, i.e. nitrogen and nickel, are austenite formers and they improve the strength and toughness.

Duplex stainless steels are strongly and successfully used in gas desulfurization and desalination plants, in oil and gas fields, and their use is growing in sectors such as architecture, biofuel production, and food and drink processing [20, 22, 23]. This is because duplex stainless steels combine good mechanical strength and corrosion resistance, particularly against pitting and crevice corrosion [20]. Furthermore, on several fields including stress corrosion cracking (SCC) resistance and pitting corrosion resistance, duplex stainless steels have showed better resistance than austenite stainless steels [21]. In terms of mechanical properties, the room temperature toughness of duplex stainless steels is typically in the order of 60J and their yield strength ranges from 550 to 690 MPa [6]. Therefore, the main advantage of duplex stainless steels is their high yield strength without losing ductility due to the two-phase structures.

There are currently 5 basic types of duplex stainless steels in use, including: lean duplex stainless steels (2101 and 2304), normal duplex stainless steel (2404 and 2205) and super duplex stainless steel (2507) [21]. Their typical chemical compositions are shown in Table 2.1 [21]. Each of these steels exhibits a different phase composition and, therefore, different properties. The ferritic structure enhances the stress corrosion resistance at expense of the ductility. On the other hand, the austenitic structure shows high toughness and corrosion resistance, but exhibits high sensitivity to chloride corrosion. Even though, duplex stainless steels offer a good combination of corrosion resistance and mechanical properties in general [24], it is important to carefully select the best material for each application.

Table 2.1 The chemical compostion of Duplex stainless steels

	Outokumpu steel name	International steel No		Chemical composition, % by weight Typical values					
		EN	ASTM	C	N	Cr	Ni	Mo	Others
Duplex	LDX 2101®	1.4162	S32101	0.03	0.22	21.5	1.5	0.3	5Mn
	2304	1.4362	S32304	0.02	0.10	23	4.8	0.3	–
	LDX 2404™	1.4662	S82441	0.02	0.27	24	3.6	1.6	3Mn
	2205	1.4462	S32205*	0.02	0.17	22	5.7	3.1	–
	2507	1.4410	S32750	0.02	0.27	25	7.0	4.0	–

2.2.2.1 Lean Duplex Stainless Steels

The two main kinds of lean duplex stainless steels are coded 2101 and 2404, after their Cr and Ni contents. The hardness of these two materials is 225 HV and 230 HV, respectively, and their tensile strength at room temperature is 650 MPa and 680 MPa, correspondingly. Both lean duplex alloys have better toughness, ductility and corrosion resistance than the austenitic stainless steels 304 and 316. Moreover, because duplex stainless steels are relatively lean in Ni or Mo, they become economically attractive than their austenitic counterparts when the price of these alloying elements increase or fluctuates [25]. The 2404 alloy shows a better corrosion resistance than the 2101 as a result of its higher Cr and Ni content, at expense of a higher cost. Although lean duplex stainless steels have been successfully used in asphalt hauling tankers, their wear resistance is quite low.

2.2.2.2 Normal Duplex Stainless Steels

Duplex stainless steels 2304 and 2205 exhibit a hardness of 210 HV and 230 HV respectively, and their corresponding tensile strengths are 630 MPa and 640 MPa. Normal duplex stainless steels show much better corrosion resistance than the lean duplex stainless steels [21, 26], and they have been used in a wide range of applications, for example: the

2304 alloy has been used for wine and food storage depots and the 2250 one has been used for the biomass processing and seawater desalination plants [1, 27]. However, they exhibit low hardness and poor tribological properties, which limit their areas of application [28].

2.2.2.3 Super Duplex Stainless Steel

Super duplex stainless steel 2507 combines the best corrosion resistance and mechanical properties of these alloys [22]. The Cr and Ni contents are 25 wt% and 7 wt% respectively, and this type of steel is used in the harshest environments. They combine the highest hardness (250HV), the highest tensile strength (730 MPa) and the best corrosion resistance among these alloys. As a result, it has been used for offshore umbilical tubing in oil and gas applications and as protective cladding [20]. The main limitation of the 2507 alloy is its low wear resistance.

2.3 Wear of Duplex Stainless Steels

In material science, wear is defined as the damage or loss of material from a solid surface by the physical interaction with another solid. Wear reduces the life span of engineering components and eventually results in costly repairs and replacements. Moreover, if unnoticed, it may cause serious safety hazards in industrial environments. Normally, the wear mechanisms are classified into several types: abrasive, adhesive, fatigue, oxidative and corrosion wear [29].

Abrasive wear is caused by the free-flow of hard particles in an open system, as in the case of ore conveyors or soil engaging tools, or by direct interaction with a solid counterpart in a constrained system, as it is the case inmetal cutting and jaw crushing. Blickensderfer et al. found that the wear rate in both open and constrained systems depends on the applied load and wear path length. However, the wear loss in constrained systems tends to be higher than in open systems because the former typically involves higher loads than the

latter [30, 31].

The adhesive wear mechanism was proposed in 1930s, to explain the shear or plastic deformation observed in worn engineering components loaded together and subjected to a sliding motion. In addition to the plastic deformation observed below the surface, debris particles are also transferred from one surface to another, typically from the softer material to harder material. This effect is exacerbated by a rough surface finish, which reduces the effective load bearing area and increases the contact stresses.

Duplex stainless steels have been largely used in many industries because of their good mechanical properties and corrosion resistance, their low cost and recyclability [32, 33]. However, they exhibit poor wear behaviour, as most stainless steels. The wear volume can be calculated using the following equation [34, 35]:

$$\mathrm{V} = \frac{k \times L \times S}{H}$$

where V is the wear volume, k is the wear coefficient, L is the load, S is the sliding distance and H is the hardness of the wearing surface.

From this equation, it becomes apparent that the wear volume is inversely proportional to the hardness. In other words, the wear will decrease when the hardness increases.

Although duplex stainless steels show excellent corrosion resistance and mechanical properties, their wear resistance is inadequate for many industrial applications. Therefore, different methods to increase the surface hardness have been investigated, in order to enhance the wear resistance while retaining the corrosion resistance of these alloys.

2.4 Surface engineering

2.4.1 Introduction

Surface engineering is a useful technology to combat erosion, wear and corrosion of engineering components. Surface engineering involves the design of treatments to enhance the surface and near-surface properties of a material, to meet the requirements of specific applications, by combining the properties of the bulk and the surface. Furthermore, surface modification treatments and coatings improve the material properties and enable their application in new fields and in a cost-effective manner [36, 37].

2.4.2 Surface Coating

Surface coatings use other elements, metals or alloys, which exhibit better properties, to cover a substrate with poor corrosion and wear resistance [38]. Physical vapour deposition (PVD) is a common surface coating technique, in which the coating material is evaporated or sputtered from a cathode and transported to the surface of the substrate in atomic, molecular or ionic form. The coating process is conducted at relatively low temperature and it does not affect the microstructure of the bulk material [39]. This method has been used for many years to deposit coatings on a wide range of components, from optical lenses to cutting tools. The typical example is PVD TiN coating to increase the wear resistance, oxidation and general corrosion resistance of titanium alloys [40, 41]. Furthermore, TiAlN coatings are frequently applied on cutting tools and they show superior wear resistance and toughness when turning stainless steels at low speed [42]. Even though these thin coatings effectively protect the substrate and enhance the tribological properties, wear resistance and low friction, they tend to fail when subjected to high loads.

2.4.3 Surface Modification

The surface modification processes alter the chemical composition or the microstructure of the substrate, and thus its properties, without building-up an additional layer or coating. This technology relies on physical and chemical principles to modify the surface and the near-surface microstructure, and ultimately improve the surface properties [43]. Some conventional surface modification methods include carburising and nitriding, and it is important to mention that in these cases there is no clear interface between the modified layer and the substrate [43, 44].

Carburising is a common thermochemical process, which introduces carbon on the surface of a component to produce a hardened layer with better wear and corrosion properties. The conventional carburising treatment is conducted at temperatures between 850°C and 1000°C. Several carburising methods have been successfully used in industry, introducing the carbon in the form of a gas, a liquid or a solid compound, namely: salt bath carburising, gas carburising and plasma carburising [45-47].

Nitriding was developed in the early 1920's to provide a method of surface hardening steel components. This process involves heating steel components in a nitrogen rich atmosphere (nitrogen or ammonia) to increase the surface hardness and the corrosion resistance [48]. When applied to hardened and tempered steels, nitriding produces a combination of high surface hardness (700 HV - 1100 HV) and a ductile core, improving both the wear characteristics and the fatigue strength. This process is carried out at relatively low temperatures, usually below the iron-nitrogen eutectoid temperature (590^{o}C), without phase transformation during the process [49]. As a result, components being treated are subjected to minimum distortion due to volume change.

2.4.4 Surface Engineering of Duplex Stainless Steel

Different coatings and surface modification methods have been applied to duplex stainless steel for several years. Paul et al. used a thermally sprayed aluminium (TSA) coating to protect duplex stainless steels against corrosion in marine environments. The TSA coating was 250-300 μm thick and extended the service life more than that 64% in chloride stress corrosion cracking (SCC) conditions [50]. However, the bonding between the coating and substrate was weak and it failed under high applied load.

Huang et al. attempted to nitrocarburise 2205 duplex stainless steels at low temperature using conventional salt bath technique. The results showed that the thickness of the nitrocarburised layer ranged from 4 μm to 28 μm, depending on the treatment temperature. Furthermore, the hardness increased to 1200 HV after the treatment and the erosion-corrosion resistance improved [27]. However, these salt bath treatments raise environmental concerns and are not entirely cost-effective [3].

2.4.5 Plasma Nitriding of Duplex Stainless Steel

Although plasma nitriding has been used for over 30 years, it has been only recently applied to stainless steels, and duplex stainless steels in particular. The plasma or ion nitriding process is conducted at low pressure, in a vacuum chamber, where the processing gas, rich in nitrogen, is ionised by an electric current, creating a glow discharge. The nitrogen ions in the plasma bombard the surface of the samples, which are kept at cathodic potential, releasing some atomic nitrogen species. The nitrogen atoms diffuse into the surfaces and may remain in solid solution or combine with alloying elements, such as Cr and Fe, to precipitate as Cr_xN or Fe_xN.

More recently, Chiu et al. used a novel active screen plasma nitriding (ASPN) technique to enhance the wear and corrosion resistance of duplex stainless steels. The ASPN method

offers such benefits over DC plasma nitriding, as reduced arcing damage, and edging effect, and maintaining a more uniform temperature inside the treatment chamber [51, 52]. The authors showed that a 9 μm-thick diffusion layer was formed at low temperature, and the hardness increased to 1100 HV which was more than 3 times higher than the untreated samples. Furthermore, the duplex stainless steel nitrided at 420°C for 10 hours also exhibited better corrosion resistance and lower mass loss in wear tests.

Kliauga et al. explored the effect of plasma nitriding on the mechanical properties of duplex stainless steel 2205. The samples were treated at temperatures between 350°C and 400°C for 20h. The metastable γ_N phase, i.e. a supersaturation of nitrogen in the γ phase, could be formed at 350°C. However, chromium and iron nitrides (Cr_XN and Fe_XN) were formed at higher temperatures or longer times. The hardness and the thickness of the diffusion layer increased with the treatment temperature and/or treatment time, but only at expense of the corrosion resistance, and the pitting corrosion resistance in particular, which became poorer after the treatment at 400°C. Therefore, it can be concluded that the plasma nitriding at a temperature in the order of 350°C is more suitable for duplex stainless steel 2205, to improve its tribological properties without losing the corrosion resistance.

2.4.6 S-Phase

Nitriding and carburising are known to improve the surface hardness, wear resistance and fatigue life of steel components. On the other hand, these treatments also tend to reduce the corrosion resistance of stainless steels by depleting the alloy from chromium when Cr_xN precipitates. The example mentioned above demonstrates that the corrosion resistance of duplex stainless steel 2507 and 2205 can be retained or even improved by conducting plasma nitriding treatments at low temperature [1, 53].

From 1980s to 2010, several researchers studied the underlying mechanisms of the

increased corrosion resistance of stainless steels plasma nitrided at low temperature. Bell, Dong and Ichi found that the precipitation of chromium nitrides in austenitic stainless steels (316 and 304) and in Co-Cr alloys could be avoided by plasma nitriding at temperatures below 400-500°C [3, 49, 52, 54]. In 2010, Dong summarised this phenomenon and provided a comprehensive interpretation: a metastable, nitrogen-supersaturated and precipitation-free γ_N phase (expanded austenite) can be formed before Cr_xN or Fe_xN precipitate, when nitrogen and carbon are introduced into the fcc structure of the substrate at low temperature. To this end, it is generally accepted that the formation of this supersaturated γ_N phase, also called S-phase, is the key to the combined excellent mechanical properties and corrosion resistance of these nitrided stainless steels [3].

To the best of our knowledge, no systemic and comprehensive research has been conducted to date, to study the effect of low temperature plasma nitriding on all grades duplex stainless steels. Therefore, this research work focuses on the effect of low temperature plasma nitriding on lean duplex stainless steels 2101 and 2404.

CHAPTER 3 EXPERIMENTS

3.1 Substrate Material

In this research project, the selected materials were lean duplex stainless steel 2101 (UNS No.S32101) and lean duplex stainless steel 2404 (UNS No.S82441), which were provided by Outokumpu corporation. The nominal chemical compositions and the GDOES results of these two materials are shown in Tables 3.1 [21] and 3.2 respectively.

Table 3.1 Chemical compositions of selected lean duplex stainless steels

Outokumpu Steel name	International steel No			Chemical composition,% by wt. Typical values					
	UNS	EN	ISO	C	N	Cr	Ni	Mo	Others
LDX 2101	S32101	1.4162	4162-321-01-E	0.03	0.22	21.50	1.50	0.30	5Mn Cu
LDX 2404	S82441	1.4662	4662-824-41-X	0.02	0.27	24.00	3.60	1.60	3Mn Cu

3.2 Sample Preparation

The received lean duplex stainless steels shaped as rectangle plates of 210x297x10 (mm^3), were cut into square slabs of 20x20x10 (mm^3) by a Struers Accutom-5 cutting machine with an abrasive silicon carbide (Si-C) blade. Then, all the samples were ground from 120 to 1200 grit using silicon carbide grinding papers. After grinding, the samples were polished using diamond paste of grades 9μm, 6μm, 3μm and 1μm on the Struers grinding/polishing machine. Finally, the polished samples were ultrasonically cleaned with soapy water and acetone and dried under hot air.

3.3 DC Plasma Nitriding

Plasma nitirding treatments were carried out in a 60kw KlÖckner DC plasma nitriding unit (Figure 3.1) at 390℃, 420℃, 450℃ and 480℃. A mixed gas of 75%H_2+25%N_2 with a pressure of 4 mbar (400Pa) was used for all the plasma treatments. The detailed treatment conditions and the sample code are listed in Table 3.2.

Table 3.2 The sample codes and surface treatment conditions

Treatment Code	Temperature,℃	Time,h	Gas composition
PN390/10	390	10	25%N_2+75%H_2
PN420/10	420	10	25%N_2+75%H_2
PN450/10	450	10	25%N_2+75%H_2
PN480/10	480	10	25%N_2+75%H_2

Prior the treatment, the samples of LDX2101 and LDX2404 were cleaned in acetone and placed on the working table of the plasma nitriding furnace. As shown in Figure 3.2, the samples were loaded closely in order to avoid potential arcing and reduce edge effect during the treatment.

The furnace was closed and the vacuum pumped down to 10-1 Pa before the gas mixture of hydrogen and nitrogen was introduced into the furnace. When the voltage was applied, the nitrogen in the chamber was ionized and bombarded the surface of the samples and plasma nitrinding was started. Because the KlÖckner DC plasma nitriding unit can allow the heating process to be managed in predetermined steps, during the treatment, the voltage, current and gas pressure were increased steadily until the set treatment temperature and pressure were achieved. The samples were then treated under the constant temperature and pressure for 10 hours. After the plasma nitriding treatment, the samples were cooled within the furnace in vacuum. After about 2 hours, the interior temperature of chamber reached about 26℃ and the furnace was then ventilated and opened to take out the treated samples.

3.4 Materials Characterisation

The microstructure, chemical composition and mechanical properties of the as-received and plasma nitrided samples were fully characterised.

3.4.1 Microstructure

3.4.1.1 SEM Observation

The microstructural characteristics of plasma nitrided samples together with wear and corrosion tested surfaces were observed by Philips 6060, Philips XL30 and Jeol-7000 SEM machines. The Philips 6060 was used mainly for chemical composition analysis by EDX; the other two were used mainly to observe the surface and cross-sectional microstructures under magnifications from 50X to 5000X.

After plasma nitriding, the treated samples were cut using the Struers Accutom-5 machine at a slow feed rate. Then, the samples were mounted in conductive Bakelite using the MET-PREP OPAL-400 machine. The mounted samples were ground and polished as described in Section 3.2 before they were etched by a solution containing 50% nitric acid (HNO_3), 25% hydrochloric acid (HCl) and 25% H_2O to reveal the microstructures for SEM examination.

3.4.1.2 X-ray Diffraction

As X-ray diffraction analysis is one of major techniques to identify the phase constituents of the nitrided layer, a Philips X` Pert diffractometer with Cu-Kα radiation was applied to all treated and untreated samples with 2θ ranging from 30°- 120° and a scanning rate of 1°/min. The recorded diffraction patterns were analysed by the software of X-Pert Highscore program for the phase identification of the nitrided surface layer and untreated surface samples.

3.4.2 Chemical composition

3.4.2.1 GDOES-measurement

The chemical composition depth distribution of nitrided samples was analysed by the LECO GDS-750 QDP Glow Discharge Optical Emission Spectrometry. This GDOES unit is a water-cooled Grimm type (Figure 3.3) with a standard 4 mm lamp. The cathode sputtering process of the Grimm type lamp is created by applying a controlled voltage to the sample surface. The surface atoms removed by sputtering diffuse into the argon plasma where excitation and emission occur. Separation of atom removal and excitation provides spectra. In this work, the operating voltage and current were set to 700V and 20mA to manage a slow sputter rate. Nitrogen was the principal interest in this work but Fe, Ni, Cr, C, N, Mo, Mn, O and H were also measured.

3.4.2.2 Energy dispersive X-ray spectroscopy (EDX)

In addition to GDOES, the Oxford EDX detector adapted to the SEM instruments was used to analysis the composition of the surface and cross-sections of plasma treated samples. The energy was chosen up to 20KeV, and INCA software was used to do the chemical elements analysis.

3.4.3 Mechanical properties

3.4.3.1 Hardness Measurement

The Mitutoyo MVK-H1 hardness tester with a Vickers indenter was used to measure the hardness of treated and un-treated samples under the loads ranging from 50g to 1000g. The hardness of each sample was measured for 5 times and the average value was calculated and reported. The distance of any two neighbouring indentations was kept at least 3 times that of the indentation size in order to avoid interference among each indentation.

The Nano Test 600 (Mico Materials Ltd, Wrexham, UK) machine was used to measure the cross-section hardness of the plasma nitride surface layers. In addition, the hardness of austenite and ferrite phases in the DSSs was also measured by relating the measured nano-hardness value to the indents revealed by post-indentation SEM observation. All the nano-hardness tests were used a depth control method with a maximum penetration depth of 0.8μm. At least 5 repeated measurements were conducted on each sample, and the data were collected by computer and analysed by Nano-test software.

3.4.3.2 Load bearing capacity tests

The load bearing capacity of untreated and plasma nitride surfaces were evaluated using the Mitutoyo MVK-H1 hardness testing machine with a Vickers indenter. The load applied to the Vickers indenter was increased from 10g to 1000g and the micro-hardness was measured as a function of the applied load.

3.4.3.3 Dry Wear Tests

Wear test was carried out at room temperature (21℃) for all experimental samples by using a reciprocating tribometer (Figure 3.4). There are two types of wear tests: (1) dry wear test in air without lubrication and (2) corrosion-wear tests in 3.5%wt NaCl solution to simulate sea water. During the wear tests, the specimen fixed on the sample stage reciprocated against a WC ball (Φ=8mm) at a frequency of 1.12Hz and with a displacement amplitude of 4 mm. The WC ball acted as a pin and created a wear track of about 4 mm in length. Two different loads of 30N and 70N were chose for the dry wear tests and one load of 70N was used for the corrosion-wear tests. The maximum Hertz contact stress on the steel sample surface has been calculated for the load of 70N based on the following [61]:

For an elastic ball of radius R, indents an elastic half-space to depth d, the contact area of radius is

$$a = \sqrt{Rd}$$

Therefore, the applied force F is:

$$F = \frac{4}{3} E^* R^{1/2} d^{3/2}$$

Where:

$$\frac{1}{E^*} = \frac{1 - {V_1}^2}{E_1} + \frac{1 - {V_2}^2}{E_2}$$

And the E_1, E_2 are the elastic module and v_1, v_2 are the Poisson ratios with each body.

Furthermore, the pressure distribution in the contact area is:

$$p(r) = P_0 (1 - \frac{r^2}{a^2})^{1/2}$$

Therefore, the P_0 is the maximum contact pressure which is given by:

$$p_0 = \frac{3F}{2\pi a^2} = \frac{1}{\pi} (\frac{6FE^{*2}}{R^2})^{1/3}$$

Based on the formula above, the maximum contact pressures of LDX 2101 and LDX 2404, which are named as P_1 and P_2, are 2.662 GPa and 2.651 GPa respectively.

3.4.3.4 Electrochemical Corrosion Tests

Corrosion resistance is one of the most important properties of stainless steel. Hence, the corrosion behaviour of the plasma nitride DSSs was compared to the un-treated samples by electrochemical corrosion tests in 3.5% NaCl solution. As shown in Figure 3.5, the sample was used as the working electrode (WE), which was hold down on a Teflon ring at the end of the flat cell. The area of the working electrode was 1cm*1cm. The open circuit potential (OCP) was first measured for 2 minutes, and then potentiodynamic polarisation tests were carried out by sweeping from -200mV of the OCP to 1200mV at a scan rate of 1mV/s. The Sequencer V4 software was used to record and analysis the data.

CHAPTER 4 RESULTS

4.1 Microstructures

4.1.1 The Microstructure of As-Received Materials

A 3D schematic of the typical microstructure of as-rolled LDX 2101 plate is shown in Figure 4.1.1-1 and two different types of microstructures can be found on longitudinal and transverse sections. All these microstructural characteristics were formed during the rolling of the steel plate. Figure 4.1.1-2 shows the detailed SEM microstructures on the longitudinal and transverse sections of the as-received LDX 2101 sample. It can be seen from Figure 4.1.1-2a that the grains on the longitudinal section are relatively thin (<10 μm) and highly elongated along the rolling direction; although the grains on the transverse section are also elongated, they are relatively thick (10 μm to 20 μm) and irregular shaped (Figure 4.1.1-2b). The chemical composition difference between the two typical grains with different contrasts was studied by EDX. As shown in Figure 4.1.1-2c, position A exhibited a higher content of Cr but a lower content of Ni when compared with position B. This indicates that position A is a ferrite grain and position B is an austenite grain, since chromium is a ferrite former and nickel is an austenite former.

The longitudinal and transverse microstructures for untreated LDX 2404 are shown in Figure 4.1.1-3, which are similar to those of LDX 2101. It can be seen that the thickness of the elongated grains ranges from 5 μm to 10 μm on the longitudinal section (Figure 4.1.1-3a). Compared with the grains on the longitudinal section, the grains on the transverse section are thicker and not so elongated (Figure 4.1.1-3b). From the EDX results (Figure 4.1.1-3c), it can be seen that the Cr content at position A is higher than that at position B, while the Ni content at position A is typically lower than that at position B. Therefore, position A should correspond to a ferrite grain and position B should correspond to an

austenite grain. This is because the austenite contains more Ni than the ferrite whilst ferrite has a higher Cr content than the austenite [55].

4.1.2 Layer Structure of Plasma Nitrided Samples

4.1.2.1 LDX2101 samples

The SEM images in Figure 4.1.2-1 show the longitudinal cross sections of samples after plasma nitriding (PN) for 10 hours at different temperatures, ranging from 390℃ to 480℃ (PN390 to PN480). The images reveal that a nitrided layer was formed on the surface of the specimens, with a clear boundary between the nitride layer and the substrate. The layer thickness observed on the PN390 sample was about 5 μm, the thicknesses of the nitrided layers increased with the treatment temperature to 8 μm, 19 μm and 25 μm for PN420, PN450 and PN480 samples, respectively. Furthermore, when the treatment temperature was below 420℃, the nitrided layer was dense, without cracks or pits, and it exhibited good corrosion resistance to the etchant [Figures 4.1.2-1a and b]. However, when the treatment temperature was over 420°C, some cracks and dark etched patches were observed (Figures 4.1.2-1c and d), indicating a poor surface layer quality and low corrosion resistance.

Figures 4.1.2-2a and b shows the typical microstructure observed on the transverse-sections of LDX 2101 samples, after plasma nitriding for 10 hours at 420℃ and 480℃, respectively. A clear boundary was found between the surface layer and the substrate, but the layer thickness is different when formed on original ferritic and austenitic grains. This indicates that the diffusion rate of nitrogen in these two phases was different during the treatment. Additionally, the surface layer formed on one of the phases after PN480 (Fig. 4.1.2-2b) was severely etched, while the PN420 sample (Fig. 4.1.2-2a) showed good corrosion resistance to the etchant for both phases. This indicates that the corrosion

resistance of the high temperature treated samples is worse than that for the low temperature treated ones.

4.1.2.2 LDX2404 samples

Figure 4.1.2-3 shows the SEM images of the longitudinal cross sections of LDX 2404 specimens, plasma nitrided at different temperatures for 10 hours. It can be clearly seen that a nitrided layer formed on the surface, and the layer thickness increased with an increase of the treatment temperature. The nitrided layer of sample PN390 showed no cracks and better corrosion resistance to the etchant than the substrate. On the other hand, the high temperature treatments resulted in a surface layer with cracks and dark etched patches (Figures 4.1.2-3c and d). Similar to the LDX 2101 samples, the nitrided layer formed on the original austenite grains showed better corrosion resistance than the nitrided layer formed on the original ferrite grains.

The typical microstructure observed on the transverse cross section of LDX 2404 samples, after plasma nitriding at 390℃, 420℃ and 480℃ for 10 hours, is shown in Figure 4.1.2-4. It can be seen that a nitrided layer was formed on the samples, and the layer thickness increased with increasing treatment temperature. The PN390 sample showed a featureless surface layer, while the layer formed on the PN420 specimen showed clearly defined grains and grain boundaries within the nitrided layer. In the case of the PN480 sample, some cracks were found in the layer, propagating parallel to the surface.

4.2 Composition & Phases

4.2.1 LDX2101 Samples

Figure 4.2.1-1 shows the typical GDOES depth-composition profiles of an LDX 2101 sample, after PN450 treatment. It can be seen that the nitrogen content at the surface reached a maximum value of 3.9 wt%, and then decreased slowly to a value of approximately 3 wt% followed by a sharp drop to the substrate content. A small peak of carbon was also observed within the surface layer, close to the interface with the substrate, which may indicate that the nitrogen introduced during the treatment pushed the pre-existing carbon inwards. The thickness of the treated layer, based on the nitrogen-depth profile, is about 18 μm, which is consistent with the thickness observed by SEM.

Figure 4.2.1-2 shows the GDOES nitrogen-depth profiles of LDX 2101 samples after plasma nitriding that for 10 hours at different temperatures, from 390℃ to 480℃. The different nitrogen diffusion depths can be clearly seen in this figure. The maximum nitrogen content in the treated layer of PN390 sample was approximately 0.6 wt%. In all the other cases, i.e. PN420, PN450 and PN480, a maximum nitrogen content of about 3.9 wt% was detected at the surface. The nitrogen content dropped sharply for PN420 sample, while PN450 and PN480 samples exhibited a plateau region with relatively constant nitrogen content of approximately 3 wt%, followed by a sharp reduction in the nitrogen content close to the interface between the surface layer and the substrate.

4.2.2 LDX2404 Samples

The typical GDOES profiles of nitrided LDX 2404 samples are shown in Figure 4.2.2. The nitrogen diffusion-depth profiles of LDX 2404 samples exhibited the same tendency as

their LDX 2101 counterparts. It can be seen that the maximum nitrogen content introduced into the surface of the sample treated at 390℃ was approximately 0.9 wt%, and the maximum nitrogen content for all the other samples, treated at 420℃, 450℃ and 480℃, was 4.9 wt%. A nitrogen plateau was observed for PN450 and PN480 samples, with an approximate nitrogen content of 3.5 wt%.

4.2.3 Comparison of LDX2101 and LDX2404 Samples

Figure 4.2.3 compares the nitrogen diffusion depth profiles of LDX 2101 and LDX 2404 samples. It can be seen that, for the same treatment condition, a marginally higher content of nitrogen (0.2 wt% to 0.8 wt%) was achieved for the LDX 2404 specimens than for the LDX 2101 ones. For example, in the case of the treatment conducted at 480℃, the nitrogen content of the LDX 2404 specimen was approximately 4.8 wt%, which is 0.9 wt% higher than its LDX2101 counterpart (3.9%wt nitrogen). On the other hand, nitrogen diffused deeper into the LDX 2101 samples than into LDX2404 for all treatment conditions, with the exception of PN390. For example, in the case of PN450 samples, nitrogen diffused approximately 8 μm into the LDX 2101 substrate, compared with the 5.6 μm observed in the LDX 2404 ones. This may be attributed to the high affinity of chromium for nitrogen and the higher content of Cr in LDX 2404 than in LDX2101 which could serve as the trapping sites for nitrogen. As a consequence of this trapping mechanism, the diffusion speed of nitrogen was reduced and resulted in thinner nitrided layers in the LDX 2404 specimens.

4.2.4 Phase identification of plasma nitride layers

As shown in Figures 4.1.2-1 and 4.1.2-3, all the samples formed a surface layer after plasma nitriding treatment. The phase composition of the surface layers formed during the plasma treatments is presented in Figures 4.2.4-1 and 4.2.4-2, together with the XRD

patterns from the as-received materials for comparison. It can be seen that the patterns obtained from the as-received LDX 2101 and 2404 specimens show the typical duplex structure, consisting of ferrite (α) and austenite (γ). Compared with the peaks of the as-received samples, all the treated specimens showed changes in the XRD patterns with considerable peak broadening. For both materials, the XRD patterns show similar peaks when treated below 480°C but with different peak intensities, depending on the treatment temperature. A detailed analysis of these peaks found that the following phases were formed during plasma nitriding: S_N, α_N and ε-Fe_3N (Figures 4.2.4-1a, b and 4.2.4-2a, b). A trace of CrN peaks can also be identified for 450°C plasma nitride samples and as evidenced in Figures 4.2.4-1b and 4.2.4-2b, a peak at 2 theta 37.5° matches CrN (111) plane. When samples were plasma nitrided at 480°C, the XRD patterns for both materials were changed and the α_N phase identified for PN390, PN420 and PN450 samples could not be found and, instead, peaks of CrN, Fe_4N and α could be indexed. The S-phase and the ε-Fe_3N phase presented for the relatively low temperature treated samples were still detected with high intensity, see Figures 4.2.4-1 and 4.2.4-2.

4.2.5 TEM Analysis

TEM characterisation was carried out on the transversal cross-section of one LDX 2404 PN420 sample. Figures 4.2.5a and b show the microstructures and the corresponding SAD patterns of the plasma nitrided surface layer from original austenite and ferrite grains respectively. It was found that a nitrogen supersaturated layer, or so-called S-phase layer, was formed on the original austenite grains and the SAD pattern analysis revealed a FCC structure (B=110, Fig. 4.2.5 a), as for the original austenite. However, the calculated d-spacing of this S-phase is larger (a=0.365nm) than the original austenite (a=0.360nm).

Similar TEM observations were also conducted on the original ferrite grains in the duplex

stainless steels investigated. The results indicated that the surface layer formed from original ferrite grains consisted of nitrogen saturated ferrite (α_N) and ε-Fe_3N needles as evidenced by the SAD pattern, shown in Figure 4.2.5 b). No chromium nitride precipitate was observed in the surface layer of this PN 420 plasma nitrided LDX2404 sample.

4.3 Hardness and Layers Thickness

4.3.1 Surface Hardness and Thickness

The hardness values measured on the untreated samples and on the nitrided layers, as a function of treatment temperature, are shown in Figure 4.3.1-1. Compared with the untreated material, all plasma nitrided samples showed an increase in surface hardness, and their hardness increased with the treatment temperature. The hardness values of LDX 2101 PN390 and PN480 samples were 697HV and 1666HV, respectively, which is nearly twice and 5 times that of the untreated material. Similarly, the hardness of the nitrided LDX 2404 samples was 717 HV, for PN390, and 1756 HV, for PN480, which is about twice and 6 times as hard as the untreated material (411 HV). When treated at 390 and 420°C, there is no significant hardness difference for these two materials; however, when treated at 450 and 480°C, the hardness of the LDX 2101 specimens is lower than the hardness of the LDX 2404 ones. This could be attributed to the higher Cr and Mo content in LDX 2404 than in LDX2101, which might have increased the nitrogen content of the surface layers. Even for the untreated condition, the LDX 2404 specimens were harder than their LDX 2101counterparts.

Figure 4.3.1-2a shows the thickness of the nitrided layers, as a function of the treatment temperature, measured on the longitudinal cross-section of the specimens. It can be seen that the thickness of the nitrided layer increased with the nitriding temperature. For the same treatment temperature, LDX 2101 samples showed a thicker layer than LDX 2404 samples. The layer thickness on both lean duplex stainless steels, measured on the transverse cross section, is shown in Figure 4.3.1-2b. The same tendency as for the longitudinal cross-section was observed with the thickness increasing with the treatment temperature. The thinnest layer formed on LDX 2101 and LDX 2404 was 5.1 μm and 4.9

μm, respectively, and the thickest layer formed on the same materials was 27.5 μm and 24.2 μm, respectively. Furthermore, when treated at 390°C, the layer thickness obtained on both LDX 2101 and LDX 2404 was nearly the same. On the other hand, for all other treatment temperatures, the layer growth rate (diffusion rate) on LDX 2101 was faster than on LDX 2404. Figures 4.3.1-2a and b show that the nitrided layers obtained on LDX 2101 were thicker than the ones on LDX 2404 for the same treatment temperature. This difference was particularly clear at high treatment temperatures, indicating that the effect of strong nitride formers, such as Cr and Mo, on the nitrogen diffusion rate is stronger at high temperatures than at 390°C.

4.3.2 Load Bearing Capacity (LBC)

The static load bearing capacity of plasma nitrided samples of both 2101 and 2404 lean duplex stainless steels was evaluated by Vickers hardness measurements at loads ranging from 0.05 kg to 1 kg. Figure 4.3.2a shows the results obtained on LDX 2101 for the five assessed conditions: the as-received sample and the plasma nitrided samples for 10 hours at four temperatures. In general, it can be seen that all plasma nitrided samples had a much higher load bearing capacity than the untreated one, particularly for loads below 200 g. When the loads were higher than 300 g, the PN390 and PN420 samples exhibited nearly the same hardness values as the untreated material. In addition, all the plasma nitrided samples showed a decrease in hardness with increasing load. The behaviour of the plasma nitrided lean duplex stainless steel resembles that of a composite sample, having a hard outer layer and a soft substrate. Therefore, when the load was low, the hard nitrided layer could bear the whole load; however, when the load exceeded a critical load, the thin hard layer could not bear the whole load and both the thin hard layer and the soft substrate contributed to the measured hardness, i.e. composite hardness. It could also be seen that the samples treated at higher temperatures had a higher LBC than those treated at low

temperatures mainly due to the thicker nitrided cases formed at higher temperatures.

Figure 4.3.2b shows the load bearing capacity of LDX 2404 samples. It can be seen that the high temperature treated samples, PN450 and PN480, exhibited hardness values over 1000 HV even under a load of 300 g. Both samples showed higher hardness values than the untreated material or the low temperature treated ones, even under a load of 1 kg. In the case of PN420 and PN390, the thin surface layers could only bear loads below 300 g and 100 g, respectively.

Therefore, both LDX 2101 and LDX 2404 samples exhibited a good bearing capacity, even at high loads, when the samples were plasma nitrided at high temperature. For the samples treated at low temperature, the load bearing capacity was below 300 g.

4.3.3 Hardness of plasma nitride layers

4.3.3.1 Microhardness

The microhardness-depth profiles of the two lean duplex stainless steels, plasma nitrided at 480℃ for 10 hours, are shown in Figure 4.3.3-1. The microhardness measured near the surface of the LDX 2101 sample was about 1200 HV, which decreased slowly to 360 HV at 42 μm from the surface. On the other hand, the surface microhardness of the LDX 2404 specimen was higher than 1400 HV and then it decreased to 360 HV at 30 μm from the surface. Therefore, it can be seen that the surface microhardness of the LDX 2404 specimen is higher than that of the LDX 2101 one, but the hardness-depth gradient was also steeper for the former than for the latter. The thickness of the nitrided layer showed an inverse correlation with the surface hardness.

4.3.3.2 Nano-indentation

The nano-indentation results obtained from 25 indentations, namely surface hardness (H)

and Young`s modulus (E), for LDX 2101 and 2404 samples after plasma nitriding at 420℃ for 10h are shown in Figures 4.3.3-2 a and b. It can be seen that the surface hardness of sample LDX 2101 fluctuated largely between 8 GPa and 13 GPa, but the variation of elastic modulusies between 186 GPa and 218 GPa. The LDX 2404 PN420 sample showed a surface hardness between 9 GPa and 16 GPa and elastic modulus between 180 GPa and 220 GPa. The average and deviation of H and E as well as the ratio of H/E are summarised in Table 4.3-1. It can be seen that the surface hardness of LDX 2101 is lower than LDX 2404, while the elastic modulus are similar for both samples.

Table 4.3-1 The average and deviation of H, E and the ratio of H/E

Sample	**LDX 2101 PN420**	**LDX 2404 PN420**
Hardness (H), GPa	10.37±1.35	12.59±1.89
Elastic modules (E), GPa	203.77±8.14	203.06±12.58
H/E	0.051	0.062

Figure 4.3.3-3 and Figure 4.3.3-4 show the SEM images, hardness maps and EDX analysis results of the chemical composition on the low and high hardness spots for PN420 treated LDX 2101 and LDX 2404 samples. The hardness distribution on the surface of the samples is not uniform, and the hard and the soft areas are related to the Cr/Ni ratio. For LDX 2101, the area with the lowest hardness, 5 GPa, corresponds to the Cr and Ni content of 22 wt% and 1.65 wt%, respectively and hence a low Cr/Ni ratio of 13.3, while the hardest area, 8.8 GPa, has the Cr and Ni content of 23 wt% and 0.92 wt%. A similar trend was observed for the LDX 2404 PN420 sample, which contained a higher content of alloying elements than LDX 2101, and hence a high Cr/Ni ratio of 25. It is well known that Cr is a ferrite forming element and Ni is an austenite forming element. Based on this, the areas with a low Cr/Ni ratio are associated with austenite grains (areas denoted as “A”), while the areas denoted as

"B" in Figures 4.3.3-3b and 4.3.3-4b, have a high Cr/Ni ratio, and hence are associated with ferrite grains. The difference in hardness of these two grains implies that the response of original austenite and ferrite to low temperature plasma nitriding was different, which will be discussed in Chapter 5.

4.4 Corrosion Resistance of Plasma Nitride Samples

Duplex stainless steels have good corrosion resistance and excellent pitting corrosion resistance in particular. The effect of plasma nitriding on the corrosion resistance of the duplex stainless steels was investigated by electrochemical corrosion tests in 3.5 wt% NaCl solutions and the results are reported here.

4.4.1 LDX 2101 Samples

Figure 4.4.1-1 shows the typical anodic polarisation curves of untreated and plasma nitrided LDX 2101 samples. The corrosion potential and the pitting potential of the untreated sample was -240 mV and 350 mV (VS SCE) respectively. The corrosion potential (Ec) of plasma nitrided samples were -370, -324, -253 and -230 mV (VS SCE) for PN480, PN450, PN420, and PN390, respectively. Only PN390 started corrosion at a higher potential than the untreated sample.

For the low temperature treated samples, the pitting potential of both PN390 and PN420 samples were increased from 350 for the untreated material to about 730 and 830 mV (VS SCE), respectively. Clearly, these two samples showed a large passive region spanning from 145 to 750 mV (VS SCE) for PN390 and from 280 to 850 mV (VS SCE) for PN420 samples. Furthermore, the current density of PN390 and PN420 samples was lower than the untreated sample for potentials over 440 and 540 mV (VS SCE), respectively.

It can be seen from Figure 4.4.1-1 that the current density for the relatively high temperature treated PN450 and PN480 increased rapidly with limited or almost no passivation. Their passive current density is at least one order of magnitude higher than that of PN390 and PN420 samples. Clearly, the high-temperature treated PN450 and PN480 showed worse corrosion resistance than the untreated sample, while the low-

temperature treated PN390 and PN420 samples showed better corrosion resistance than the untreated sample at potentials above 450 for PN390 and 530 mV (VS SCE) for PN420. It is also evident that the corrosion behaviour of PN390 is better than PN 420 in terms of a high corrosion potential and lower passive corrosion density.

SEM observations were carried out on all corroded samples to investigate the corrosion mechanisms involved. Figure 4.4.1-2 shows the SEM images of an untreated sample before and after the corrosion test. Compared with the featureless surface morphology of the sample before the test (Figure 4.4.1-2a), the surface of the corroded sample showed several pits, some of which were elongated in shape as labelled “A” in Figure 4.4.1-2b. This morphology is consistent with the microstructure features shown in Figure 4.1.1-2, and the elongated shaped pits could be related to the rolling structure of the duplex stainless steel samples. Other pit morphologies were also observed, such as the large and deep holes labelled “B” in Figure 4.4.1-2b, and shown at higher magnification in Figure 4.4.1-2c. These holes typically consisted of a deep pit in the centre, surrounded by small pits around the edge.

The morphology observed on the 390°C treated sample (PN390), is illustrated in Figure 4.4.1-3. It can be seen that very few changes were observed after the corrosion tests, and no signs of either intergranular corrosion or pitting could be seen under low magnification SEM observation (Figures 4.4.1-3a VS. b). The observations at a higher magnification (Figure 4.4.1-3c) only revealed grinding marks with no pits, indicating that PN390 exhibited good corrosion resistance. With increasing the treatment temperature to 420°C, the PN420 samples began to show signs of corrosion on the tested surface, particularly pitting corrosion (Fig. 4.4.1-4). Figure 4.4.1-4c shows a typical pit observed on sample PN420, which is of much smaller than the pits observed on the untreated specimen (Fig.

4.4.1-2c).

The surface morphology of the samples treated at relative high temperatures is shown in Figures 4.4.1-5 and 4.4.1-6. Compared with the untreated material, both the PN450 and the PN480 specimens were severely corroded, which is in line with the corrosion curves showed in Fig. 4.4.1-1. Under high magnification (Figure 4.5.1-5c) the tested surface of the PN450 sample showed signs of selective corrosion, which could be associated with the formation of CrN and the selective attack around these Cr depleted areas. In the case of PN480 (Figure 4.5.1-6), the surface was extensively corroded, which should be attributed to an extensive precipitation of CrN when the treatment temperature increased. Therefore, the PN390 condition showed the best corrosion resistance, compared with the untreated material and with the plasma nitrided samples at higher temperatures.

4.4.2 LDX 2404 Samples

The anodic polarisation curves of untreated and plasma nitrided LDX 2404 samples are shown in Figure 4.4.2-1. The corrosion potential (Ec) for this set of samples was about -304(PN480), -268 (PN450), -234 (PN420), -188(untreated) and -183 mV (VS SCE) (PN390). Except for PN390, all plasma treated samples showed a lower corrosion potential than the untreated sample. The pitting potential of the untreated material was 1079 mV (VS SCE), where a sudden change in the slope of the current density curve is observed in Figure 4.4.2-1. For the plasma nitrided samples, the pitting potential was 800 and 860 mV (VS SCE) for PN420 and PN390, respectively.

Similar to the anodic polarisation curves of LDX 2101, the LDX 2404 specimens nitrided at low temperatures, PN390 and PN420, showed a wide passive region after an initial activation. In contrast, no or limited passivation was observed for PN450 and PN480 treated LDX 2404 samples. The passive current density of PN450 and PN480 samples is at

least 10 times higher than that of PN390 and PN420 samples. Consequently, the PN450 and PN480 samples showed much worse corrosion resistance than PN390 and PN40 samples although they still showed showed at a higher passive current density than the untreated specimen.

The surface morphology of the untreated LDX 2404 sample before and after the corrosion test is shown in Figure 4.4.2-2. The surface of the untreated sample after the test exhibited signs of corrosion in the form of pits, similar to the ones observed on the LDX 2101 specimen (Fig.4.4.1-2). The elongated shape of the pits could be once again attributed to the rolling structure of the sample. Figure 4.4.2-2c shows a typical corrosion crater at high magnification, having a deep central pit surrounded by small pits. Judging from the surface morphology after the test, the LDX 2404 specimen showed fewer pits than its LDX 2101 counterpart.

SEM observations on plasma nitrided samples before and after the corrosion tests were carried out and the images are illustrated in Figures 4.4.2-3 to 4.4.2-6. The PN390 sample showed very mild change after the corrosion test and no pits could be found on the surface at low magnification SEM observation. This shows an improvement in the corrosion resistance over the untreated material. However, a few small pits can be seen on the corroded surface at high magnification (Figure 4.4.2-3c), indicating that when treated at 390°C (PN390), the corrosion resistance of LDX 2404 was lower than LDX 2101. Many small pits were observed after the corrosion test on the surface of PN420 (Fig. 4.4.2-4b) and a typical pit is shown in Figure 4.4.2-4c. These pits were shallower than the ones observed on the untreated material. Clearly, the corrosion resistance of PN420 is better than the untreated substrate but worse than PN390.

The specimens treated at relatively high temperatures (PN450 and PN480) were severely

corroded (Figures 4.4.2-5 and 4.4.2-6). It can be seen that the most of the surfaces were corroded and only a few patches of the nitrided layer remained on the surface (Figures 4.4.2-5b and 4.4.2-6b). Therefore, the corrosion resistance of plasma nitride LDX 2404 samples showed the same trend as their LDX 2101 counterparts; while the samples treated at low temperatures (390 and 420°C) showed better corrosion resistance than the untreated sample. The degraded corrosion resistance of PN450 and PN480 samples were attributed to the formation of CrN and the depletion of Cr in the adjacent areas.

In conclusion, both LDX 2101 and LDX 2404 showed a better corrosion resistance than the untreated material after plasma nitriding at 390 and 420°C. Further increasing the treatment temperature led to the reduced corrosion resistance for both materials.

4.5 Tribological Properties

It is well known that plasma nitriding can improve the wear resistance of stainless steels, and its effect on lean duplex stainless steels in particular was assessed by wear testing with a reciprocating ball-on-disc tribometer, under dry and wet (3.5 wt% NaCl) conditions with a counterpart ball of WC.

4.5.1 Dry Wear of LDX 2101

4.5.1.1 Dry wear loss

The results of the dry wear tests conducted on LDX 2101 samples under loads of 30 N and 70 N can be seen in Figure 4.5.1-1. For the dry wear tests conducted at 30 N, the wear loss of the untreated sample was 5.3 $x10^3$ μm^2 and the wear losses corresponding to the plasma nitrided samples were reduced to 95 μm^2 and 41 μm^2 for PN390 and PN420, respectively, while the wear loss for the high temperature treated samples, PN450 and PN480, was below the detection limits. Figure 4.5.1-2a shows the 2D profiles of the wear tracks left on the untreated and on the plasma nitrided samples after the wear tests under a load of 30 N. The wear track observed on the untreated specimen was very deep, while the PN390 sample only showed a narrow and shallow wear track. Sample PN420 showed a wear track depth comparable to the thickness of the nitrided layer, while the other samples exhibited no detectable wear track.

When wear tested at 70 N (Figure 4.5.1-1), the wear loss of the untreated samples increased further. PN390 and PN420 also showed severe wear loss, which is mainly because of the thin nitrided layers (5 μm and 8 μm thick for these two samples). The surface nitride layers collapsed under the high load used in this test and hence the tungsten carbide ball (counterpart) worn through the nitrided layer. In addition, the hard wear debris particles, released from the nitrided layer, are abrasive and may accelerate the wear.

On the other hand, the PN450 and PN480 samples retained their wear resistance even under 70N and exhibited a wear loss of only 2.6 and 6.5 μm^2, respectively. The 2D profiles of the wear tracks left on the samples after the wear tests conducted at 70 N are shown in Figure 4.5.1-2b. It is clear that the size of the wear track increased with decreasing treatment temperature, but all the nitrided samples showed better wear resistance than the untreated material, particularly after high temperature plasma nitriding treatments.

4.5.1.2 Post wear test SEM observation

Figure 4.5.1-3 shows the SEM observation and the EDX results of the untreated LDX 2101 sample, tested under 70 N. The width of the wear track on this sample was approximately 1700 μm, and substantial wear tracks or grooves can be seen, running parallel to the sliding direction of the tungsten carbide ball, which are signs of abrasive wear. In addition, craters were also observed in the wear track, indicating of adhesive wear. A large amount of wear debris can be seen in Figure 4.5.1-3b, accumulated at both ends of the track. The EDX results showed the typical chemical composition of the untreated material outside the wear track (point A), while the same analysis conducted inside the wear track (point B) revealed a high oxygen content. This implied that oxidation occurred at the high temperature developed by the friction between the tungsten carbide ball and the sample.

The images obtained from the wear tracks of plasma nitrided samples tested at 70 N, are shown in Figure 4.5.1-4. It can be seen that the wear resistance improved with increasing the treatment temperature. In the case of the PN390 sample, the wear track exhibits grooves associated with abrasive wear and a large number of holes which were attributed to adhesive wear mechanisms. In some areas, the original treated surface is still visible, indicating a better wear resistance compared with the untreated material. The PN420 specimen exhibited shallower wear grooves than the PN390, which is a sign of better wear

resistance. For treatment temperatures over 450°C, PN450 and PN480, the samples exhibited high wear resistance and no clear wear tracks were observed on their surfaces.

Figure 4.5.1-5 shows the morphology of the wear track produced on plasma nitrided samples during the wear tests at a low load of 30 N. Compared with the wear tracks formed under 70 N, the wear track formed under 30N on PN390 exhibited shallow and thin wear grooves with some patches of oxide debris (Fig.4.5.1-5a). However, the original grinding marks can still be seen on the both sides of the wear track. For PN420, only scattered fine wear grooves can be found in the middle of the wear track and very few sings of adhesive wear could be identified (Fig.4.5.1-5b). For the PN450 and PN480 specimens, no wear track could be found (Fig.4.5.1-5c & d). Hence, the samples treated at temperatures over 420°C showed good wear resistance.

4.5.2 Corrosion wear of LDX 2101

4.5.2.1 Corrosion wear loss

The results from the corrosion-wear tests are summarised in Figure 4.5.2-1. It is of interest to note that it followed a different trend to the dry wear. The corrosion-wear loss for the untreated specimen was 1.5 x 10^3 μm^2. When treated at or above 420°C, the corrosion-wear loss measured on the plasma treated samples significantly increased with increasing treatment temperature: 2.8 x 10^2 μm^2 for PN390, 2.1 x 10^2 μm^2 for PN420, 1.2 x 10^3 μm^2 for PN450 and 1.3 x 10^4 μm^2 for PN480. However, PN420 showed the lowest corrosion-wear of 2.1 x 10^2 μm^2 compared with untreated material, the PN390 and PN420 samples showed improved corrosion-wear resistance and PN480 exhibited reduced corrosion wear resistance, with almost no change for PN450. This indicates that the high temperature treated samples lost their wear resistance when tested in a corrosive environment mainly due to their reduced corrosion resistance. The 2D profiles of the corrosion-wear tracks are

shown in Figure 4.5.2-2. It can be seen that the corrosion-wear tracks observed on samples PN450 and PN480 were wider and deeper than the untreated sample. However, the PN390 and the PN420 specimens showed shallower and narrower track profiles. Once again, this indicates that the low temperature treated samples exhibit improved corrosion-wear resistance.

4.5.2.2 Post-wear SEM observation

The morphology of the corrosion-wear track produced on the untreated sample under 70 N is shown in Figure 4.5.2-3. Overall, this sample showed a smooth surface with some pits and abrasive wear grooves, which are more clearly shown in the high magnification image in Figure 4.5.2-3b. Samples PN390 and PN420 showed better corrosion-wear resistance than the untreated material. In the case of sample PN390, the surface showed a featureless morphology, with no pits or grooves, and only a few pits can be found on the surface of the PN420 specimen (Figure 4.5.2-4a and b).

Figure 4.5.2-5 shows the SEM images of the corrosion-wear track of samples treated at high temperature. The PN450 sample exhibits large pits and corrosion products on the surface. The high magnification image in Figure 4.5.2-5b shows deep pits and corrosion products adhered around them. The EDX results revealed a high content of oxygen in point A, together with chlorine and a much lower content of Cr, indicating that the material had been corroded by the NaCl solution. The surface of the PN480 specimen was seriously corroded and showed large pits and a large amount of corrosion products on the surface (Figure 4.5.2-6b). In summary, the plasma nitrided samples showed better corrosion-wear resistance when the treatment temperature was below 420°C but reduced corrosion-wear resistance was found for 480°C treated sample.

In conclusion, compared with the untreated LDX 2101 sample, all plasma nitrided

specimens showed better wear resistance under dry wear conditions, and the low temperature treated samples produced better results in the corrosion-wear tests.

4.5.3 Dry Wear of LDX 2404

4.5.3.1 Dry wear loss

Figure 4.5.3-1 shows the results of dry wear tests conducted on LDX 2404 specimens under 30 N and 70 N. The wear loss measured on the untreated samples under 30 N load was 7.8 x 10^3 μm^2, compared with 1.3 x 10^2 μm^2 for PN390 and 71μm^2 for the PN420 samples. The wear loss of the PN450 and PN480 samples was below the detection limits. The 2D profiles of the wear tracks produced on the untreated and plasma nitrided samples tested under 30 N are shown in Figure 4.5.3-2a. A wide and deep wear track can be seen for the untreated material, while the PN390 sample showed a small wear track and all other plasma nitride samples showed no measurable wear.

The wear loss increased when the testing load increased to 70 N. The wear loss measured on the untreated material was 1.9 x 10^4 μm^2. In the case of the plasma nitrided samples, the wear loss of PN390 sample was 2.1 x 10^4 μm^2, which is even larger than the untreated sample. This is mainly because the thin hardened case collapsed under high load of 70N and the debris from the damaged hardened surface acted as an abrasive third body, thus increasing the wear rate. The wear area losses of PN420, PN450 and PN480 was 1.4 x 10^2 μm^2, 51 μm^2 and 69 μm^2 respectively, which is much lower than that of the untreated material. From Figure 4.5.3-2b, it can be clearly seen that the untreated and the PN390 samples showed similar wear track profiles, while the PN420, PN450 and PN480 specimens showed much shallower and narrower wear tracks.

4.5.3.2 Post-wear SEM observation

The morphology of the wear track produced on the untreated sample was studied by SEM

(Figure 4.5.3-3). It can be seen that the wear track was approximately 1200 μm wide, with many wear grooves running parallel to the sliding direction. The image in Figure 4.5.3-3b also reveals a large amount of wear debris, which was produced by abrasive wear. The EDX results presented in Figure 4.5.3-3c, show that the debris accumulated on the sides of the wear track contained oxygen (point A) because of the high temperature developed upon the sliding between the tungsten carbide ball and sample.

Figure 4.5.3-4 shows the wear track on plasma nitrided samples tested at 70 N. For the PN390 sample, the wear grooves were typically deep and large, which is in agreement with the high wear loss presented in Figure 4.5.3-1. The wear surfaces of the PN420, PN450 and PN480 samples showed signs of mild wear, with only a few fine wear grooves visible over the original grinding marks, illustrating the good wear resistance of these samples.

Figure 4.5.3-5 shows the SEM observations of the wear track on plasma nitrided samples tested under 30 N. The PN390 sample exhibited wear pits in the middle of the track and wear grooves on the sides. For the PN420, the number of wear pits decreased and only fine wear grooves can be found, indicating a mild wear regime. When treated over 450°C, the samples showed excellent wear resistance with very few signs of wear. Therefore, when tested under a load of 30 N, most of the treated samples showed good wear resistance, in particular those samples treated at high temperature; when tested at a load of 70 N, only the samples treated at high temperature, i.e. PN450 and PN480, showed good results.

4.5.4 Corrosion Wear of LDX2404

4.5.4.1 Wear area Loss

Figure 4.5.4-1 shows the corrosion-wear loss of untreated and plasma nitrided LDX 2404 samples. The corrosion-wear loss of the untreated material is 1.2×10^3 μm^2, and the corrosion wear of the plasma nitrided samples is 4.0×10^2 μm^2 for PN390, 1.5×10^2 μm^2

for PN420, 2.3 x 10^3 μm^2 for PN450 and 1.2 x 10^4 μm^2 for PN480. Similar to LDX 2101 samples,, i.e. the samples treated at high temperature showed poor results, while the PN390 and PN420 specimens, treated at low temperature, showed better corrosion-wear resistance compared with the untreated material. Figure 4.5.4-2 showed the 2D profile of the wear tracks after corrosion-wear for all samples tested under a load of 70 N. It can be seen that both PN450 and PN480 samples showed deep and wide corrosion-wear tracks. On the other hand, the PN390 and PN420 specimens showed shallower and narrower tracks than the untreated sample. Therefore, the samples treated at high temperature are not suitable for corrosion-wear environments. This could attribute to the precipitation of Cr_xN, which increased the hardness at expense of the corrosion resistance of the material.

4.5.4.2 Post-wear SEM observation

The SEM images of the corrosion-wear track of untreated samples are shown in Figure 4.5.4-3. Several wear grooves and some pits can be seen on the wear track of this sample. Observations conducted at a higher magnification revealed that many corrosion products had accumulated at the end of the wear track. Figure 4.5.4-4 shows the corrosion-wear tracks on samples PN390 and PN420 observed by SEM. Compared with untreated sample, both samples showed better corrosion-wear resistance. Few wear grooves were found in the middle of the wear track of PN390, and some pits can be seen in the high magnification image in Figure 4.5.4-4b, near the ends of the track. PN420 showed better corrosion-wear results than PN390, only some wear grooves were observed and the original grinding marks are clearly visible in most of the worn surface.

Figure 4.5.4-5&6 shows the morphology of the corrosion-wear tracks formed on the samples treated at high temperatures, PN450 and PN480, tested under a load of 70 N. large

pits and corrosion products are visible on the surface of the PN450 sample. The high magnification image in Figure 4.5.4-5b reveals deep pits and corrosion products accumulated on the wear track. The EDX results showed a high content of oxygen in point A, on the wear track, together with chlorine and a much lower content of Cr , similar to the phenomenon observed on sample LDX 2101 PN450. This means that the precipitation CrN produced during the high temperature treatments reduced the corrosion resistance and the most of debris was oxide. In the case of PN480, the surface was more severely corroded than PN450. The whole wear surface was extensively corroded and the corrosion products had accumulated on the surface of the wear track (Figure 4.5.4-6a). Furthermore, Figure 4.5.4-6b shows many cracks on the nitrided layer, indicating the modified layer lost the protective function, exposing the substrate to the corrosive solution.

In summary, plasma nitrided samples showed better corrosion-wear resistance only when treated at temperatures below 420°C.

CHAPTER 5 DISCUSSION

5.1 The Response of Duplex Stainless Steels to Plasma Nitriding

It is widely reported that low temperature plasma (or gas) nitriding/carburising of austenitic stainless steels will produce a so-called S-phase layer on the surface [HD Review]. This S-phase is a nitrogen/carbon supersaturated, FCC structured solid solution, which not only increases the hardness and wear properties but also maintains a good corrosion resistance of austenitic stainless steels.

Relatively, much less research has been directed to the low temperature nitriding and carburising of duplex stainless steels. Some researchers [56, 57] claimed based on XRD pattern analysis that similar to austenitic stainless steels, single S-phase layer can be formed on the duplex stainless steels by low temperature plasma/gas nitriding/carburising. They proposed that as nitrogen is an austenite former the ferrite in the original microstructure will first be converted to austenite and then form S-phase. This assumption implies that not only the fcc structured austenite grains became S-phase, but also the bcc structured ferrite grains transformed to austenite fcc structure with supersaturated nitrogen/carbon during low-temperature nitriding and/or carburising.

However, the XRD patterns obtained from this research as shown in Figures 4.2.4-1 and 2 differ greatly from the typical XRD pattern reported by many researchers for S-phase. Indeed, strong peaks of nitrogen saturated bcc α-Fe (indexed as α_N) can be observed for most of the samples nitrided below 480°C.

The potential causes for the despondencies observed between this and other work could be

twofold. Firstly, as shown in Figures 4.2.4-1 and 2 the main peaks from the expanded austenite (i.e. S-phase) and expanded ferrite (α_N) are broadened shifted and highly overlapped, which makes it difficult, if not impossible to conclusively identify the phases in the treated surface layers. Secondly, it has been found for the first time that the XRD patterns obtained from the same nitrided material but different surfaces are different, probably due to the highly preferred orientation of the austenite and ferrite grains. Figure 5.1 superimposed two sets of XRD patterns taken from the nitrided longitudinal and transvers sections and it can be seen that the XRD pattern from the nitrided transverse section showed strong S-phase peaks of (111) and (200) and a weak peak of (110)α_N, while the XRD pattern taken from the nitrided longitudinal section revealed a strong (110)α_N, some potential ε-Fe_3N peaks and weak S-phase peaks. Most probably, the XRD patterns obtained by some other researchers are taken from the transverse section with strong S-phase peaks of (111) and (200).

Therefore, the above discussion points to the reasonable assumption that it is difficult, if not impossible for the bcc ferrite in duplex stainless steels to transfer to fcc S-phase during low-temperature plasma nitriding. This is partially supported by the observation that low temperature nitriding/carburising of ferritic stainless steels [56] cannot form S-phase layer on the surface. Instead, nitrides of ε-Fe_3N and γ'-Fe_4N were detected from the surface treated layer.

Detailed TEM characterisation of LDX PN420 sample has further clarified the response of original austenite and ferrite in the DDSs to low temperature plasma nitriding. As shown in Figure 4.2.5, the original austenite phase has transferred into S-phase, while the original ferrite phase was supersaturated with nitrogen and needle-like nitride of ε-Fe_3N was precipitated from it. This TEM observation has proved that that a single S-phase layer

cannot be formed on duplex stainless steels by low temperature plasma nitriding.

5.2 Comparison between LDX2101 and LDX2404

5.2.1 Surface hardness and thickness

The repose of two lean duplex stainless steels, LDX2101 and LDX2404 to plasma nitriding in terms of the hardness and thickness of plasma nitride case as a function of treatment temperature ranging from 390 to 480°C was systematically studied in this research and the results have been reported in the preceding chapter.

In general, both materials showed similar temperature effect on the thickness and hardness of the nitride cases formed during plasma nitriding. As shown Figure 4.3.1-1, the surface hardness of these two lean duplex stainless steels increased with increasing the treatment temperature from 390 to 480°C. Similarly, the thickness of the surface engineered layers formed during the plasma nitriding on the both longitudinal (Fig. 4.3.1-2a) and transverse (Fig. 4.3.1-2b) sections of these two lean duplex stainless steels followed the same trend: the thickness of the surface layer increased with the increase of the treatment temperature when treated for the same time. This seems understandable as both materials are lean duplex stainless steels.

However, some differences have been also noted for these lean duplex stainless steels. As depicted in Figure 4.3-1-1, although the difference in the surface hardness of low-temperature (PN390 and PN420) plasma nitrided LDX2101 and LDX2404 sample is within the experimental errors, the relatively high-temperature （PN450 and PN480） treated LDX2404 is harder than LDX2101.

More significant effect of treatment temperature has been found on the thickness of the surface treated cases form on these two materials when treated for 10 hours at temperatures

above 420°C. It can be clearly seen from Figures 4.3.1-2a & 2b that the surface case on both the longitudinal and transverse sections is thinner when formed on LDX2404 than on LDX2101.

By way of example, Figure 4.3.3-1 shows the hardness depth profiles across the cross sections of PN480 treated LDX 2101 and 2404. It can be seen that within the first 28 μm the PN480 treated LDX 2404 possesses a higher hardness than the PN480 treated LDX 2101; however, the order is reversed within the depth of 29-42 μm. This is in line with the discussion on the results shown in Figures 4.3.1-1 to 4.3.1-3 i.e. The surface and near surface of the plasma nitrided LDX 2404 is harder than that of LDX 2101 but the total layer thickness is thicker when formed on the latter than on the former.

The mechanism involved could be explained by the trapping of nitrogen atoms by the strong nitride forming elements in these duplex stainless steels. As reviewed by Dong, there is a strong affinity between N and strong nitride forming elements such as Cr and Mo. Therefore, such strong nitride forming elements can on the one hand attract N to form a high nitrogen content in surface but on the other hand they would become traps to retard or stop further inward diffusion of nitrogen atoms.

As has shown in Table 3.1.2, although both LDX2101 and LDX2404 are lean duplex stainless steels, the former contained more nitride formers (16.442 wt% Cr and 0.248 wt% Mo) than the latter (18.072 wt% Cr and 1.621 wt% Mo). Therefore, when nitrogen diffused into the surface of these steels during plasma nitriding, some nitrogen atoms are fired stopped or trapped by the strong nitride formers of Cr and Mo and the rest diffuse further into the subsurface. Therefore, the trapping effect of the strong nitride formers of Cr and Mo mainly depends on the amount of Cr and Mo in these materials. As LDX2404 contains more Cr and Mo than LDX 2101, it is expected that during plasma nitriding more nitrogen

was trapped in the near surface areas of LDX2404 than in LDX2101. Consequently, the hardness of the surface and near surface is higher in LDX2404 than in LDX2101 due to the well-known solid solution hardening of the interstitial alloying element of nitrogen.

According to the trapping effect, the more the strong nitride formers in the steel, the stronger the solid solution hardening in the surface and near surface but the less the nitrogen can diffuse into the subsurface within the same treatment period. Therefore, the trapping effect is stronger in LDX2404 than in LDX2101 as the former contains more Cr and Mo than the latter. As a result, nitrogen can diffuse deeper in LDX2101 than in LDX2404 and hence the hardened case is thicker when formed on LDX2101 than on LDX2404 as is evidenced in Figures 4.3.1-1 and Figures 4.3.1-2a,b.

5.2.2 Dry wear resistance

Some common observations could be made for the wear of plasma nitrided LDX2404 and LDX2101: (1) when tested under 30N, the wear of the plasma nitrided LDX2404 and LDX2101 reduced when increasing the treatment temperature; (2) when treated under the same conditions, the wear of both plasma nitrided steels increased dramatically when the load increased from 30N to 70N.

The first observation could be explained by the fact that when the treatment temperature increased, both the hardness and the thickness of the plasma nitride layers increased significantly (Figs 4.3.1-1 and 4.3.1-2a, b). The second observation is understandable since the wear of a given material normally increases with an applied load for abrasive wear [58]. In this study, the dry wear of both the plasma nitrided materials against a WC ball is dominated by abrasive wear as evidenced by the parallel wear groves observed (e.g. Figs. 4.5.3-4 &5).

However, some different wear behaviour has also been observed when comparing the wear behaviour of plasma nitrided DX2404 and LDX2101. For example, when tested under a relatively high load of 70N, more wear was observed from PN390 treated LDX2404 than from PN390 treated LDX2101 although they have almost the same surface hardness and layer thickness. Indeed, the wear of PN390 treated DX2404 is even larger than that of the untreated DX2404. This seemingly abnormal wear behaviour of the PN390 treated DX2404 could be investigated by careful examining the wear tracks formed. It can be seen from Figure 4.5.3-2b that the depth of the wear track formed after sliding against a hard WC ball under 70 N is about 70 μm, which is five times that of the hardened case formed on the PN390 treated LDX2404 sample.

Hence, the mechanism for the abnormally large wear of the PN390 treated LDX2404 could be proposed as follows: (i) under a high load of 70N, the Hertz stress field extended beyond the hardened case into the substrate, (ii) plastic deformation occurred in the relatively soft substrate (<400HV0.05), (iii) without mechanical support, the hard nitride case collapsed and (iv) the hard debris thus formed served as abrasives and produced very severe abrasive wear. This is evidenced by the typical abrasive wear grooves formed in the deep wear tracks (Fig. 4.5.3-4a) and by the fact that without hard debris the wear of the untreated LDX2404 is even lower than the PN390 treated material.

As can be seen from Fig. 4.5.1-2b, the maximum depth of the wear track formed after the same wear test on the PN390 treated LDX2101 is about 10 μm. Although the maximum wear depth in the middle of the wear track also exceeded the thickness of the plasma nitride case (~ 5 μm) formed on PN390 treated LDX2101, both side areas of the wear track are still within the hardened case. This is evidenced by some retained hardened surface areas as shown in Figure 4.5.1-4. Damages of the hardened case have also occurred at some areas of the wear track and the debris thus formed should have caused further

abrasive wear. However, as reported in Section 4.3.3, the PN390 treated LDX2101 surface layer had a high nano-hardness than the PN390 treated LDX2404 surface. According to the abrasive wear theory, the relatively soft wear debris should cause mild abrasive wear and hence the wear of the PN390 treated LDX2101 is much lower than the PN390 treated LDX2404.

5.2.3 Corrosion Behaviour

The corrosion behaviour of plasma nitride LDX 2101 and LDX2404 was assessed using electrochemical tests and the results have been reported in Section 4.4. To compare the electrochemical corrosion behaviour of these two plasma nitrided materials, corrosion potential Ecorr and corrosion current density Icorr have been calculated from the anodic polarisation curves shown in Figures 4.4.1-1 and 4.4.2-1 and the quantitative results are compared in Table 5.1.

It can be seen from Figure 4.4.1-1, Figure 4.4.2-1 and Table 5.1 that the corrosion properties of untreated LDX2404 is better than LDX2101 in terms of the higher corrosion potential and a much higher pitting potential of the former than the latter although the corrosion current density followed opposite trend. This could be attributed the larger amount of alloying elements of Cr, Ni and Mo in LDX2404 than in LDX2101.

For the plasma nitride materials, when plasma nitrided under the same conditions, the plasma nitrided LDX2404 possesses better corrosion properties than plasma nitrided LDX2401 as evidenced by the increased corrosion potential and reduced corrosion current density. This is could be mainly attributed to the different amounts of alloying elements of Cr, Ni

Table 5.1 Results of corrosion tests for LDX 2101 and LDX 2404

	LDX 2101		LDX 2404	
Sample code	I_{corr}(mA/cm^2)	E_{corr}(mV)	I_{corr}(mA/cm^2)	E_{corr}(mV)
Unt.	1.69E-04	-240	1.03E-03	-181.41
PN390	1.72E-03	-230	3.22E-04	-169.65
PN420	4.50E-04	-252.75	2.62E-04	-233.93
PN450	1.26E-03	-324.4	4.48E-04	-267.9
PN480	1.37E-03	-369.49	6.13E-04	-304.14

and Mo in these two materials. As shown in Tables 3.1 and 2, compared with LDX2101, LDX2404 contains a higher amount of strong nitride formers of Cr and Mo. According to the trapping theory, after plasma nitriding more nitrogen will be in the nitrided surface formed on LDX2404 than on LDX2101, which is proved in Figure 4.2.3. It is well-know that nitrogen in solid solution can effectively enhance the corrosion properties of stainless steel and hence better corrosion resistance is expected for nitrided LDX2404 than for LDX2101 when treated at the same temperature. Furthermore, the higher level of Ni in LDX2404 than in LDX2101 should have also contributed the better corrosion properties of the former than the latter.

5.3 Corrosion-Wear

Corrosion-wear is one of the most important properties required for some important applications and in this study the corrosion-wear behaviour of two plasma nitrided lean duplex stainless steels, LDX2101 and LDX2404 has been evaluated by conducting sliding reciprocating wear in 3.5% NaCl solution.

It can be seen from Figures 4.5.2-1 and 4.5.4-1 that the corrosion-wear for both plasma nitrided materials decreased first and then increased with the plasma nitriding temperature

with the minimum corrosion-wear being observed for PN420 treated samples. Clearly, this differs from the temperature dependence of dry wear of the plasma nitride materials. In general, the dry wear of the plasma nitride LDX2101 and LDX2404 is reduced by increasing the treatment temperature (Figures 4.5.1-1 and 4.5.3-1).

The difference in the treatment temperature dependence of dry wear and corrosion-wear could be attributed to the difference in their damage mechanisms. As discussed earlier, the material loss of the plasma nitride materials during dry wear is mainly via abrasive and adhesive wear. It is known that abrasive wear of a surface is inversely proportional to its hardness and that adhesive wear of a surface is also affected by the plastic deformation and ductility of the surface. After plasma nitriding, the surface hardness has been effectively increased and the ductility and hence plastic deformation tendency could be reduced, which contributed to reduced abrasive and adhesive wear during dry reciprocating wear.

However, according to corrosion-wear theory [59, 60], not only the corrosion-wear of a surface depends on its hardness and hence wear resistance but also its corrosion resistance i.e. depending on the synergy of wear and corrosion. The dry wear of low-temperature treated PN390 and PN420 samples is larger than the relatively high-temperature treated PN450 and PN480 samples (Fig. 4.5.1-1); however, the corrosion resistance of the low-temperature treated PN390 and PN420 samples is much better than the relatively high-temperature treated PN450 and PN480 samples (Fig 4.4.1-1 & 4.4.2-1 and Table 5.1). Therefore, it is the synergy of relatively good wear resistance and corrosion resistance that makes the best corrosion-wear behaviour of the PN420 treated samples.

Clearly, the optimum plasma treatment conditions depend on the application conditions and hence the property requirement. For dry wear, PN450 is the best treatments for both materials whilst for corrosion-wear in simulated sea water, PN420 is the optimal treatment.

CHAPTER 6 CONCLUSIONS AND FURTHER WORK

6.1 Summary and Conclusions

Plasma nitriding of lean duplex stainless steels LDX 2101 and LDX 2404 with nitrogen has been conducted at temperatures ranging from 390 to 450℃ for 10 hours in a gas mixture of 25%N_2 and 75%H_2. Based on the experimental results obtained from this MRes research, the following conclusions can be drawn:

1) Nitrogen can diffuse into LDX 2101 and LDX 2404 lean duplex stainless steels to form a hardened surface case during plasma nitriding. The thickness of the surface nitrided case formed on the LDX 2101 and LDX 2404 lean duplex stainless steels ranges from 5 to 28 μm, which increased with the treatment temperature. The plasma nitride case is thicker when formed on LDX 2101 than on LDX 2404 especially when treated at 420, 450 and 480°C.

2) The response to plasma nitriding of the original ferrite and austenite phases in the LDX 2101 and LDX 2404 lean duplex stainless steels differs greatly mainly due to their different structures and compositions. The original austenite grains in the surface of the LDX 2101 and LDX 2404 lean duplex stainless steels transferred into S-phase (i.e. nitrogen supersaturated expanded austenite) whilst ε-Fe_3N needles were embed in nitrogen saturated ferrite grains (α_N).

3) Plasma nitriding method can effectively improve the surface hardness of all plasma nitride samples, which are increased with increasing the plasma nitriding temperature when treated for a fixed time of 10 hours. The 480°C treated PN480

samples showed an improvement of surface hardness of 6 times compared with untreated materials. The load bearing capacity can also been significantly enhanced by plasma nitriding, which shows the same temperature dependence as for the surface hardness.

4) When treated at 450 and 480°C for 10 hours, the plasma nitrided LDX2404 possessed a higher surface hardness than plasma nitrided LDX2101. Comparison of the hardness depth distribution across the 480°C/10h treated two lean duplex stainless steels revealed that although the PN480 plasma nitrided LDX2404 showed a higher hardness than LDX2404 in the first 28 μm, the total hardened case formed on the PN480 treated LDX2101 is thicker than formed on PN480 treated LDX2404.

5) The effect of plasma nitriding on the corrosion behavior of LDX 2101 and LDX 2404 lean duplex stainless steels is closely related to the treatment temperature. The low-temperature PN390 and PN420 treatments can increase the potting potential of LDX 2101 and LDX 2404 materials. For both LDX 2101 and LDX 2404 materials, the corrosion properties of the low-temperature treated PN390 and PN420 samples outperformed the relatively high-temperature treated PN450 and PN480 samples.

6) The effect of plasma nitriding on the corrosion behavior of the LDX 2101 and LDX 2404 lean duplex stainless steels is also related to their chemical compositions. When treated under the same conditions, the plasma nitrided LDX 2404 outperformed LDX2101 in terms of higher corrosion potential and lower corrosion current density.

7) When tested under 30N, the dry wear resistance of both LDX 2404 and LDX2101steels can be drastically improved by all the plasma nitriding treatments developed from the research project. In general, the higher the plasma nitriding temperature, the better the dry wear resistant of the treated both materials mainly because of the effectively enhanced hardness and load bearing capacity.

8) When tested under 70N, the dry wear of all the plasma nitrided as well as the untreated samples increased. The best PN450 treatment can increase the dry wear resistance by 8.1 x 10^3 and 3.7 x 10^2 times for LDX 2101 and LDX2404 respectively. However, the wear of PN390 treated LDX2404 sample is even larger than that of the untreated materials. This observed seemingly abnormal wear could be attributed to the low load bearing capacity of the PN390 treated LDX2404 sample and the severe abrasive action of the hard debris when the hardened surface layer collapsed under the high load.

9) Unlike dry wear, the corrosion-wear resistance of both LDX 2101 and LDX2404 materials can be effectively improved only by low temperature PN390 and PN420 treatment since corrosion-wear is the synergy of wear and corrosion. The PN420 treatment showed the best improvement in corrosion-wear resistance by 7.4 and 8.1 times for LDX 2101 and LDX2404 respectively.

10) The optimised plasma nitriding treatment depends on application conditions and requirement. For both LDX 2101 and LDX2404 lean duplex stainless steels, plasma nitriding for 10 hours at 450℃ (i.e. PN450) and at 420℃ (i.e. PN420) have

been identified as the best plasma nitriding treatment respectively for dry wear and corrosion-wear applications.

6.2 Suggested Future Work

As planned, the response of lean duplex stainless steels LDX2101 and LDX2404 to plasma nitriding was investigated and the results have demonstrated that the low-temperature plasma nitriding treatments developed from the present study can effectively increase the hardness, try wear and corrosion-wear properties of these two lean duplex stainless steels. To fully advance scientific understanding, some future work is suggested and outlined below.

1. To conduct detailed TEM analysis of 450 and 480°C plasma nitrided LDX2101 and LDX2404 samples to study the distribution of CrN in PN450 and Fe_4N in PN480 samples.

2. To investigate the mechanism involved in the observed effect of microstructural orientation on plasma nitriding response.

3. To start the repose of lean duplex stainless steels LDX2101 and LDX2404 to plasma alloying with carbon (i.e. carburising) and both C and N (i.e. nitrocarburising).

References

1. Li, W., Zhao Xinwei, Huo Chunyong, Feng yaorong, *The characteristic of 2205 duplex stainless steel and application in natural gas pipeline.* JOURNAL OF GUANGDONG NON- FERROUS METALS, 2005. **15**(2.3): p. 628-632.
2. Fredriksson, W. and K. Edström, *XPS study of duplex stainless steel as a possible current collector in a Li-ion battery.* Electrochimica Acta. **79**: p. 82-94.
3. Dong, H., *S‐phase surface engineering of Fe‐Cr, Co‐Cr and Ni‐Cr alloys* International Materials Reviews, 2010. **55**: p. 65-98.
4. Samuels, L.E., *Steel-makers and knotted string: Harry Brearley: 2nd ed., edited by P. R. Beeley and P. J. Beeley, Institute of Materials, London, 1995, 276 pages, $40.00 (hardcover) (available in the U.S.A. from Ashgate Publishing Co., Brookfield, Vermont).* Materials Characterization, 1996. **36**(1): p. 51-52.
5. Cobb, H.M., *History of Stainless Steel* Vol. 2. 2010, Materials Park, OH, USA ASM International 374.
6. Baddoo, N.R., *Stainless steel in construction: A review of research, applications, challenges and opportunities.* Journal of Constructional Steel Research, 2008. **64**(11): p. 1199-1206.
7. Lo, K.H., C.H. Shek, and J.K.L. Lai, *Recent developments in stainless steels.* Materials Science and Engineering: R: Reports, 2009. **65**(4–6): p. 39-104.
8. Singh, R., *Chapter 8 - Stainless Steels*, in *Applied Welding Engineering*. 2012, Butterworth-Heinemann: Boston. p. 65-73.
9. Cobb, H.M., *History of Stainless Steel*. 2010, Materials Park, OH, USA: A S M International.
10. Cobb, H.M., *The History of Stainless Steel.* ASM International®, 2010: p. 185.
11. Basson, E., *WORLD STEEL IN FIGURES 2012.* 2012.
12. ISSF, *The Stainless Steel Family*. 2012, International Stainless Steel Forum: Belgium. p. 5.
13. Tasker, J., *Austenitic Steels: Non-stainless*, in *Encyclopedia of Materials: Science and Technology (Second Edition)*, K.H.J. Buschow, et al., Editors. 2001, Elsevier: Oxford. p. 411-415.
14. McGuire, M.F., *Austenitic Stainless Steels*, in *Encyclopedia of Materials: Science and*

Technology (Second Edition), K.H.J. Buschow, et al., Editors. 2001, Elsevier: Oxford. p. 406-410.

15. Ma, D.-s., et al., *Microstructure and Mechanical Properties of Martensitic Stainless Steel 6Cr15MoVn.* Journal of Iron and Steel Research, International, 2012. **19**(3): p. 56-61.
16. Garrison Jr, W.M., *Stainless Steels: Martensitic*, in *Encyclopedia of Materials: Science and Technology (Second Edition)*, K.H.J. Buschow, et al., Editors. 2001, Elsevier: Oxford. p. 8804-8810.
17. Shaigan, N., et al., *A review of recent progress in coatings, surface modifications and alloy developments for solid oxide fuel cell ferritic stainless steel interconnects.* Journal of Power Sources, 2010. **195**(6): p. 1529-1542.
18. Cortie, M., *Ferritic Stainless Steels*, in *Encyclopedia of Materials: Science and Technology (Second Edition)*, K.H.J. Buschow, et al., Editors. 2001, Elsevier: Oxford. p. 3037-3039.
19. Xu, W., P.E.J.R.D.d. Castillo, and S.v.d. Zwaag, *A combined optimization of alloy composition and aging temperature in designing new UHS precipitation hardenable stainless steels.* Computational Materials Science, 2009. **45**(2): p. 467-473.
20. Stainless, T., *Practical Guidelines for the Fabrication of Duplex Stainless Steels*, ed. T. Stainless. Vol. 2. 2009, Lodon, UK: The International Molybdenum Association (IMOA).
21. Outokumpu, *Duplex 2507,2205,2304,4501,LDX2101,LDX2404 data sheet*, in *Outokumpu steel*, O. steel, Editor. 2013, Outokumpu steel: Outokumpu steel. p. 1.
22. Sato, Y.S., et al., *Microstructure and mechanical properties of friction stir welded SAF 2507 super duplex stainless steel.* Materials Science and Engineering: A, 2005. **397**(1–2): p. 376-384.
23. Jiang, D.-w., et al., *22Cr High-Mn-N Low-Ni Economical Duplex Stainless Steels.* Journal of Iron and Steel Research, International, 2012. **19**(2): p. 50-56.
24. Wei, Z., et al., *Study of mechanical and corrosion properties of a Fe–21.4Cr–6Mn–1.5Ni–0.24N–0.6Mo duplex stainless steel.* Materials Science and Engineering: A, 2008. **497**(1–2): p. 501-504.
25. Aribo, S., et al., *Erosion–corrosion behaviour of lean duplex stainless steels in 3.5%*

NaCl solution. Wear, 2013. **302**(1–2): p. 1602-1608.

26. Moradi, M., et al., *Effect of marine Pseudoalteromonas sp. on the microstructure and corrosion behaviour of 2205 duplex stainless steel.* Corrosion Science, 2014. **84**(0): p. 103-112.
27. Huang, R., et al., *Surface modification of 2205 duplex stainless steel by low temperature salt bath nitrocarburizing at 430 °C.* Applied Surface Science, 2013. **271**(0): p. 93-97.
28. Hussain, E.A.M. and M.J. Robinson, *Erosion–corrosion of 2205 duplex stainless steel in flowing seawater containing sand particles.* Corrosion Science, 2007. **49**(4): p. 1737-1754.
29. Ashby, M.F. and D.R.H. Jones, *Chapter 28 - Friction and Wear*, in *Engineering Materials 1 (Fourth Edition)*, M.F. Ashby and D.R.H. Jones, Editors. 2012, Butterworth-Heinemann: Boston. p. 417-430.
30. Blickensderfer, R., *Design criteria and correction factors for field wear testing.* Wear, 1988. **122**(2): p. 165-182.
31. R. Blickensderfer, B.W.M., and J.H. Tylczak, *Comparison of Several Types of Abrasive Wear Tests*, in *Proceedings of the International Conference on Wear of Materials*. 1985, American Society of Mechanical Engineers. p. P313.
32. Do Nascimento, A.M., et al., *Wear resistance of WCp/Duplex Stainless Steel metal matrix composite layers prepared by laser melt injection.* Surface and Coatings Technology, 2008. **202**(19): p. 4758-4765.
33. Fargas, G., A. Mestra, and A. Mateo, *Effect of sigma phase on the wear behavior of a super duplex stainless steel.* Wear, 2013. **303**(1–2): p. 584-590.
34. RABINOWICZ, E., *Friction and wear of materials.* ASM Metals Handbook, 1966. **18**.
35. ARCHARD, J.F., *Contact and rubbing of flat surfaces.* 1953.
36. Fuentes, G.G., *Chapter 14 - Surface Engineering and Micro-Manufacturing*, in *Micromanufacturing Engineering and Technology*. 2010, William Andrew Publishing: Boston. p. 221-240.
37. Smallman, R.E. and R.J. BiShop, *Chapter 12 - Corrosion and surface engineering*, in *Modern Physical Metallurgy and Materials Engineering (Sixth edition)*. 1999, Butterworth-Heinemann: Oxford. p. 376-393.
38. Catherine M. Cotell, J.A.S.a.N.R.L., *Surface Engineering*. ASM handbook, ed. J.A.S.

Catherine M. Cotell, and Fred A. Smidt, Jr. Vol. 5. 1994, ASM International: ASM International. 8-9.

39. Wu, W., et al., *Design and characterisation of an advanced duplex system based on carbon S-phase case and GiC coatings for 316LVM austenitic stainless steel.* Surface and Coatings Technology, 2009. **203**(9): p. 1273-1280.

40. Hua, M., et al., *Patterned PVD TiN spot coatings on M2 steel: Tribological behaviors under different sliding speeds.* Wear, 2006. **260**(11–12): p. 1153-1165.

41. Ávila, R.F., et al., *Comparative analysis of wear on PVD TiN and (Ti1−x Alx)N coatings in machining process.* Wear, 2013. **302**(1–2): p. 1192-1200.

42. Al-Bukhaiti, M.A., et al., *Tribological and mechanical properties of Ti/TiAlN/TiAlCN nanoscale multilayer PVD coatings deposited on AISI H11 hot work tool steel.* Applied Surface Science, (0).

43. Liang, W., *Surface modification of AISI 304 austenitic stainless steel by plasma nitriding.* Applied Surface Science, 2003. **211**(1–4): p. 308-314.

44. Kaklamani, G., et al., *Nitrogen plasma surface modification enhances cellular compatibility of aluminosilicate glass.* Materials Letters, 2013. **111**(0): p. 225-229.

45. Kula, P., et al., *"Boost-diffusion" vacuum carburising – Process optimisation.* Vacuum, 2014. **99**(0): p. 175-179.

46. Buhagiar, J., et al., *Augmentation of crevice corrosion resistance of medical grade 316LVM stainless steel by plasma carburising.* Corrosion Science, 2012. **59**(0): p. 169-178.

47. Gregory, J.C., *A salt bath treatment to improve the resistance of ferrous metals to scuffing, wear, fretting and fatigue.* Wear, 1966. **9**(4): p. 249-281.

48. Grün, R. and H.-J. Günther, *Plasma nitriding in industry—problems, new solutions and limits.* Materials Science and Engineering: A, 1991. **140**(0): p. 435-441.

49. Liu, R., et al., *Surface modification of a medical grade Co-Cr-Mo alloy by low temperature plasma surface alloying with nitrogen and carbon.* Surface and Coatings Technology, (0).

50. Paul, S., et al., *Thermally Sprayed Aluminum (TSA) Coatings for Extended Design Life of 22%Cr Duplex Stainless Steel in Marine Environments.* Journal of Thermal Spray Technology, 2013. **22**(2-3): p. 328-336.

51. Chiu, L.H., et al., *Microstructure and Properties of Active Screen Plasma Nitrided*

Duplex Stainless Steel. Materials & Manufacturing Processes, 2010. **25**(5): p. 316-323.

52. Sun, Y. and T. Bell, *Plasma surface engineering of low alloy steel.* Materials Science and Engineering: A, 1991. **140**(0): p. 419-434.
53. Li, X.Y., et al., *Low temperature plasma surface alloying and characterisation of a superduplex stainless steel.* International Heat Treatment and Surface Engineering. **0**(0): p. 1749514813Z.00000000090.
54. Sun, Y.B., T., *Low Temperature Plasma Nitriding Characteristics of Precipitation Hardening Stainless Steel* Surfce Engineering, 2003. **19**: p. 331-336.
55. El-Hossary, F.M., *The influence of surface microcracks and temperature gradients on the rf plasma nitriding rate.* Surface and Coatings Technology, 2002. **150**(2–3): p. 277-281.
56. Larisch, B., U. Brusky, and H.J. Spies, *Plasma nitriding of stainless steels at low temperatures.* Surface and Coatings Technology, 1999. **116–119**(0): p. 205-211.
57. Blawert, C., et al., *Structure and composition of expanded austenite produced by nitrogen plasma immersion ion implantation of stainless steels X6CrNiTi1810 and X2CrNiMoN2253.* Surface and Coatings Technology, 1999. 116–119(0): p. 189-198.
58. Scott, D., Wear / edited by Douglas Scott, ed. H. Herman and D. Scott. 1979, New York (etc.)
59. Bachus, L.C., Angel, 16 - Avoiding wear in centrifugal pumps. 232-237.
60. Marinescu, J.D.R., W. Brian; Dimitrov, Boris; Inasaki, Ichiro, Tribochemistry of Abrasive Machining-15. Elsevier Inc. 587-633.
61. Johnson, K. L, 1985, Contact mechanics, Cambridge University Press.

List of Figures

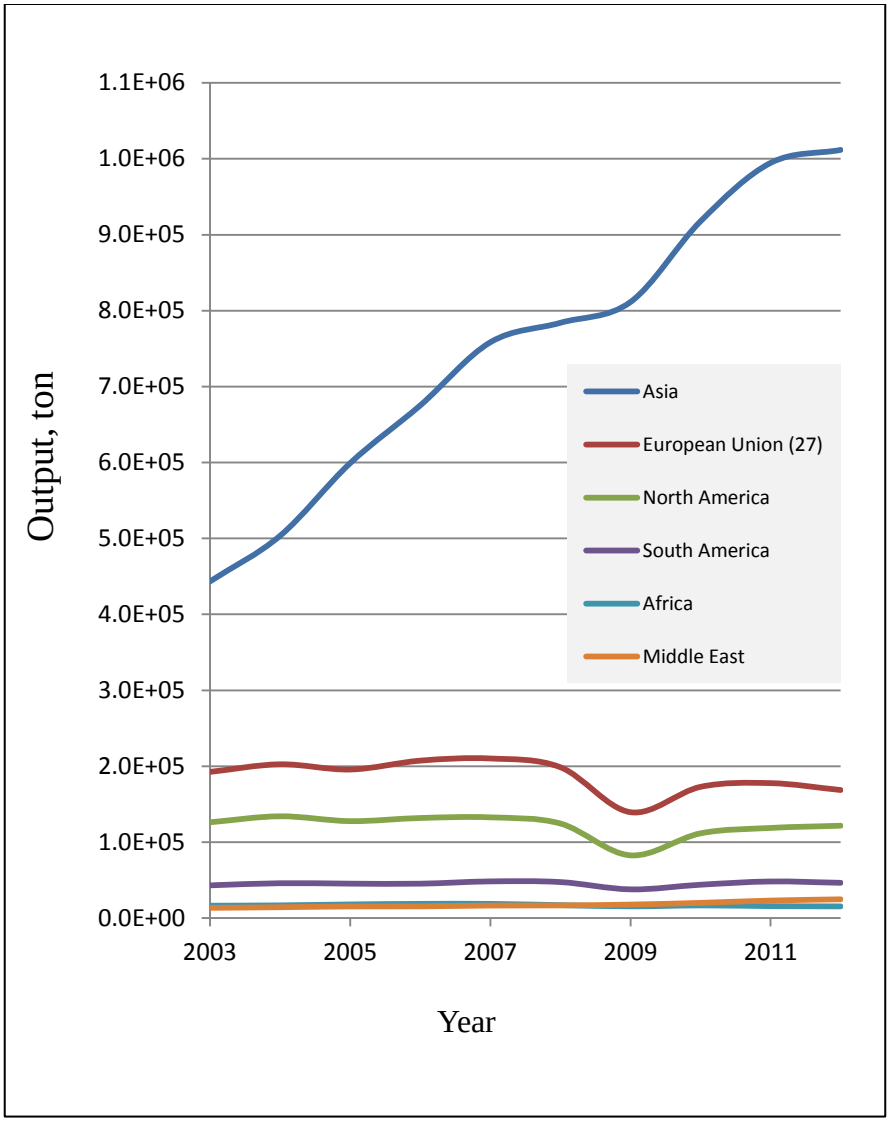

Figure 2.1 Total production of austenite stainless steels in the world
(Source: world steel https://www.worldsteel.org/publications/bookshop.html)

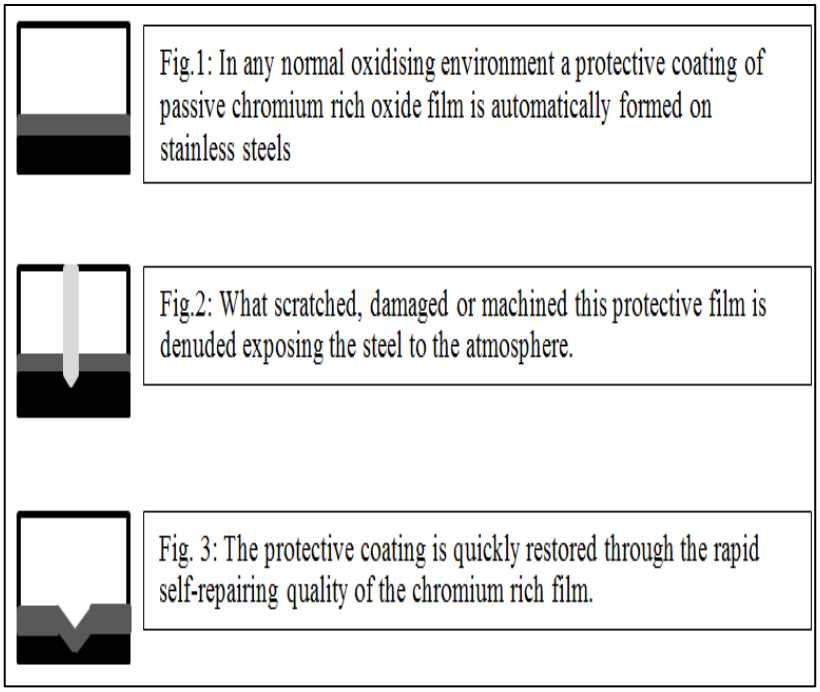

Figure 2.2 The self-repairing principle of stainless steels.

Figure 3.1 The KlÖckner DC plasma unit

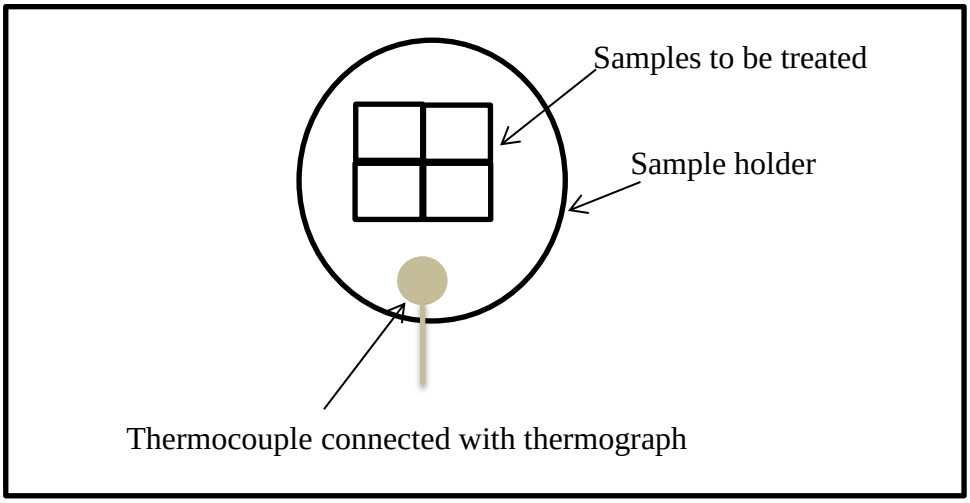

Figure 3.2 The Schematic diagram of plasma nitriding table setup for the treatment of duplex stainless steel samples

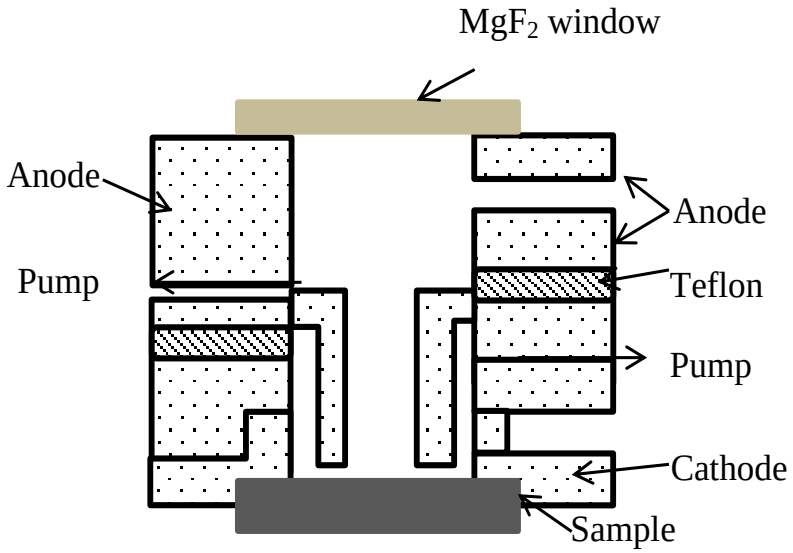

Figure 3.3 The Schematic diagram of the Grimm lamp acted as a source in GDOES analysis

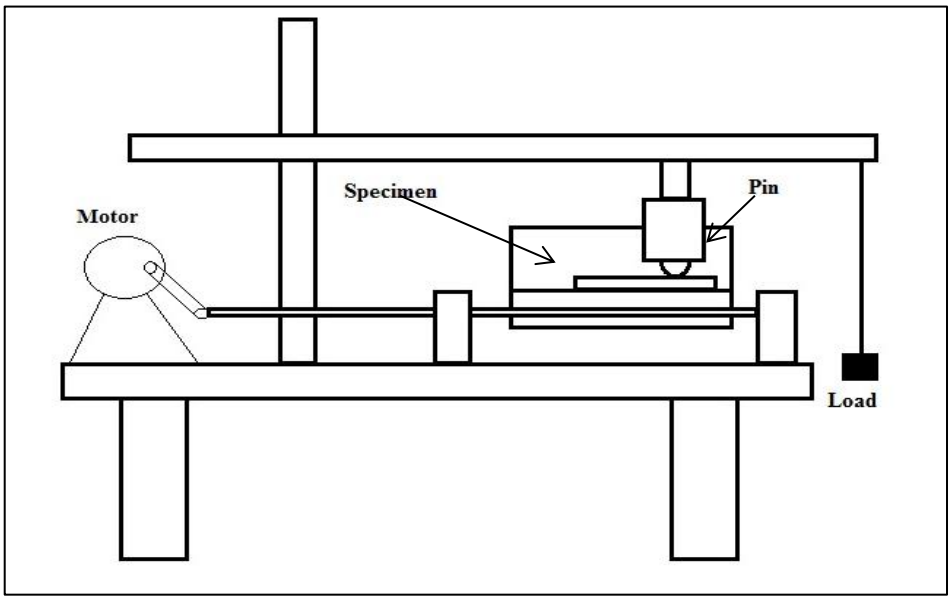

(a)

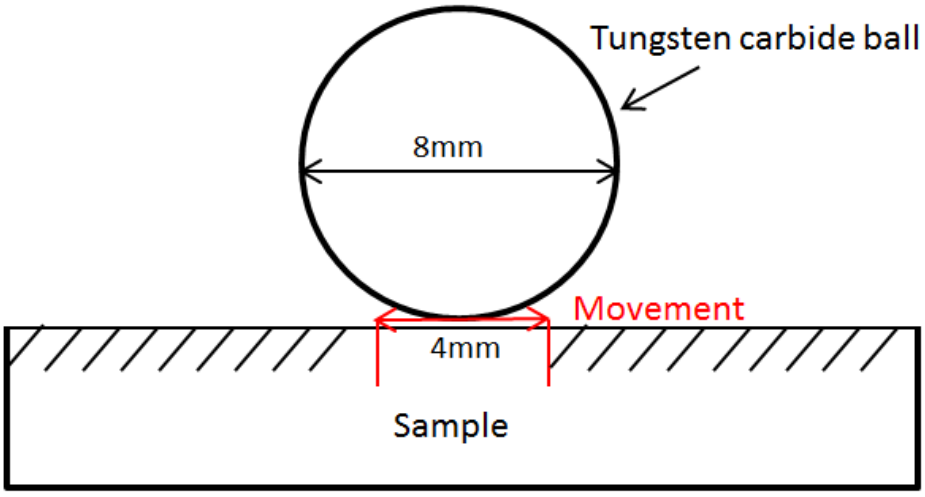

(b)

Figure 3.4 Schematic diagram of the reciprocating wear machine (a) and the geometry of the contact surface in wear tests (b)

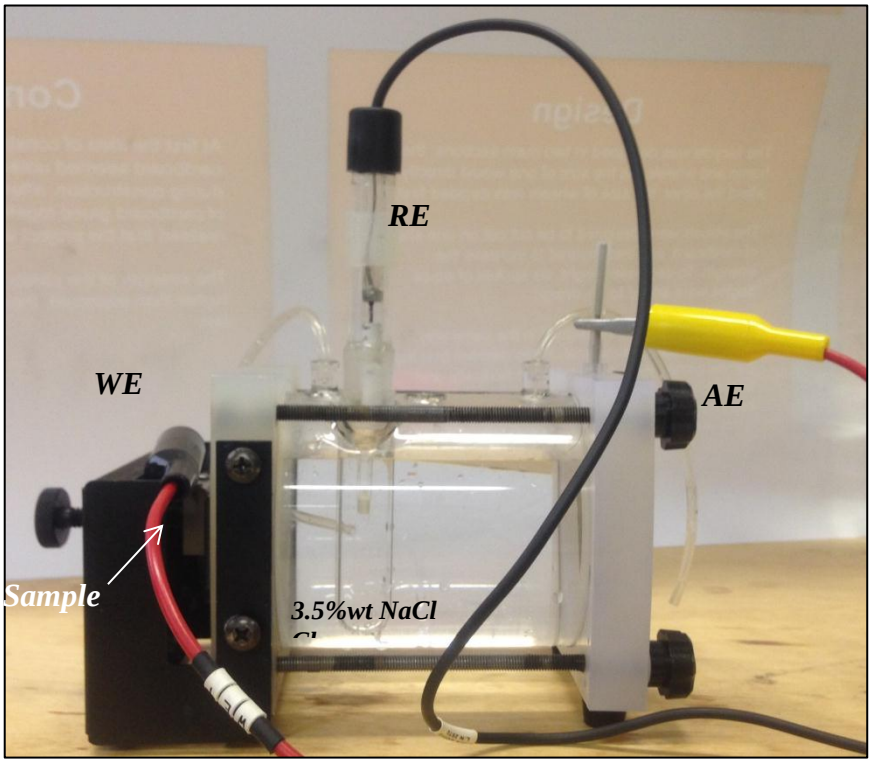

Figure 3.5 The Corrosion test unit

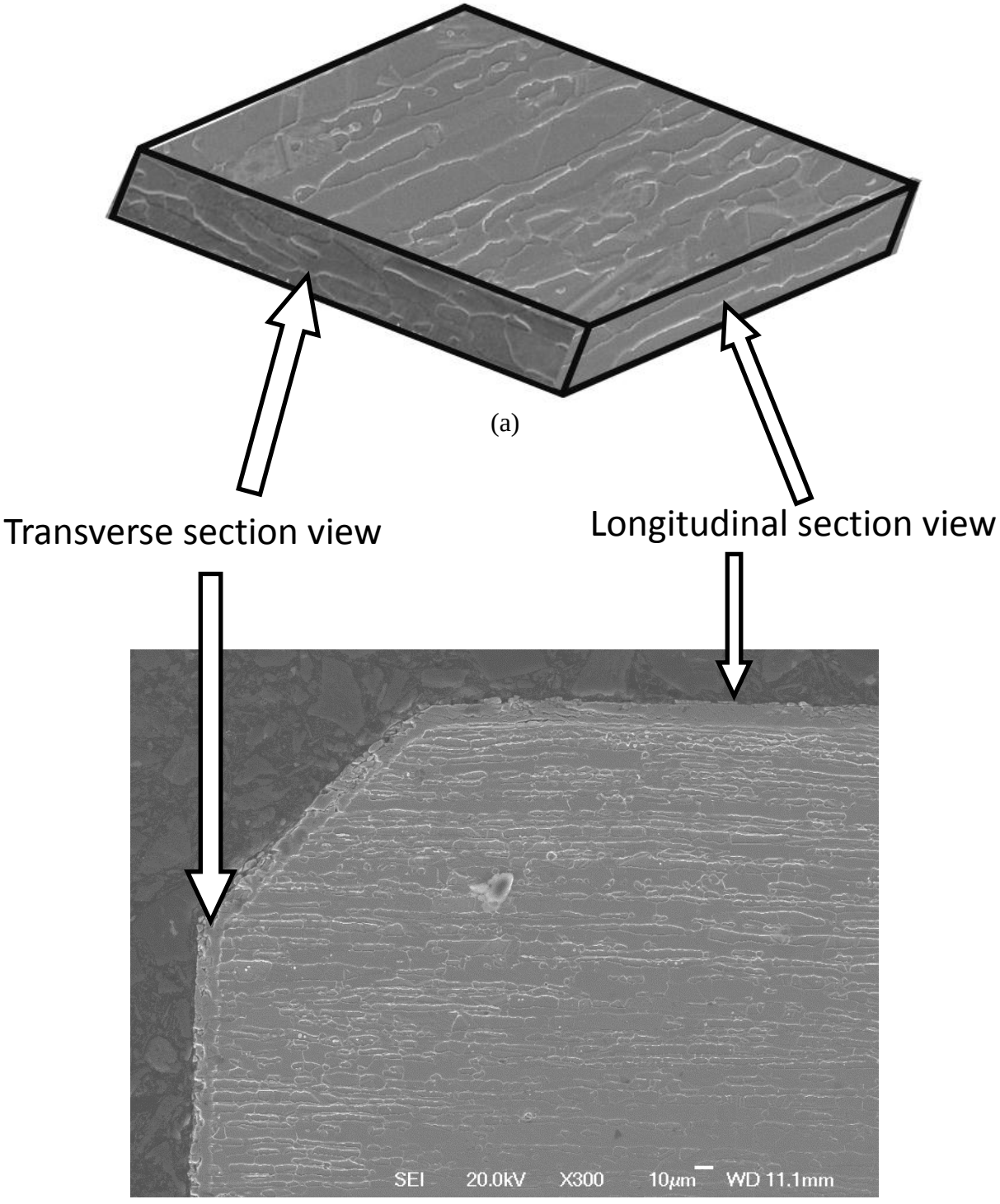

(a)

(b)

Figure 4.1.1-1 (a) As-received rolled type thin 2101 plate and (b) mounted sample for observation

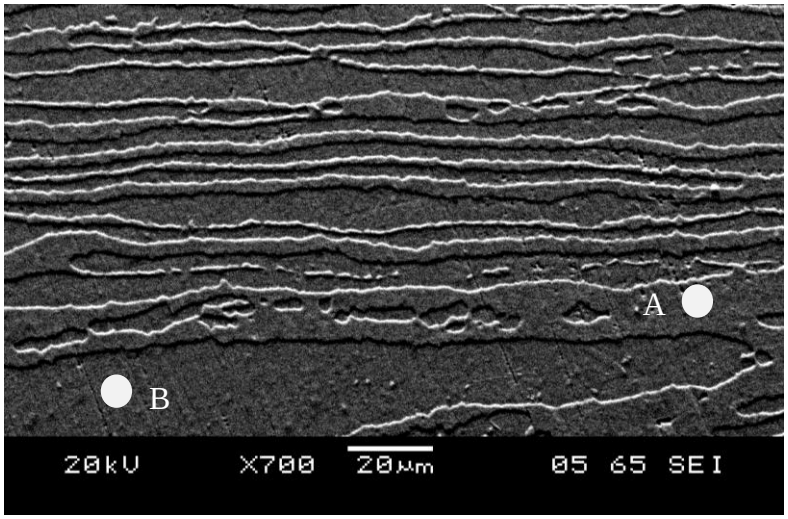

(a)

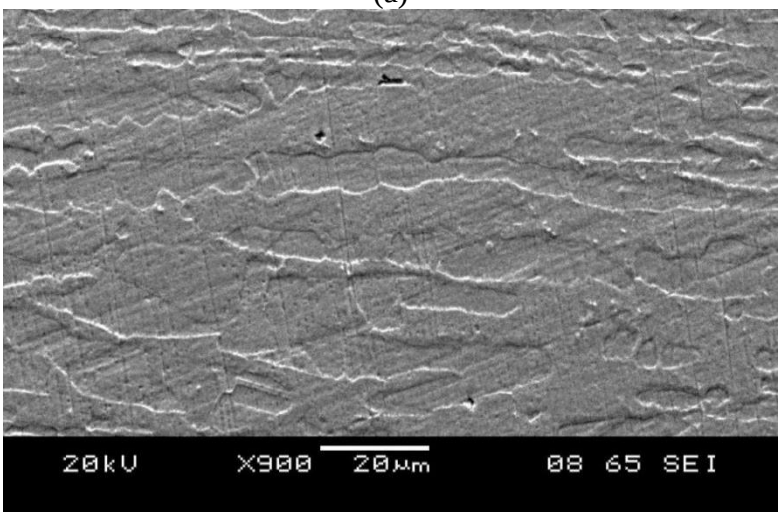

(b)

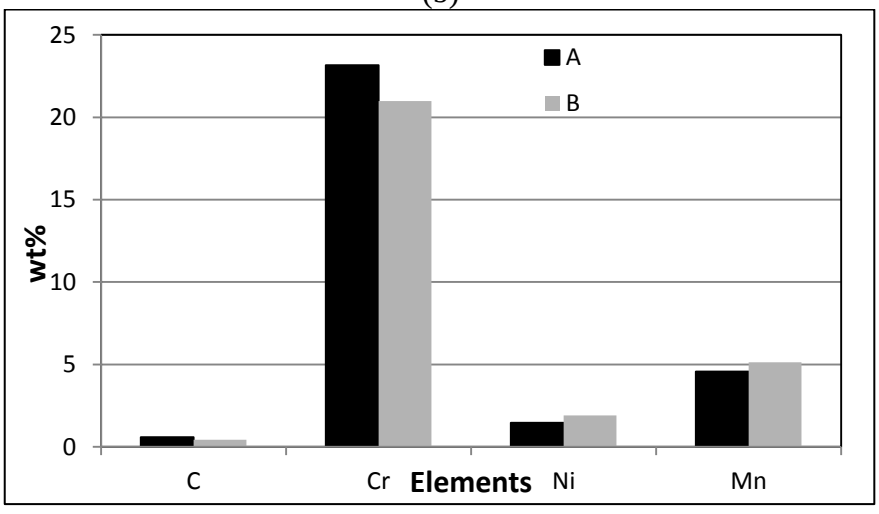

(c)

Figure 4.1.1-2 Longitudinal (a) and transverse (b) view SEM images and EDX analysis at ferrite (A) and austenite (B) grains(c) of as-received LDX 2101 material.

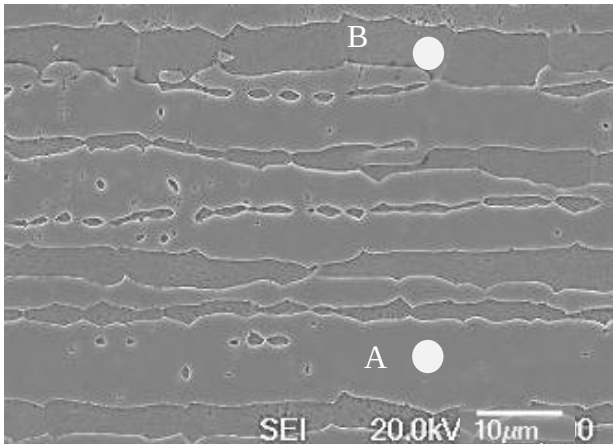

(a)

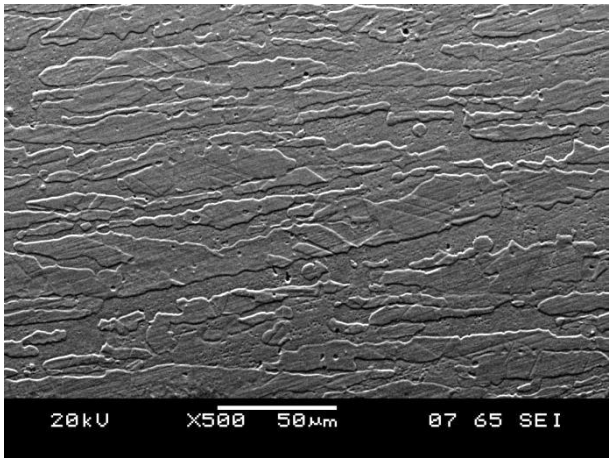

(b)

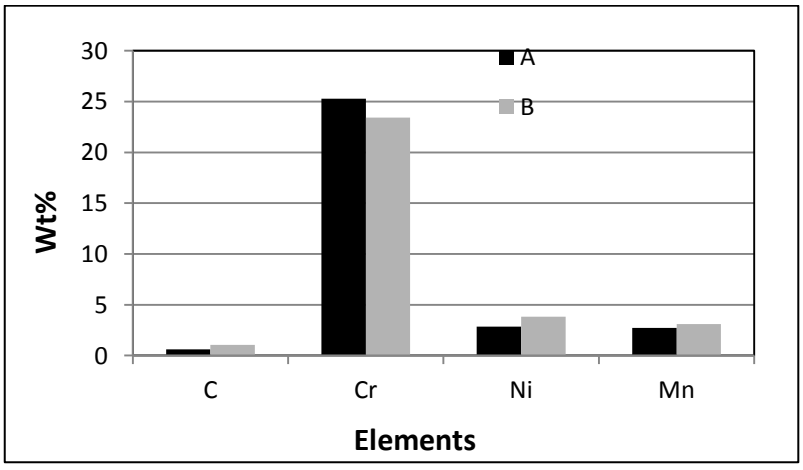

(c)

Figure 4.1.1-3 longitudinal (a) and transverse (b) view SEM images and EDX analysis at ferrite (A) and austenite (B) grains (c) of as-received LDX 2404 plate.

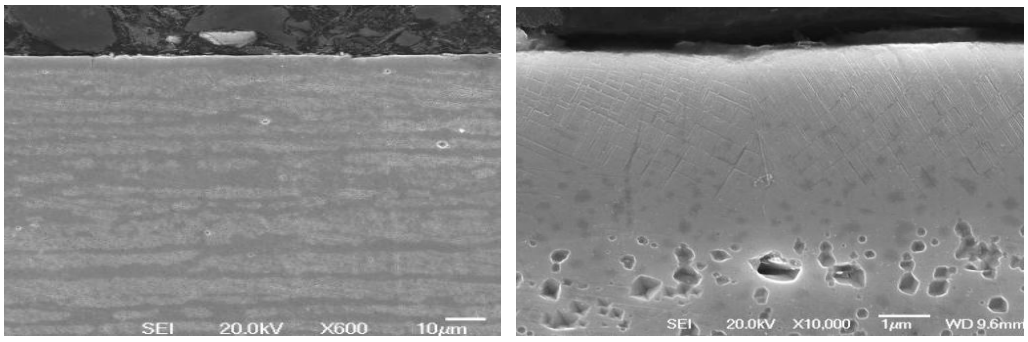

(a)

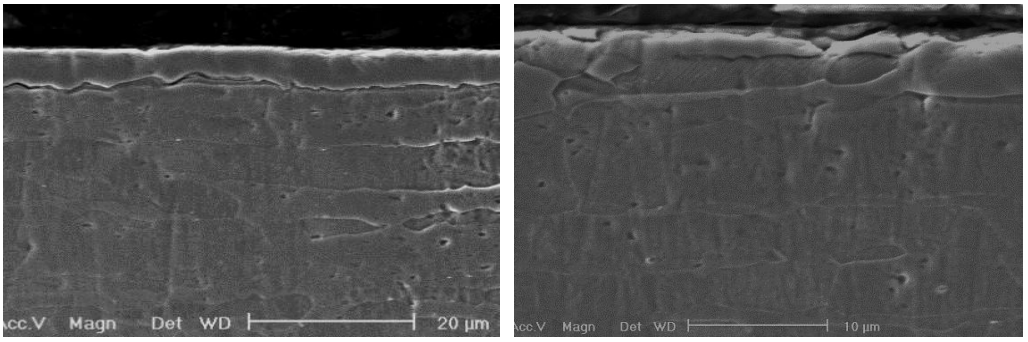

(b)

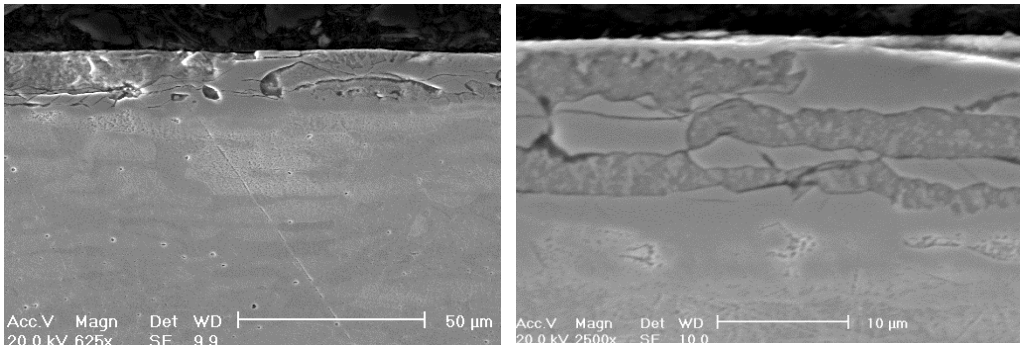

(c)

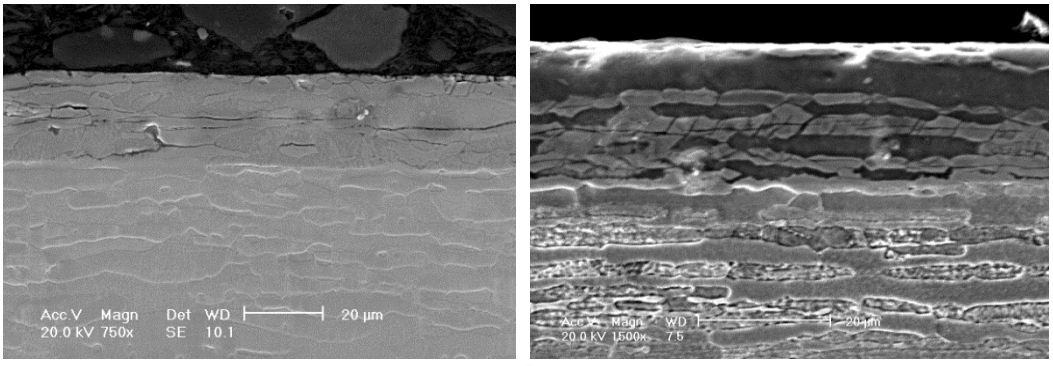

(d)

Figure 4.1.2-1 longitudinal view SEM images of plasma nitrided 2101 samples produced at different temperatures for 10 hours: PN390 (a); PN420 (b); PN450 (c) and PN480 (d).

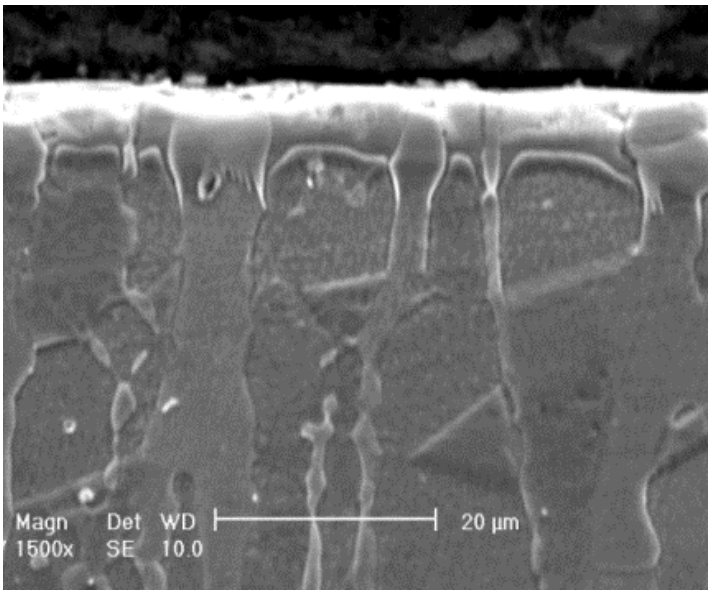

(a)

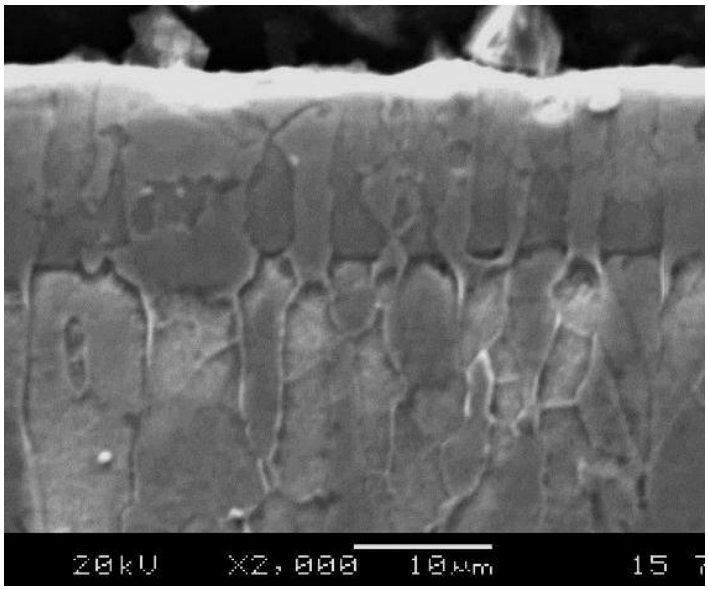

(b)

Figure 4.1.2-2 Transverse section SEM images of plasma nitrided LDX 2101 samples under (a) 420 and (b) 480°C treatment temperatures.

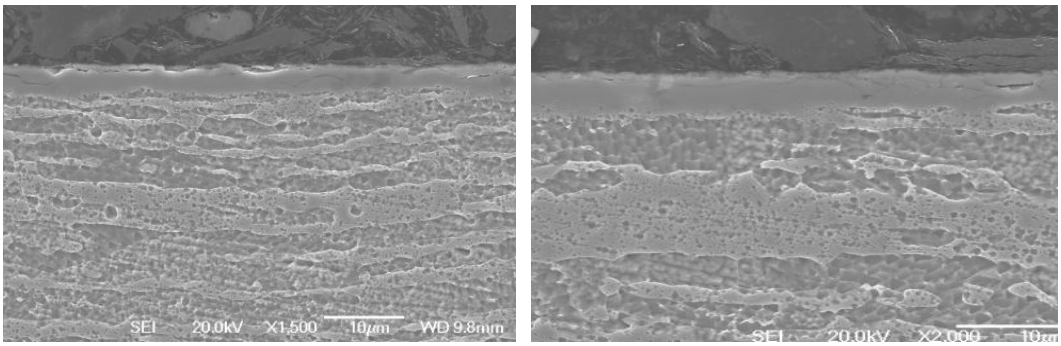

(a)

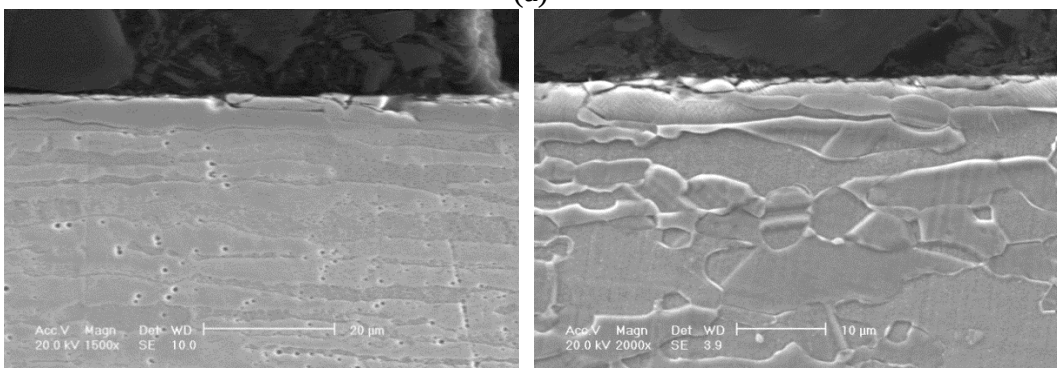

(b)

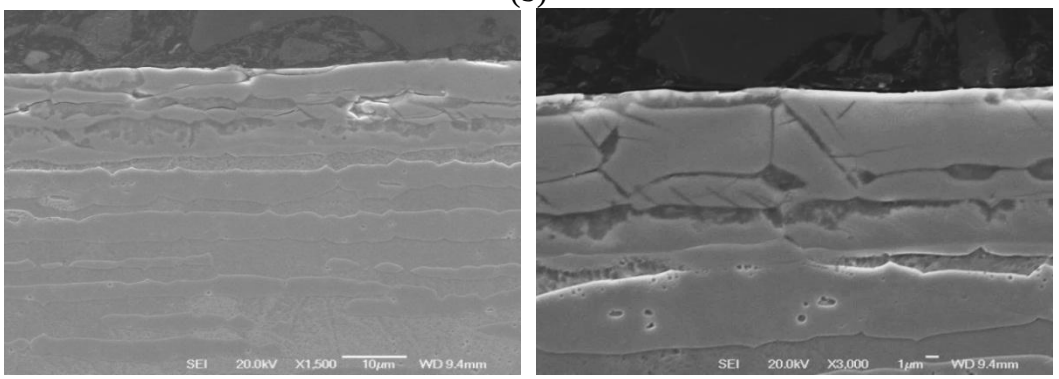

(c)

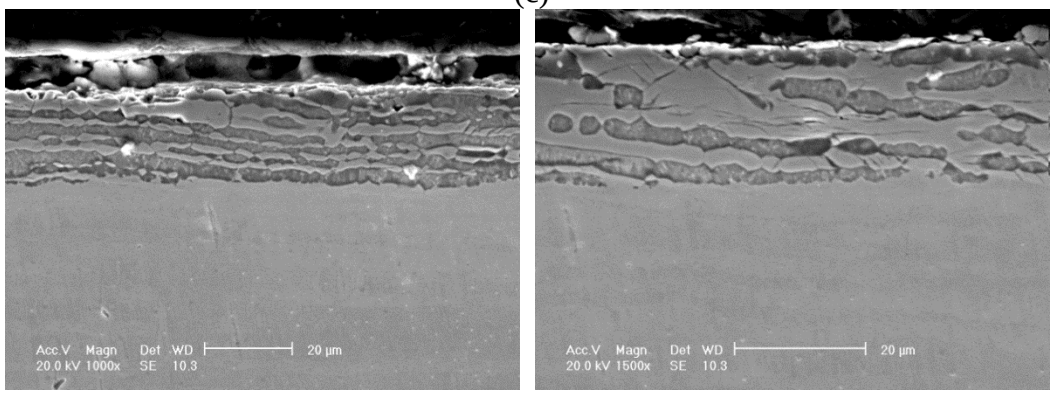

(d)

Figure 4.1.2-3 The longitudinal view SEM images of plasma nitrided 2404 samples u (a) PN390; (b) PN420; (c) PN450 and (d) PN480.

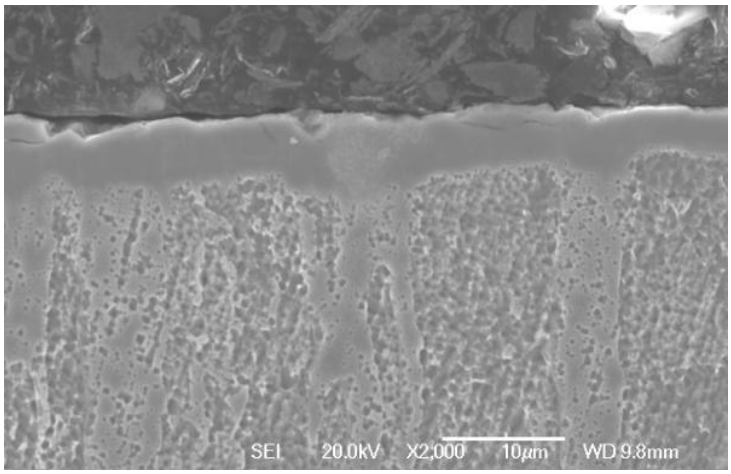

(a)

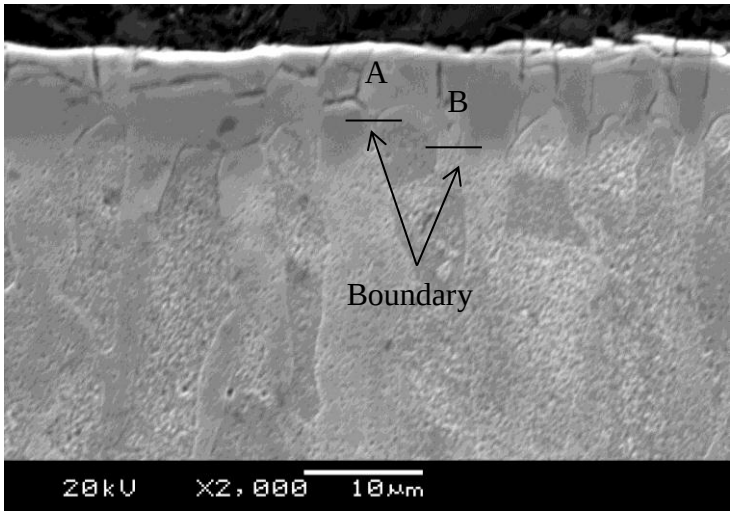

(b)

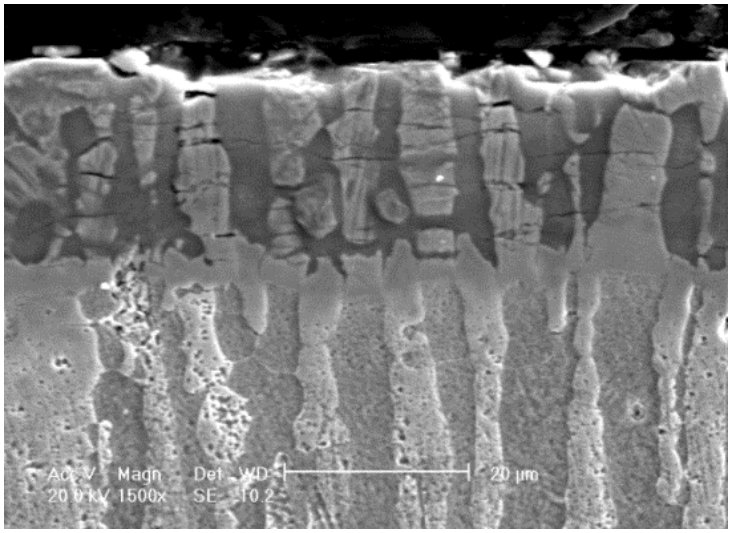

(c)

Figure 4.1.2-4Transverse section SEM images of plasma nitrided LDX 2404 samples treated at temperatures of (a) 390; (b) 420 and (c) 480 °C.

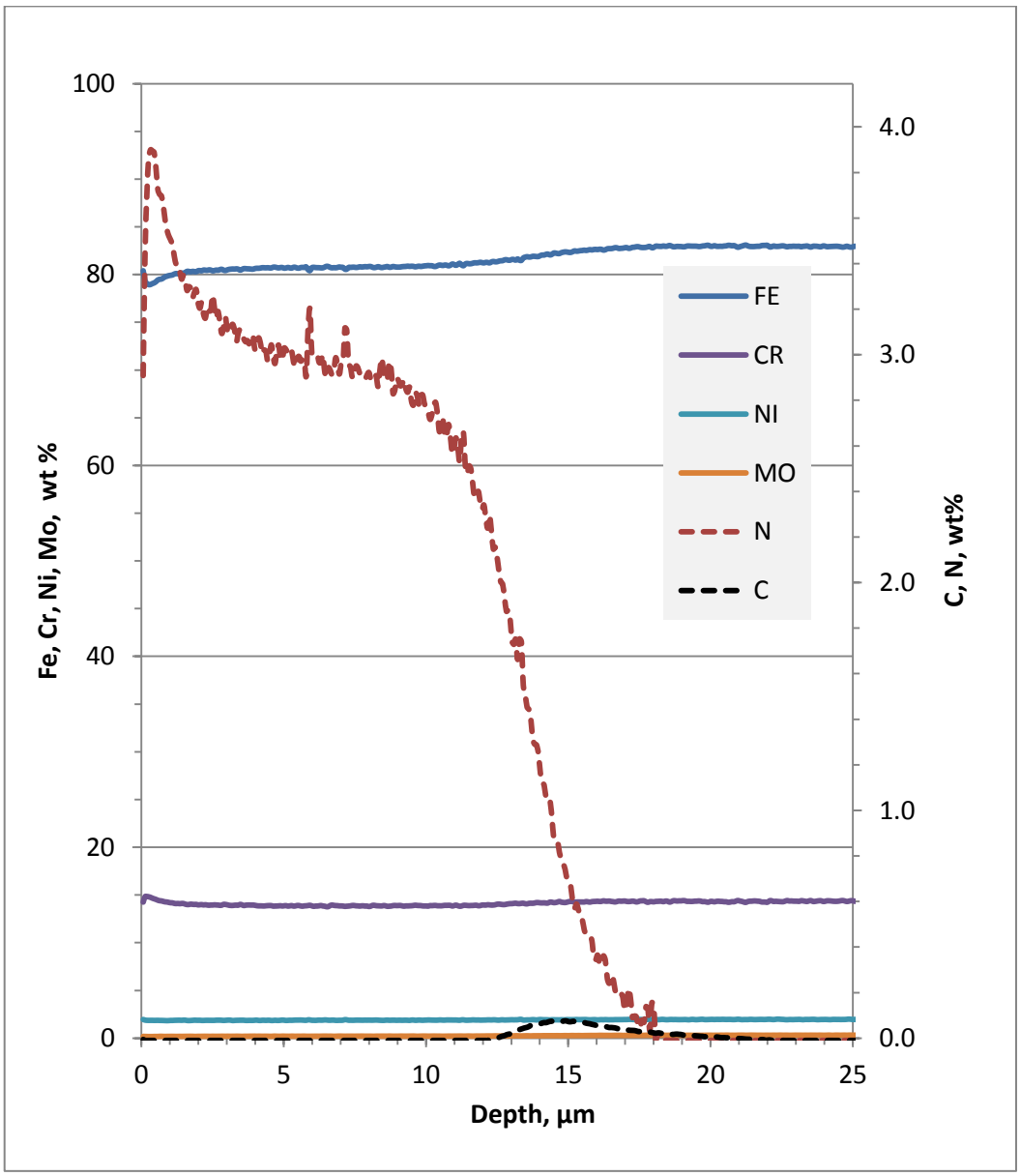

Figure 4.2.1-1 GDOES elements depth profiles of LDX2101 PN450 sample.

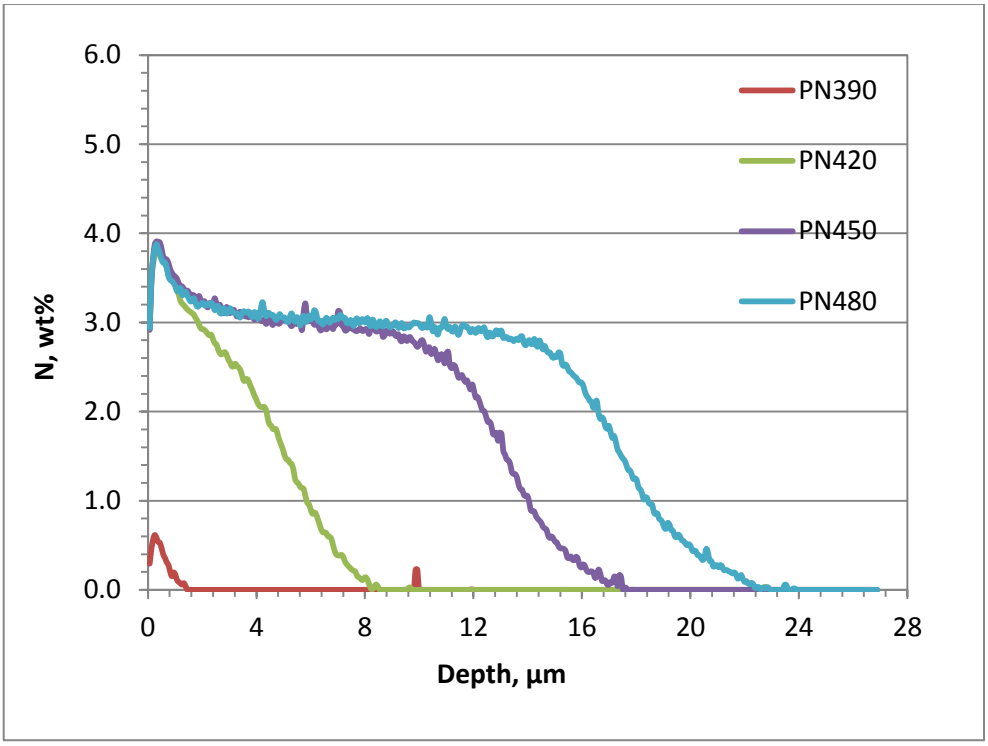

Figure 4.2.1-2 Temperature effect of nitrogen diffusion depth profiles of PN390/10, PN420/10, PN450/10 and PN480/10 of LDX2101.

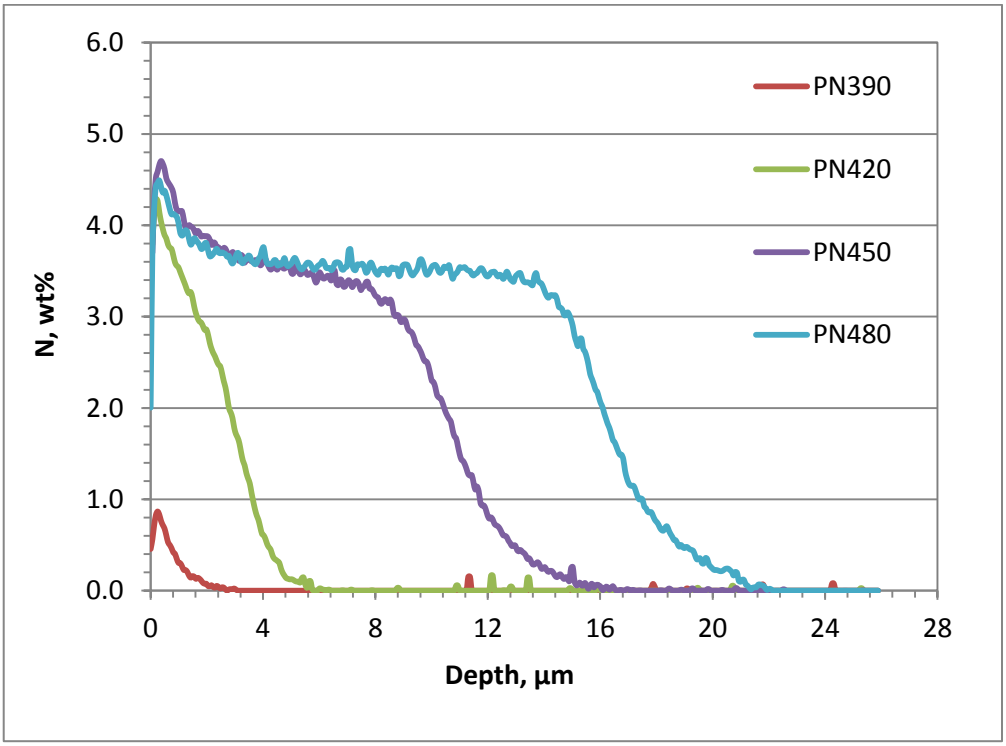

Figure 4.2.2 Temperature effect of nitrogen diffusion depth profiles of PN390/10, PN420/10, PN450/10 and PN480/10 of LDX2404.

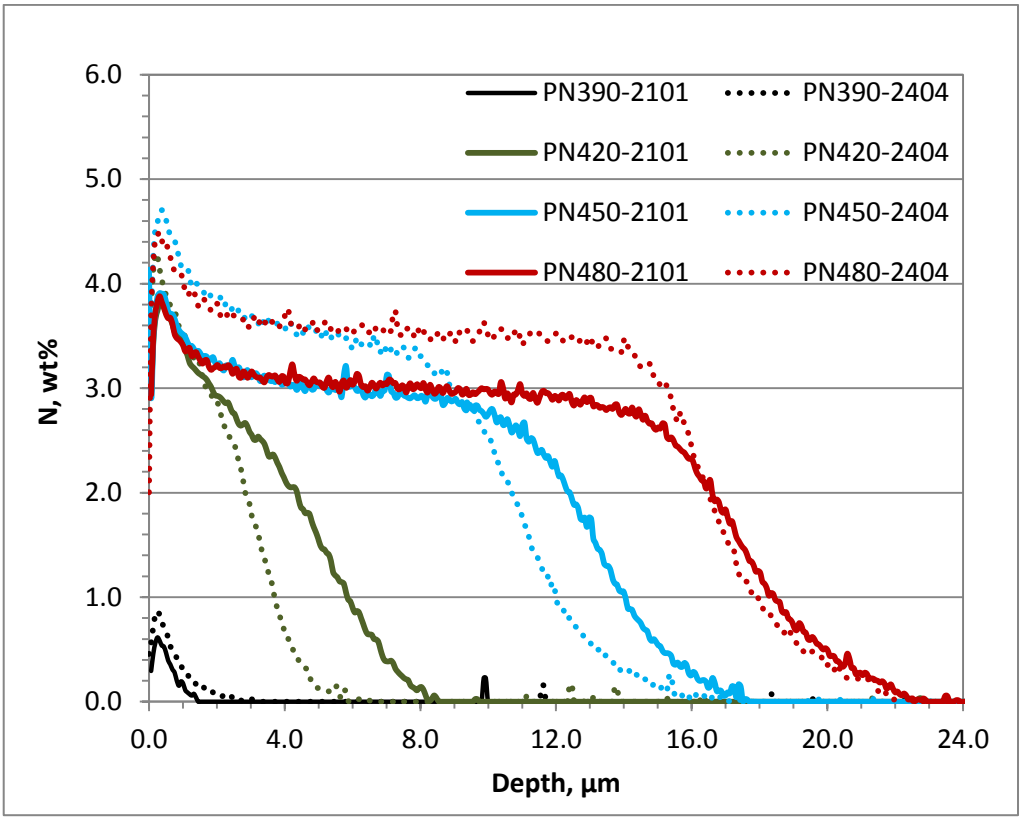

Figure 4.2.3 The comparison of nitrogen diffusion depth profiles between LDX 2101 and LDX 2404 under different treatment temperatures for 10 hours.

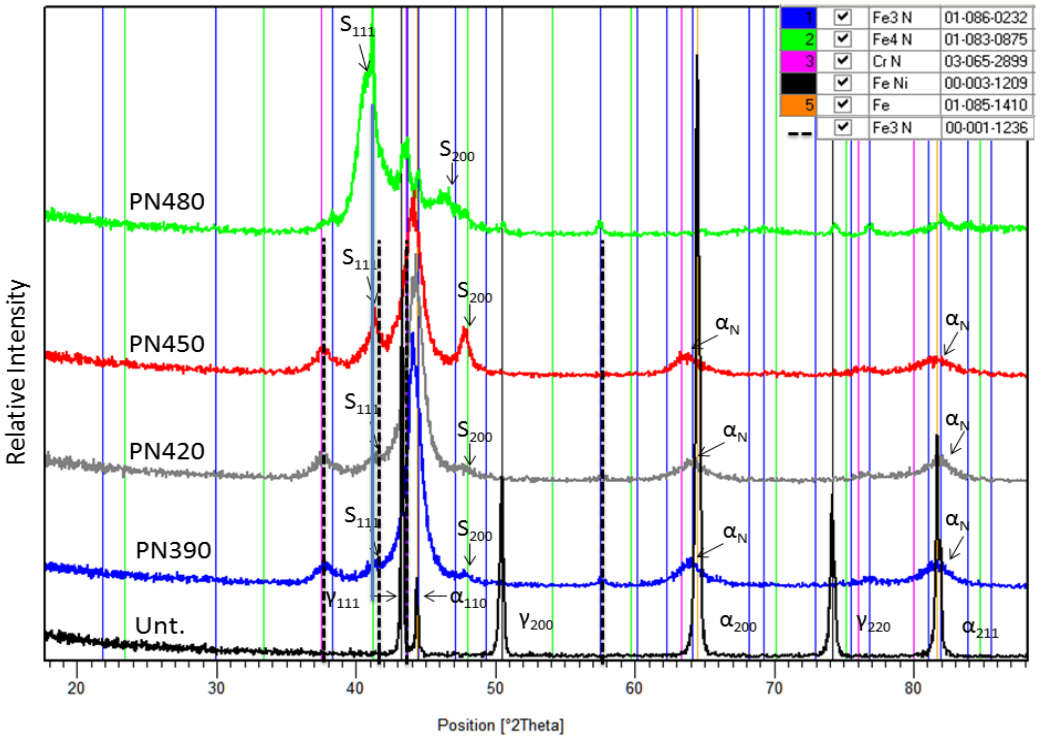

(a)

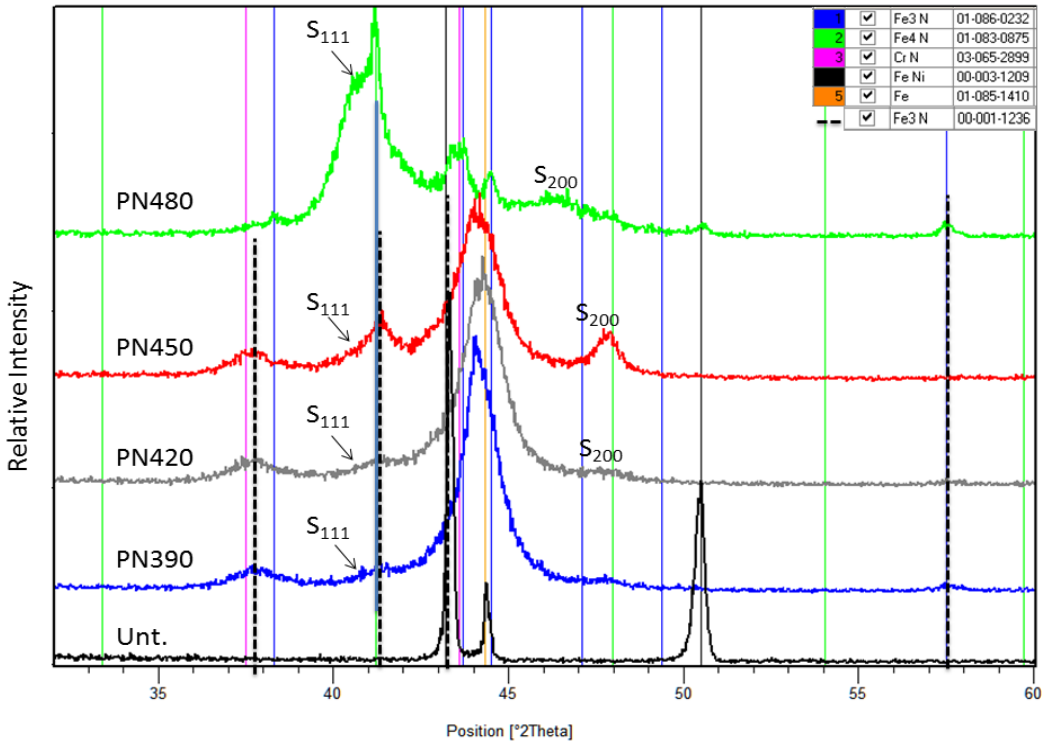

(b)

Figure 4.2.4-1 XRD patterns of plasma nitride LDX2101samples with as-received sample (Unt) for comparison: (a) whole scanned patterns and (b) detailed patterns within 2 thetas of 32 to 60°.

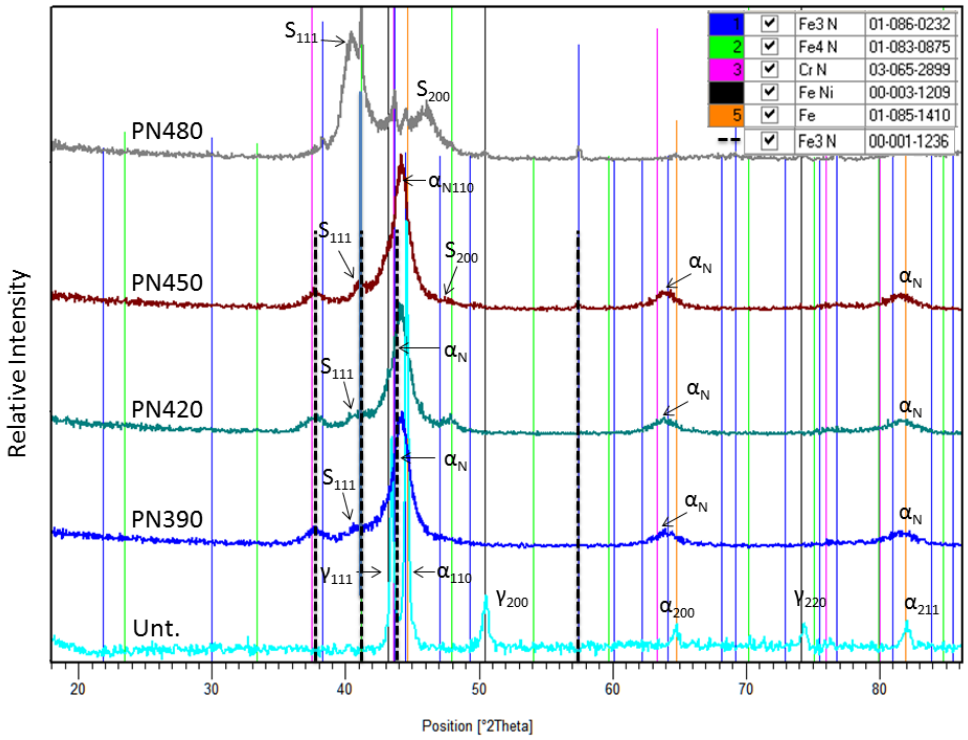

(a)

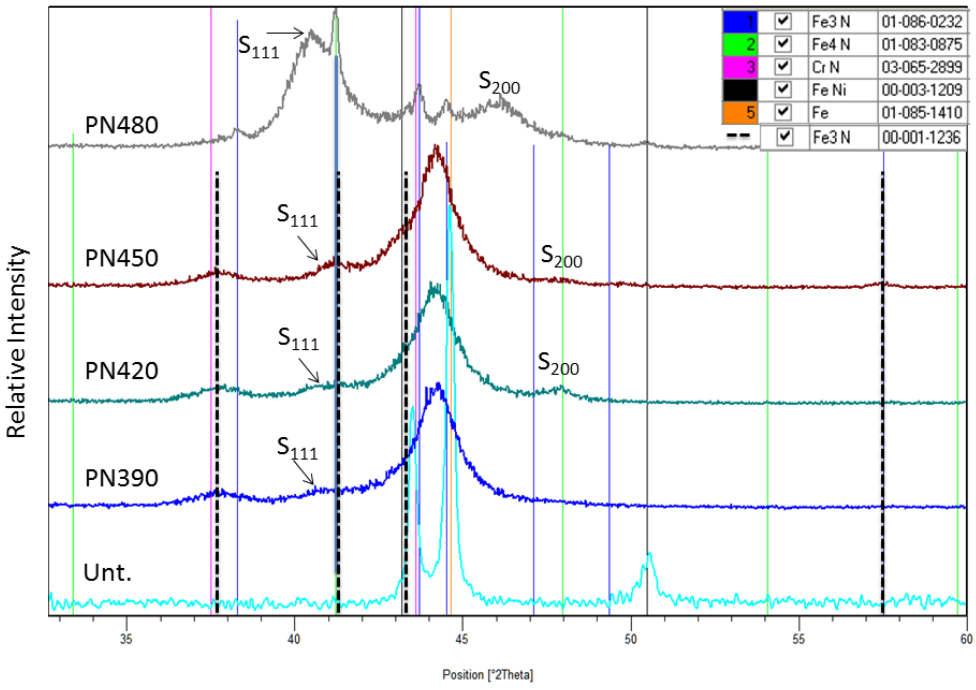

(b)

Figure 4.2.4-2 XRD patterns of plasma nitride LDX2404 samples with as-received sample (Unt) for comparison: (a) whole scanned patterns and, (b) detailed patterns within 2 thetas of 32 to 60°.

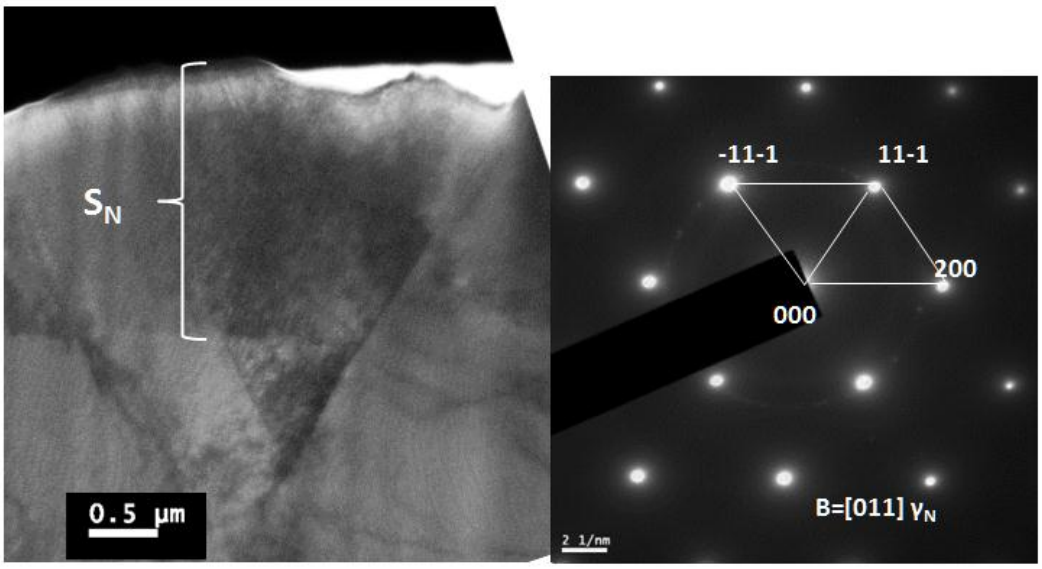

(a)

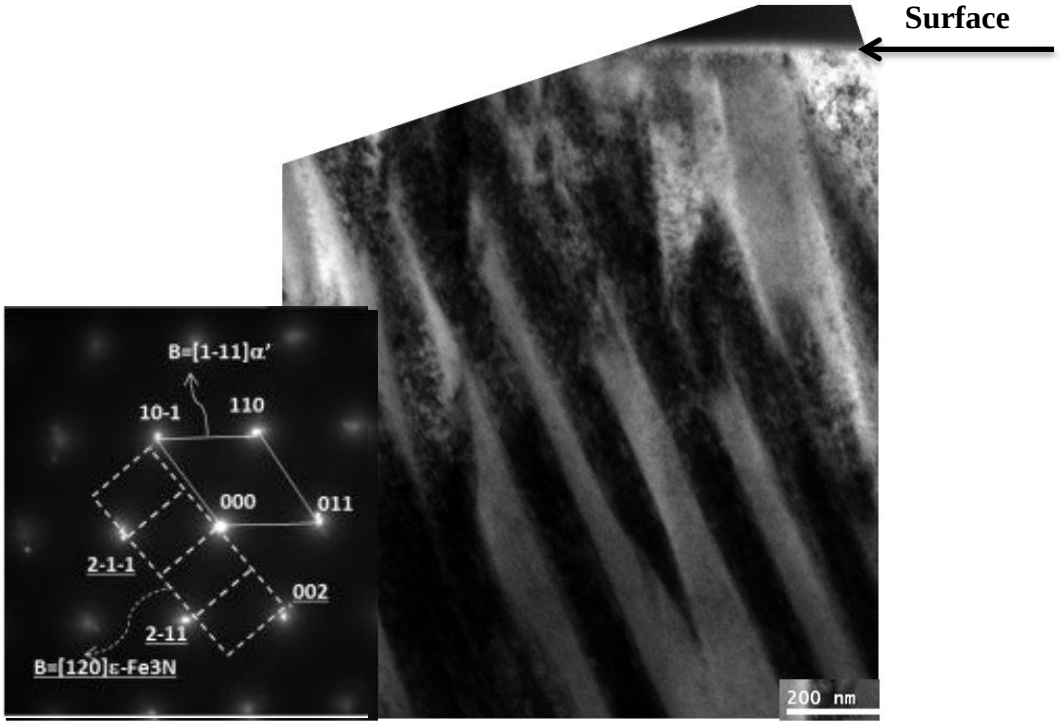

(b)

Figure 4.2.5 TEM microstructure and corresponding SAD patterns from LDX 2101 PN420 sample, (a) nitride surface layer from an original austenite grain; (b) nitride surface layer from an original ferrite grain.

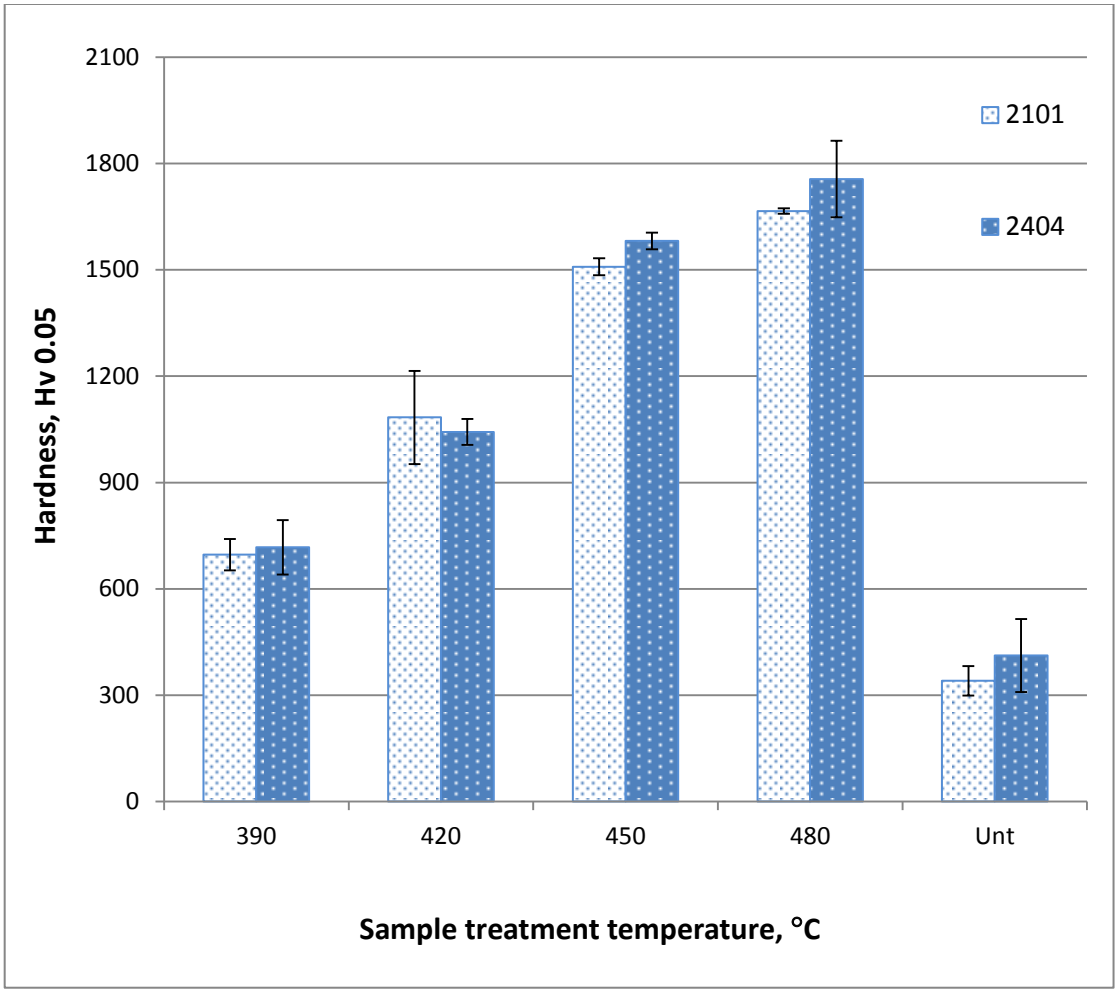

Figure 4.3.1-1 Surface hardness of 10 hours plasma nitrided and untreated LDX2101 and LDX2404 samples.

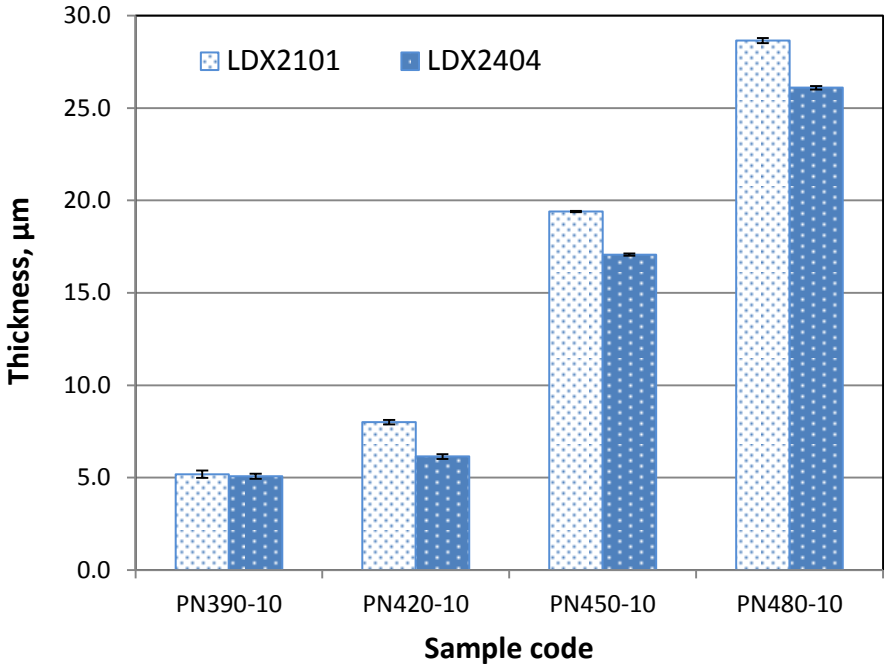

(a)

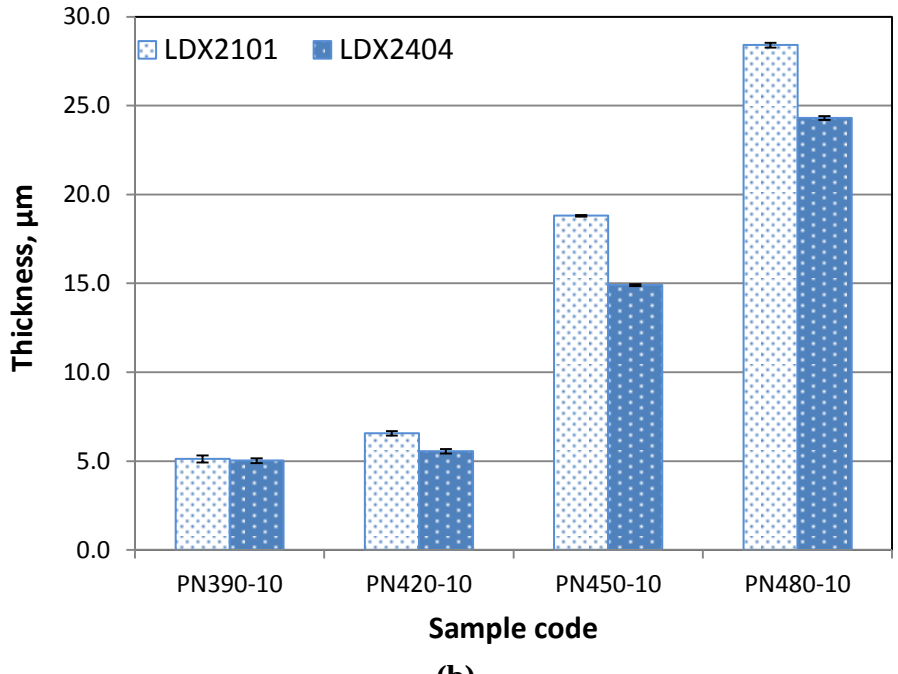

(b)

Figure 4.3.1-2 Nitrided surface layer thickness of 10 hours plasma nitrided LDX2101 and LDX2404 samples: (a) longitudinal section and (b) transverse section.

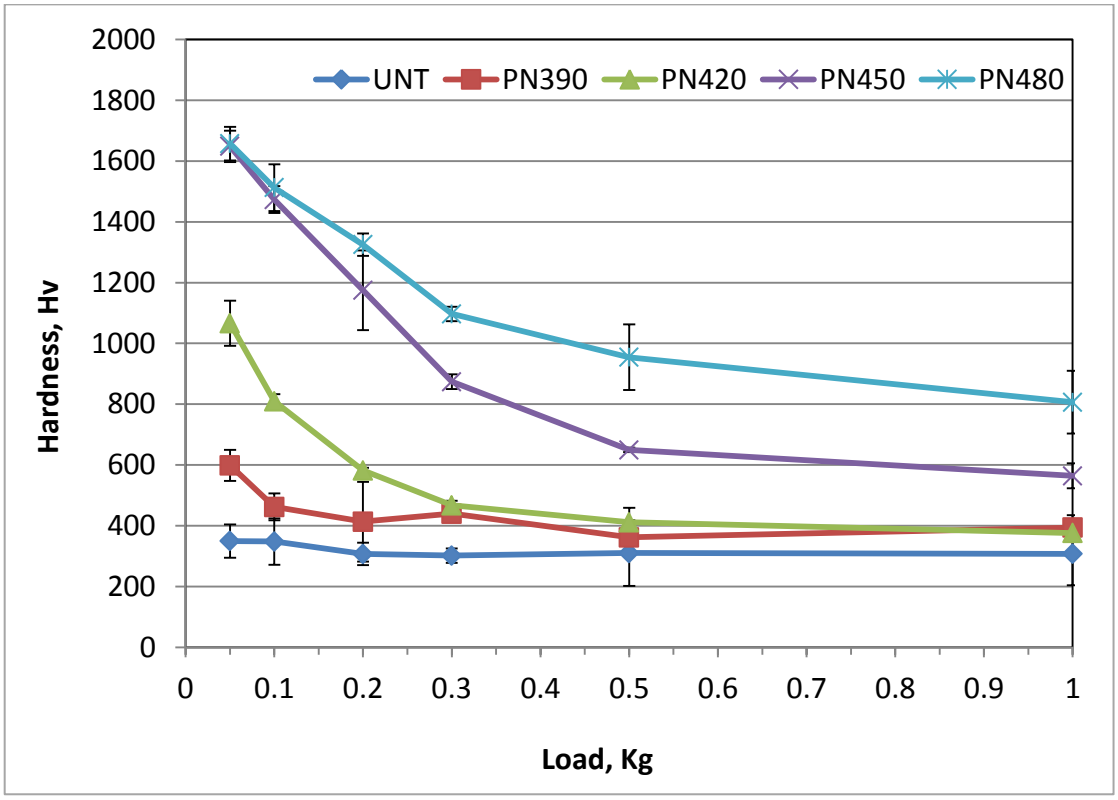

(a)

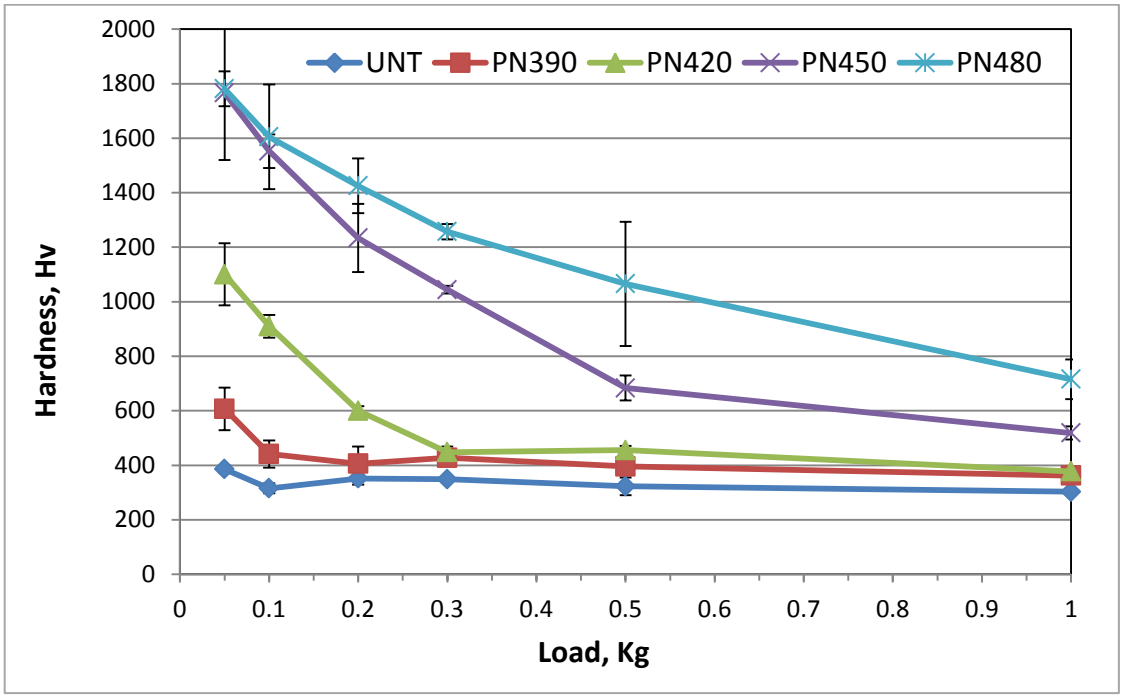

(b)

Figure 4.3.2 The load bearing capacity of plasma nitrided samples comparing with untreated sample, (a) LDX2101 and (b) LDX2404.

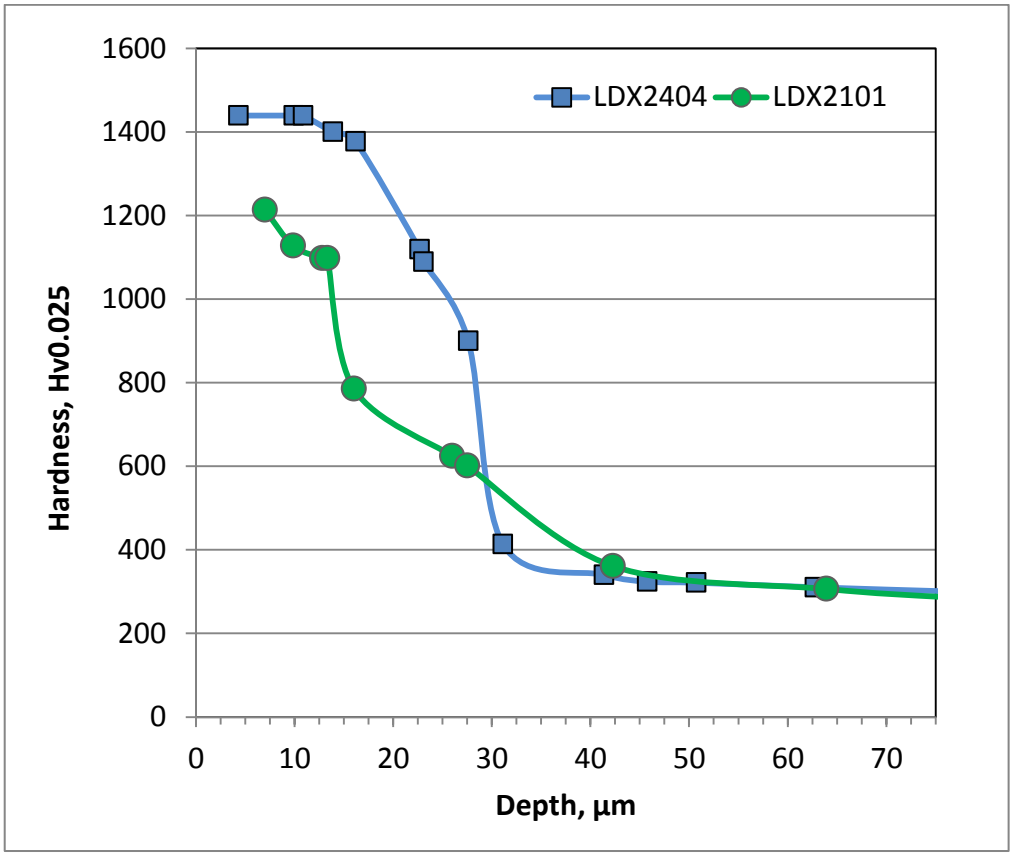

Figure 4.3.3-1 The microhardness depth profiles of PN480 treated samples of LDX 2101 and LDX2404 under 480℃ for 10 hours.

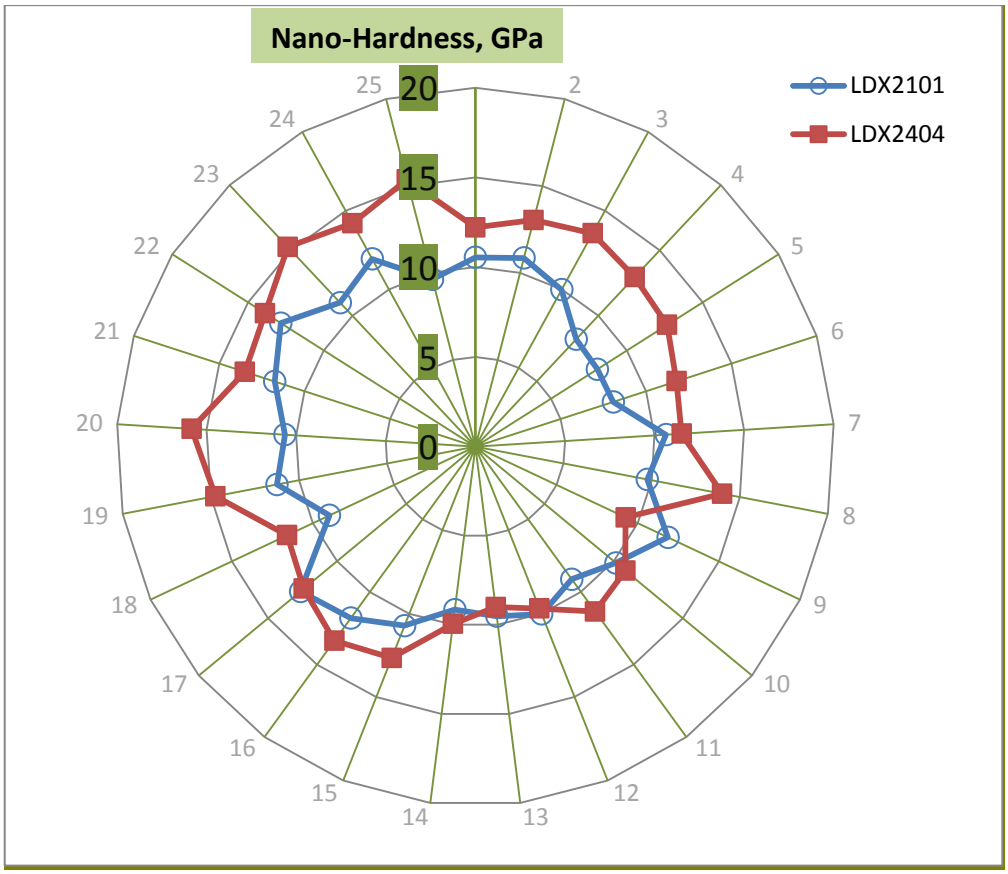

(a)

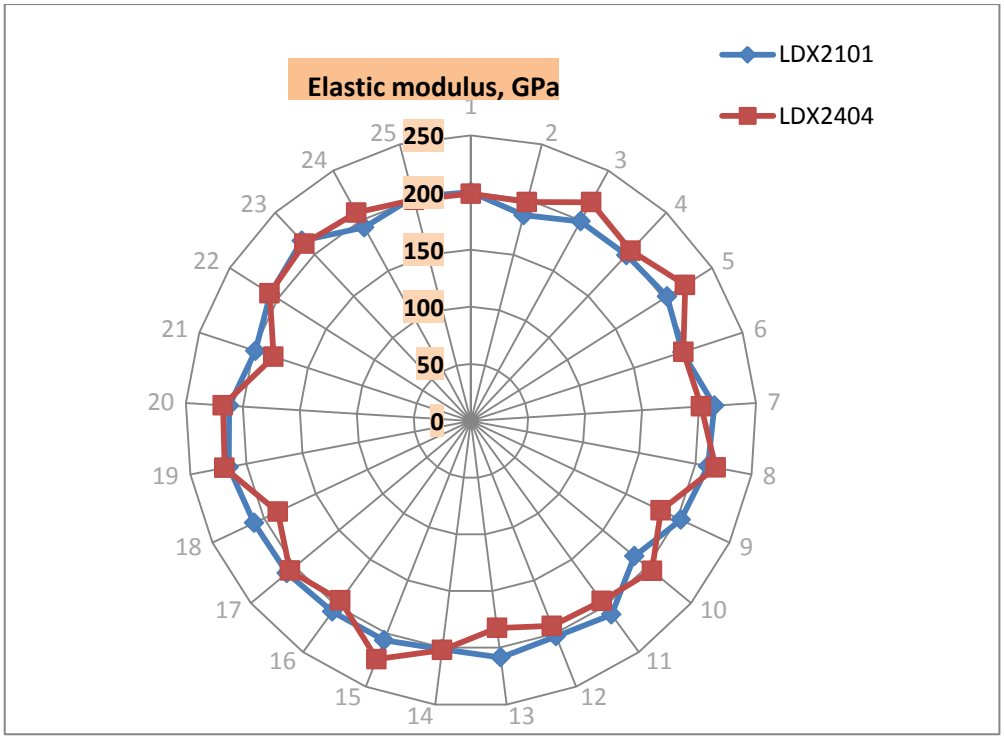

(b)

Figure 4.3.3-2 Comparing of LDX2101 and LDX2404 PN420 samples, (a) Nano-Hardness and (b) Elastic modulus

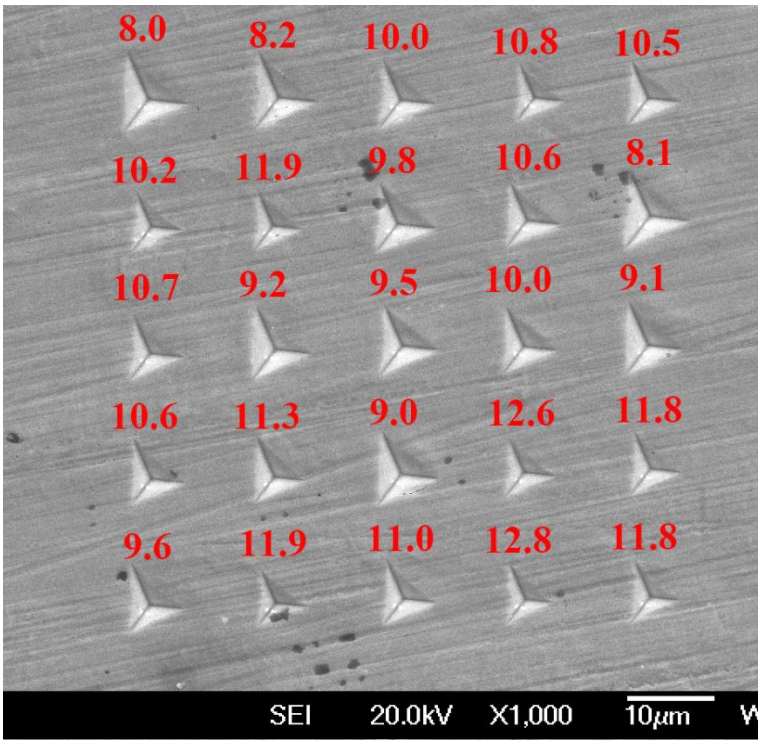

(a)

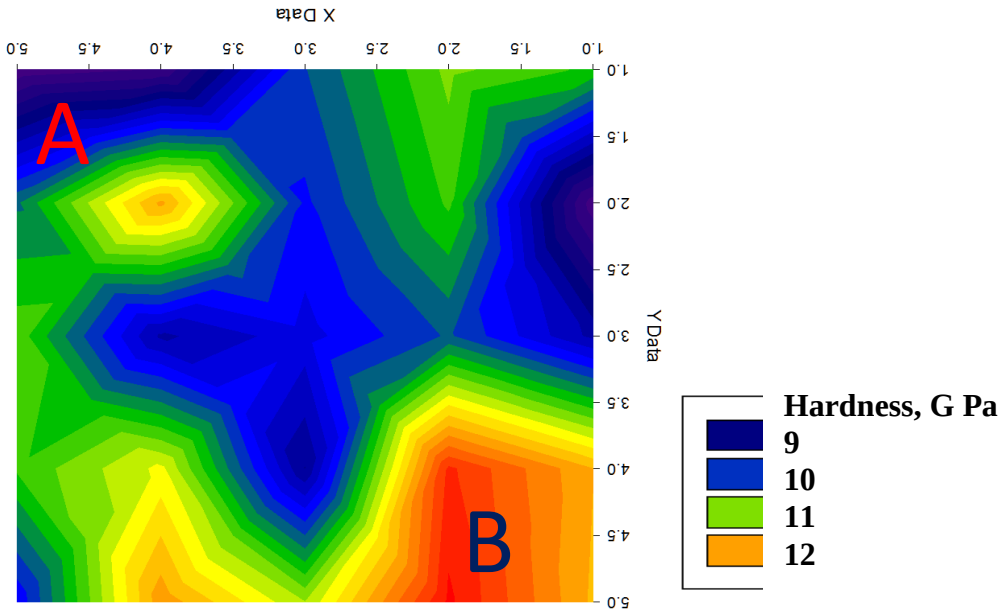

(b)

EDX spot	Cr	Ni	Cr/Ni	Nanohardness
A	21.52	1.65	13.04	8.0
B	23.36	0.92	25.40	11.8

(c)

Figure 4.3.3-3 LDX 2101 PN420 sample: (a) SEM image of Nano-indents with hardness values; (b) hardness value distribution and (c) EDX analysis in area 'A' and 'B', as denoted.

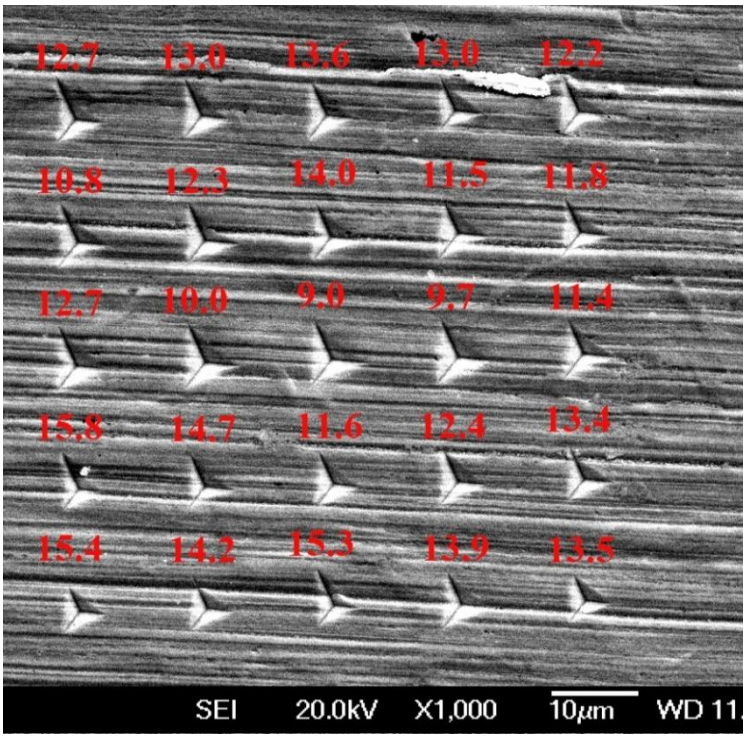

(a)

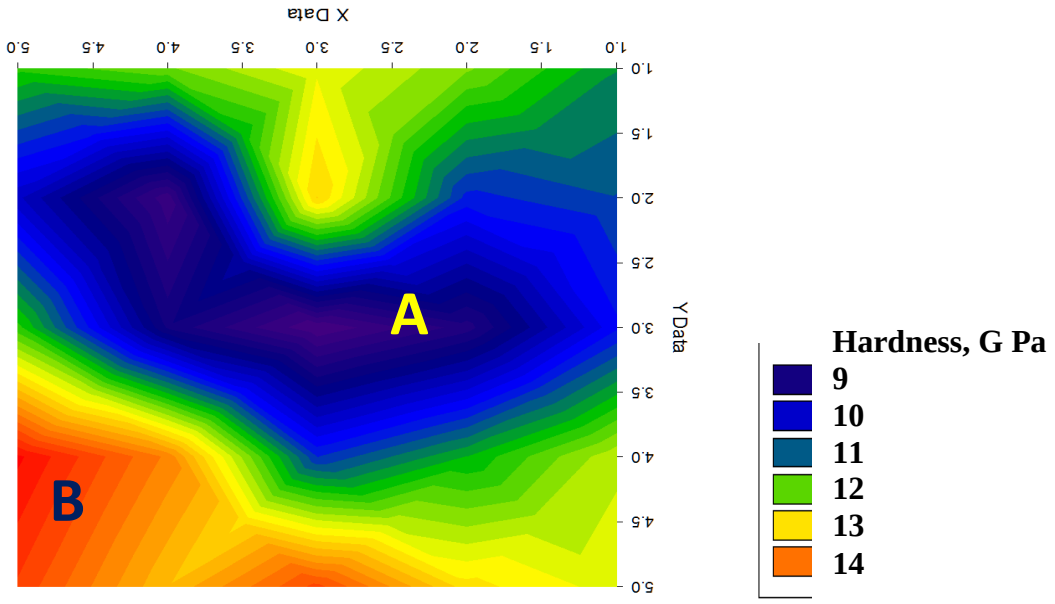

(b)

	Spectrum	Cr	Ni	Cr/Ni	Nanohardness
A	**1**	**24.51**	**4.27**	**5.74**	**9.0**
B	**6**	**26.66**	**2.96**	**9.00**	**15.3**

(c)

Figure 4.3.3-4 LDX2404 PN420: (a) SEM image of Nano-indents with hardness values; (b) hardness value distribution and (c) EDX analysis in area 'A' and 'B', as denoted.

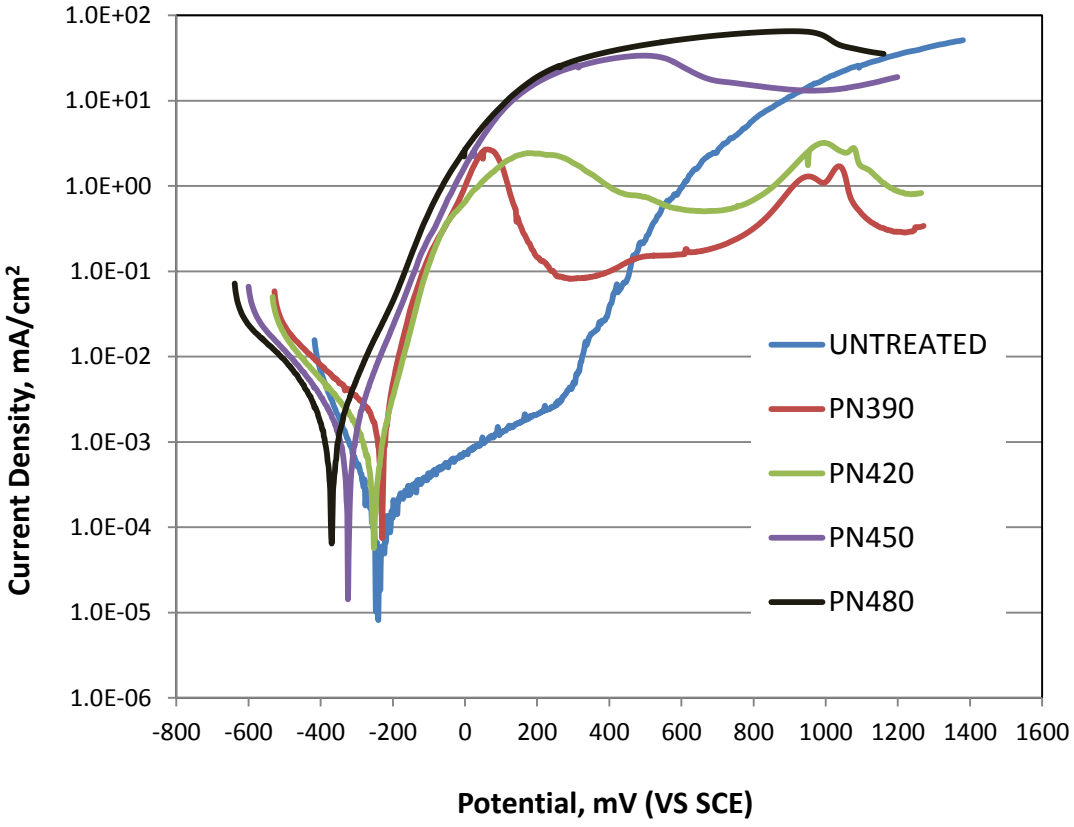

Figure 4.4.1-1 Anodic polarization curves for untreated and plasma nitride samples of LDX 2101

(a)

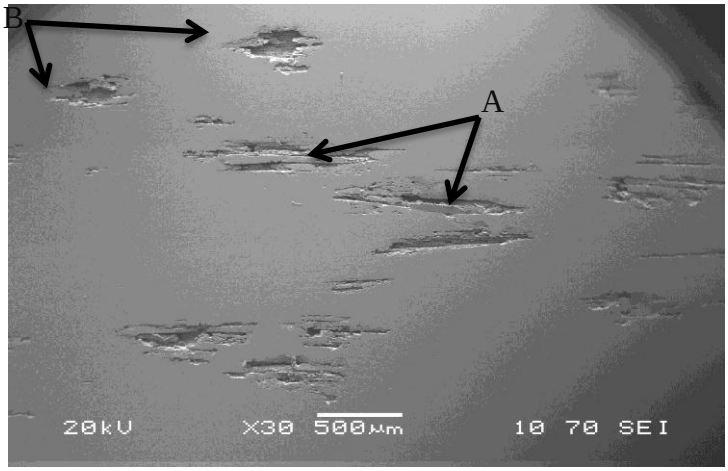

(b)

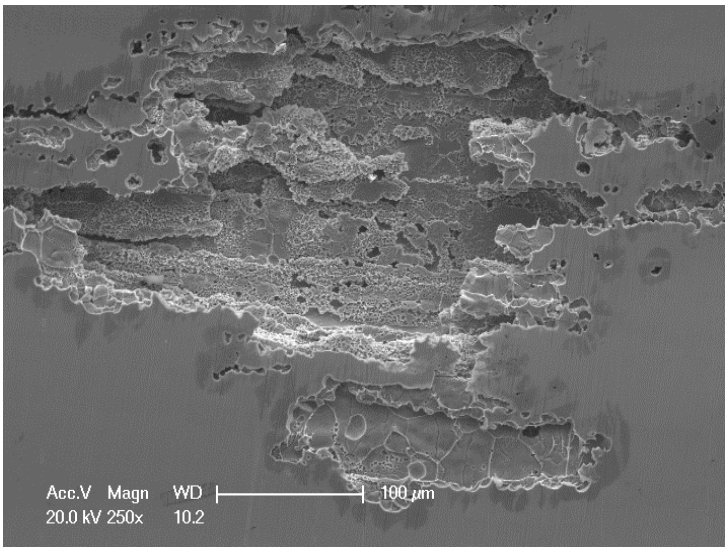

(c)

Figure 4.4.1-2 SEM images of untreated LDX 2101 sample surfaces: (a) before corrosion test, (b) post corrosion test and (c) higher magnification image of area 'B' in (b).

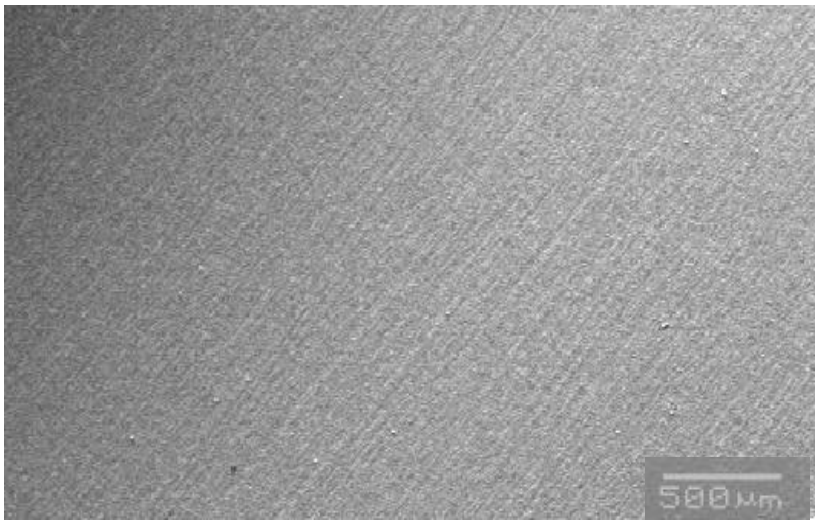

(a)

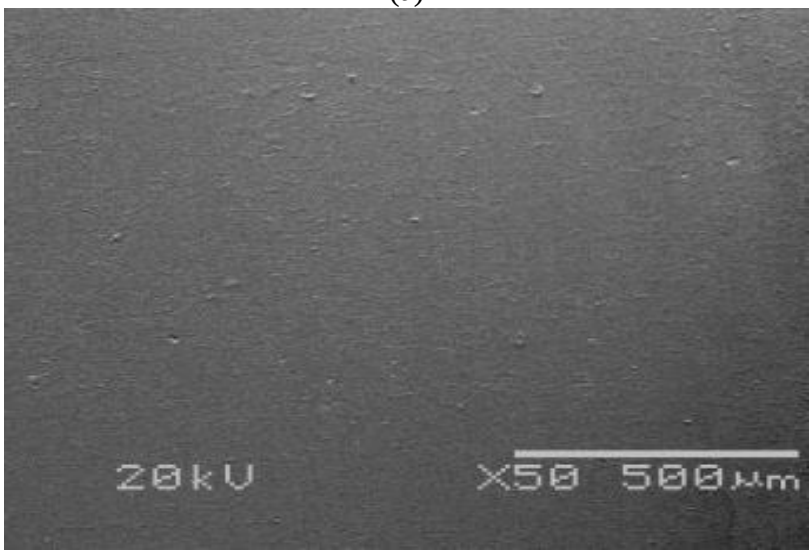

(b)

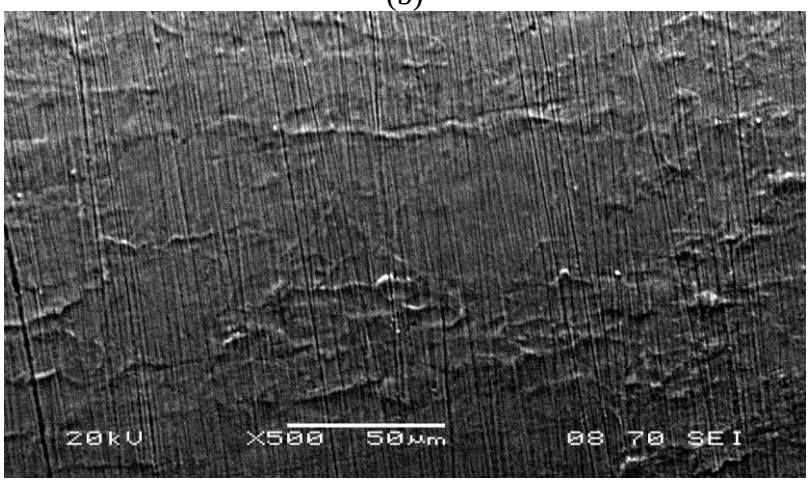

(c)

Figure 4.4.1-3 SEM images of LDX 2101 PN390 sample surfaces: (a) before corrosion test, (b) post corrosion test and (c) higher magnification image of part of (b).

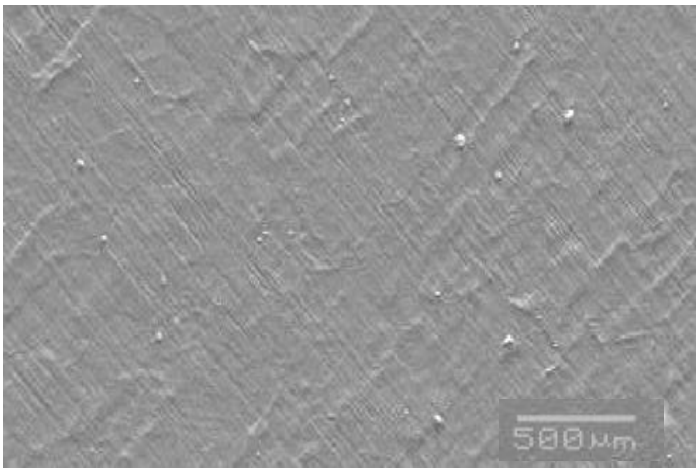

(a)

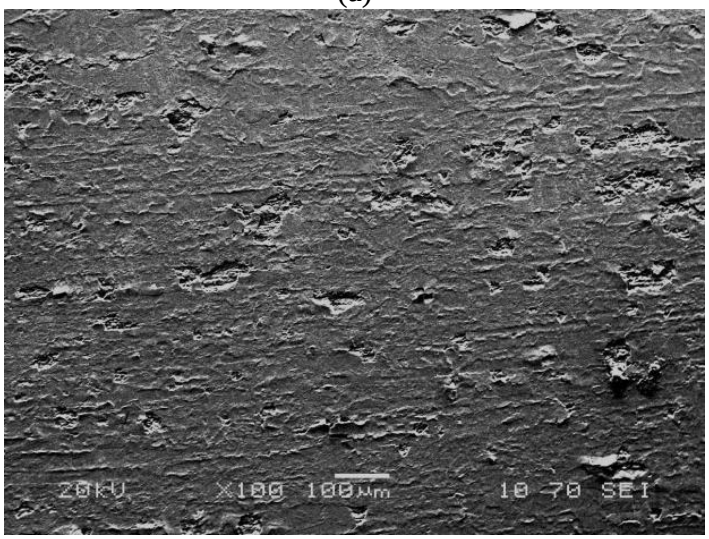

(b)

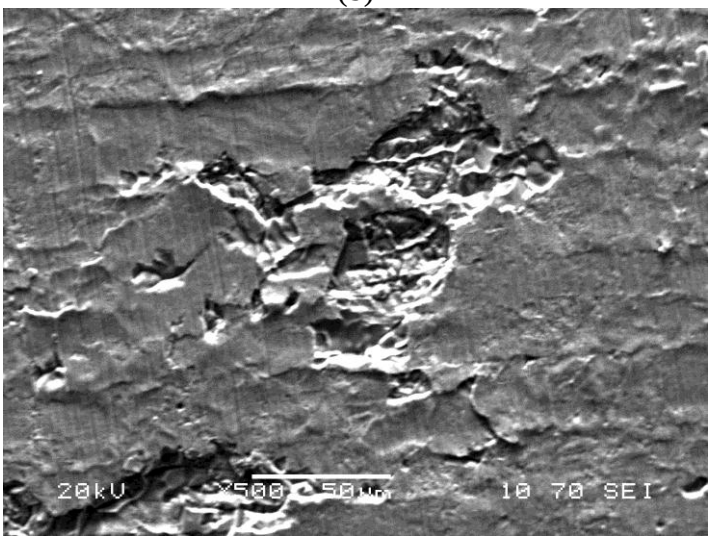

(c)

Figure 4.4.1-4 SEM images of LDX 2101 PN420 sample surfaces: (a) before corrosion test, (b) post corrosion test and (c) higher magnification image of part of (b).

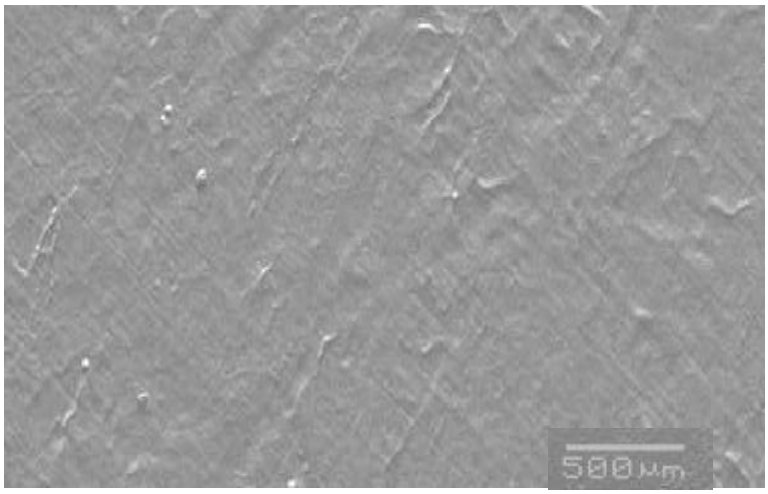

(a)

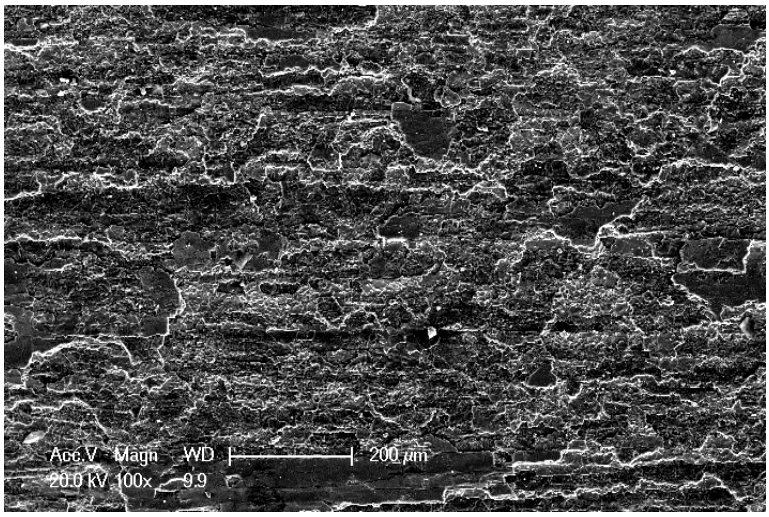

(b)

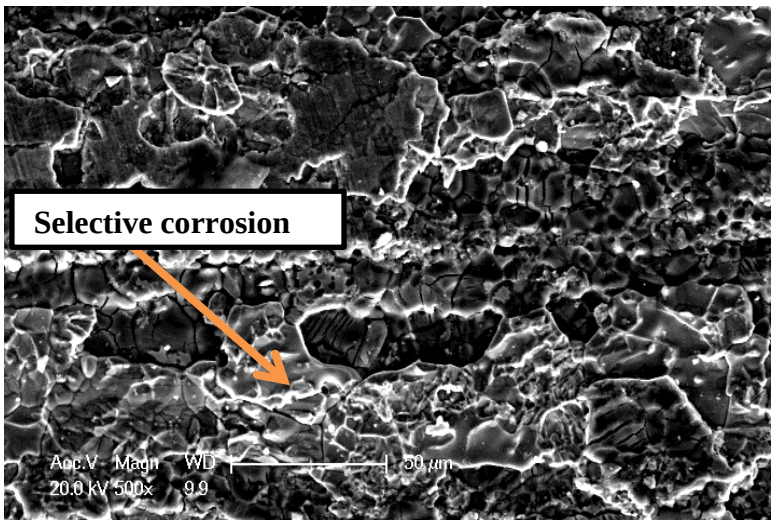

(c)

Figure 4.4.1-5 SEM images of LDX 2101 PN450 sample surfaces: (a) before corrosion test, (b) post corrosion test and (c) higher magnification image of part of (b).

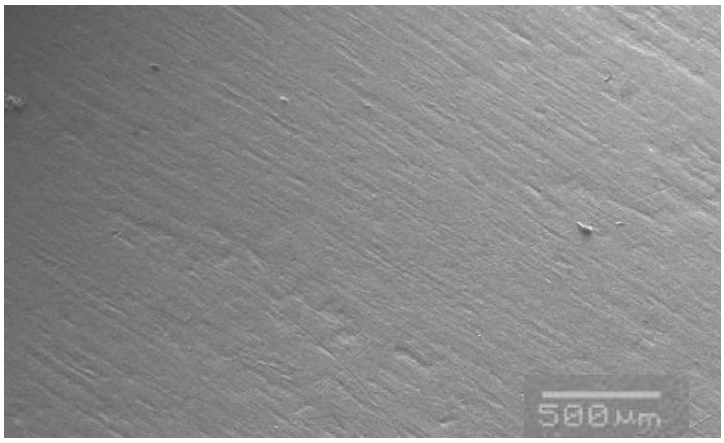

(a)

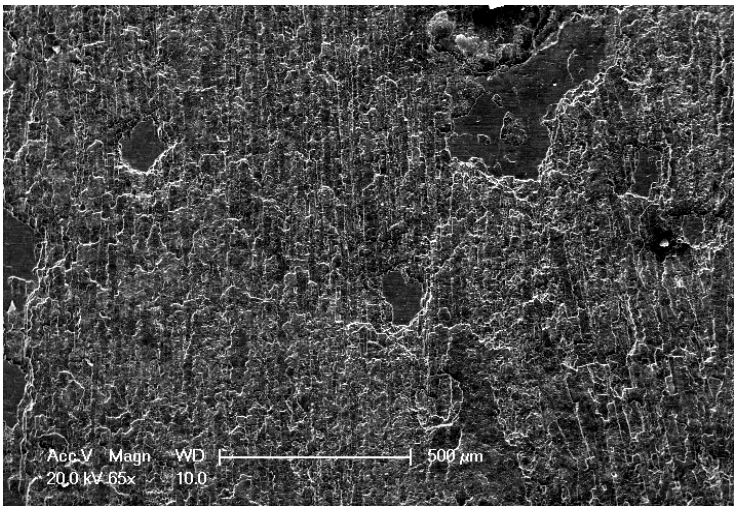

(b)

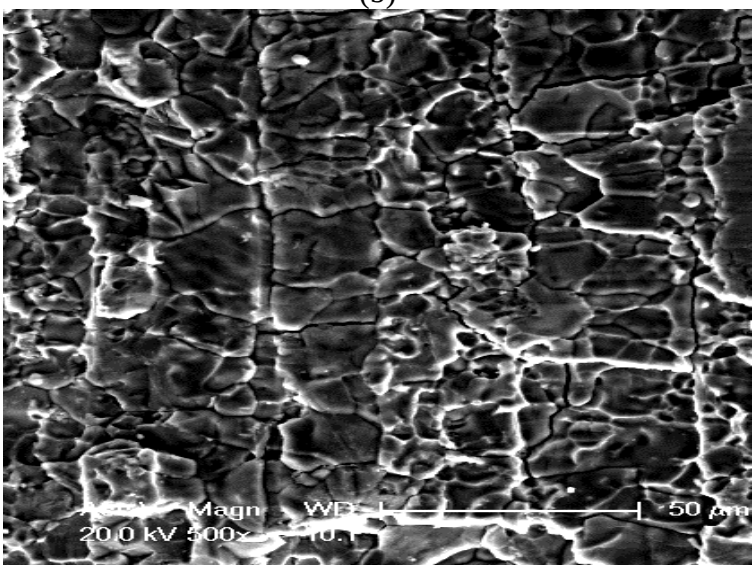

(c)

Figure 4.4.1-6 SEM images of LDX 2101 PN480 sample surfaces: (a) before corrosion test, (b) post corrosion test and (c) higher magnification image of part of (b).

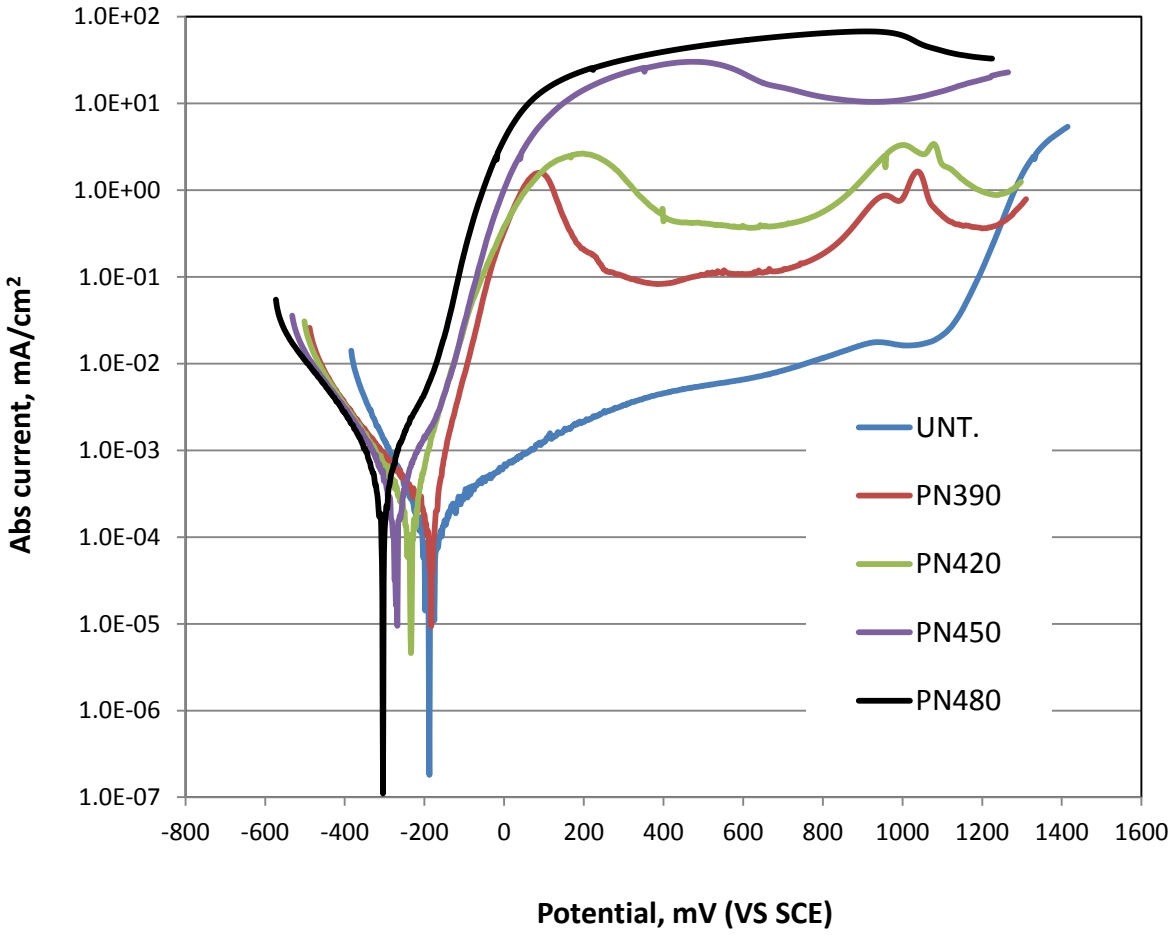

Figure 4.4.2-1 Anodic polarization curves for untreated and plasma nitride samples of LDX 2404 steel.

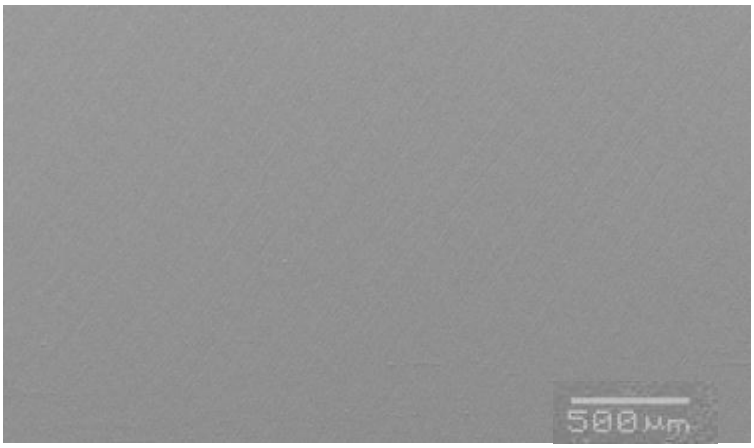

(a)

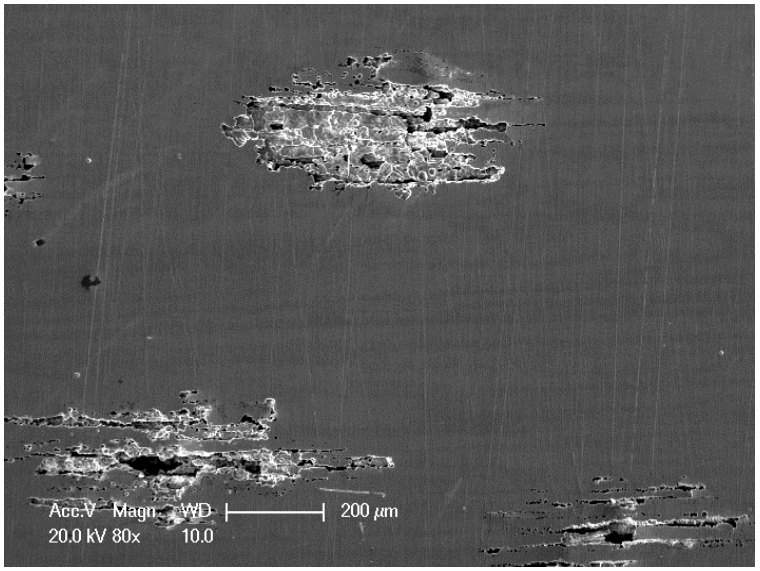

(b)

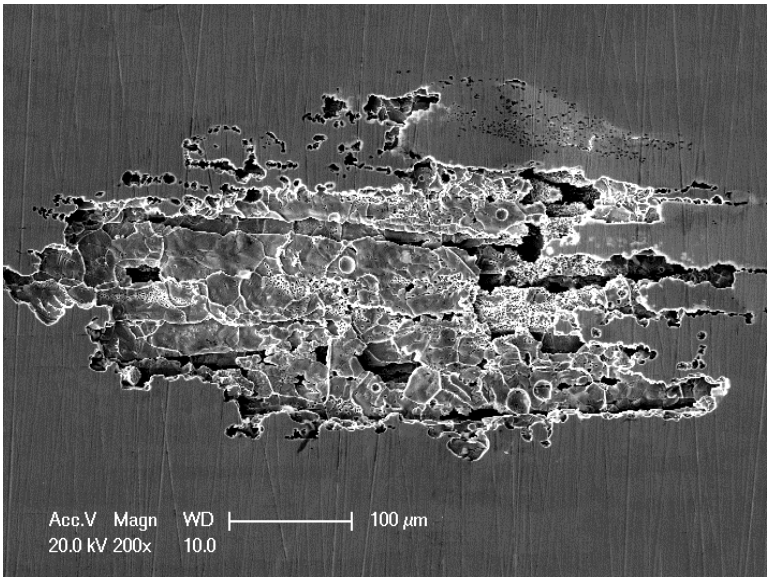

(c)

Figure 4.4.2-2 SEM images of (a) before treatment, (b) corroded area of untreated sample overview and (c) higher magnification picture for LDX 2404.

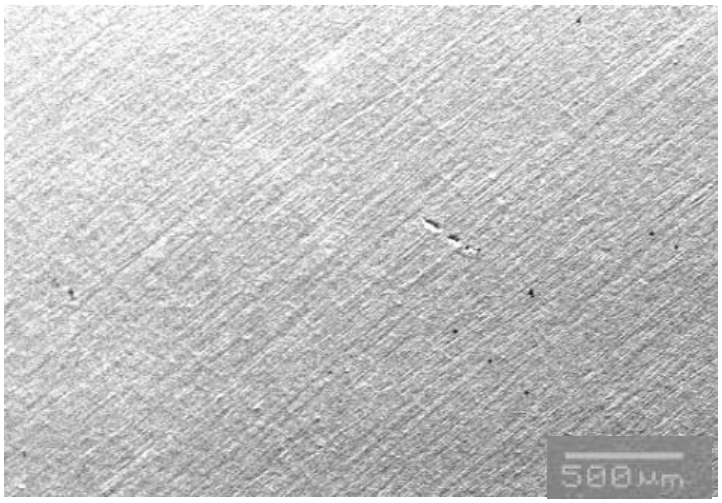

(a)

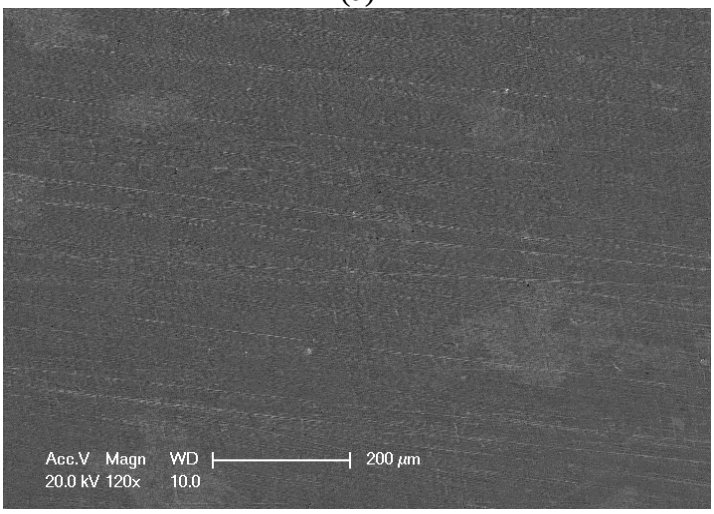

(b)

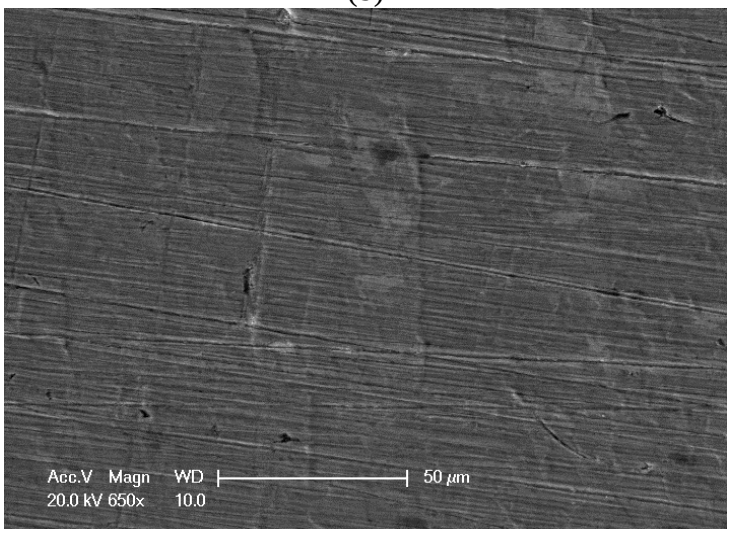

(c)

Figure 4.4.2-3 SEM images of LDX 2404 PN390 sample surfaces: (a) before corrosion test, (b) post corrosion test and (c) high magnification image of part of (b).

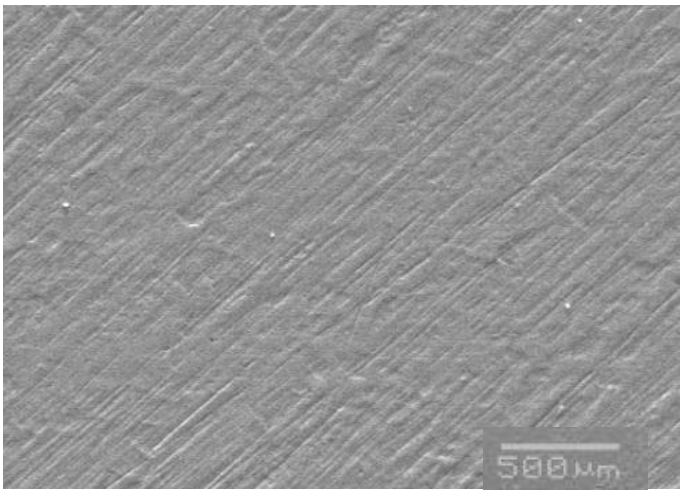

(a)

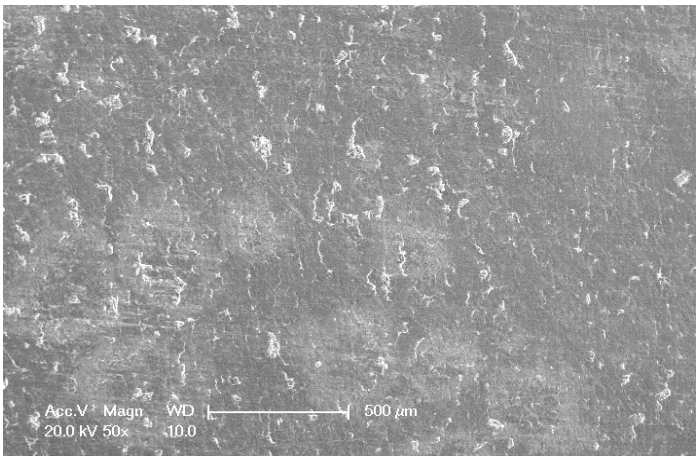

(b)

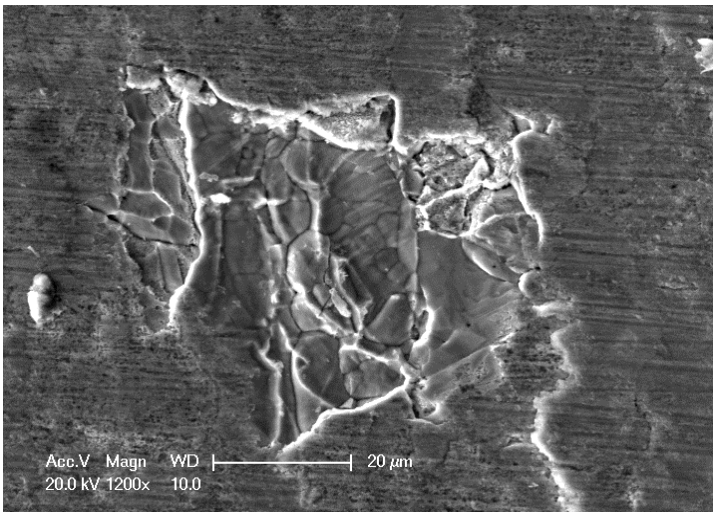

(c)

Figure 4.4.2-4 SEM images of LDX 2404 PN420 sample surfaces: (a) before corrosion test, (b) post corrosion test and (c) high magnification image of part of (b).

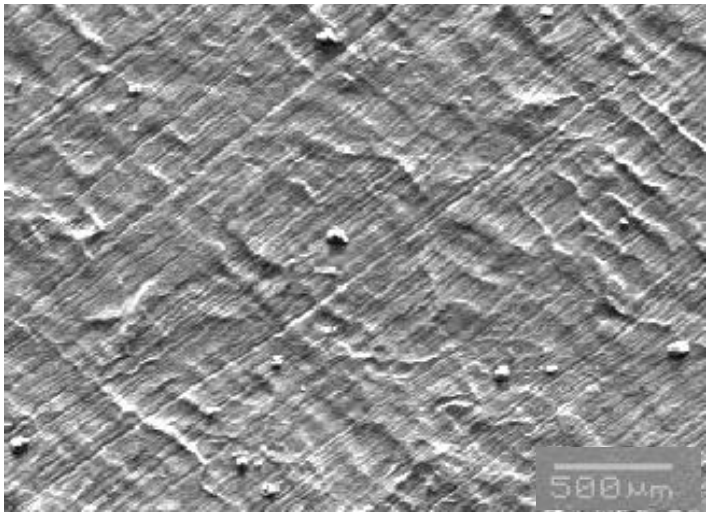

(a)

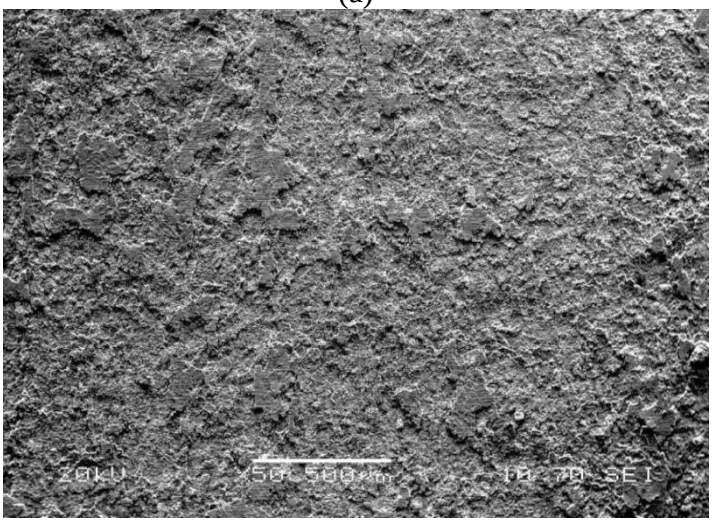

(b)

(c)

Figure 4.4.2-5 SEM images of LDX 2404 PN450 sample surfaces: (a) before corrosion test, (b) post corrosion test and (c) high magnification image of part of (b).

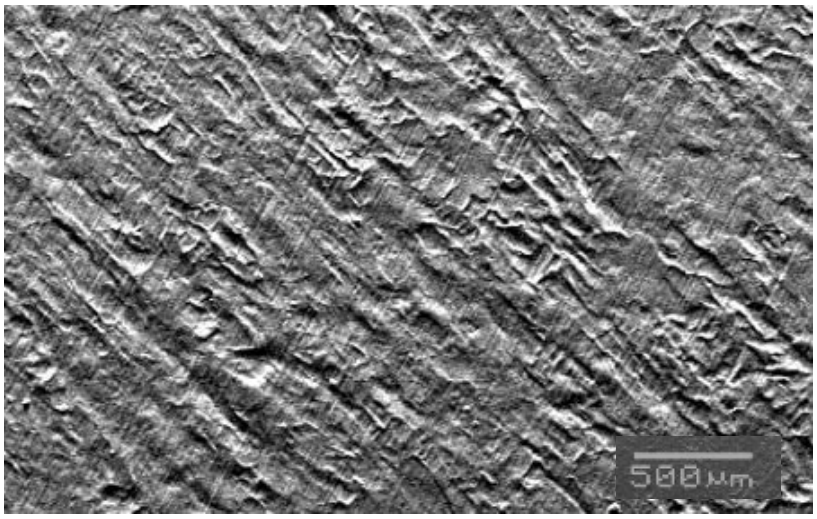

(a)

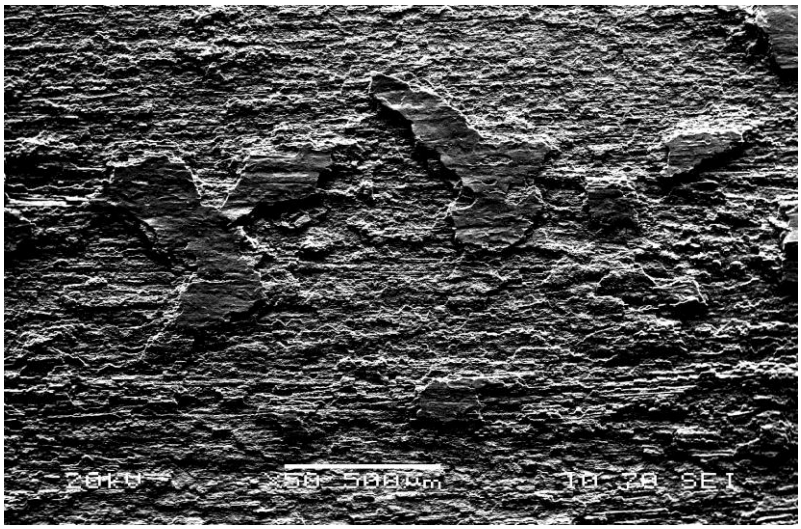

(b)

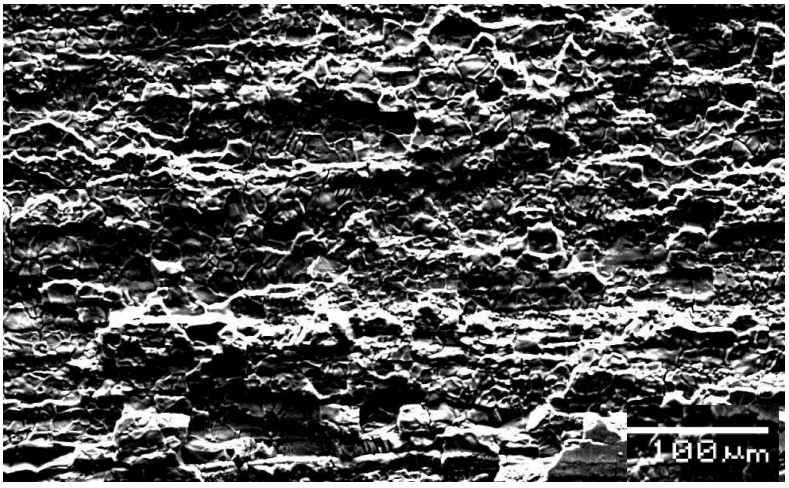

(c)

Figure 4.4.2-6 SEM images of LDX 2404 PN480 sample surfaces: (a) before corrosion test, (b) post corrosion test and (c) high magnification image of part of (b).

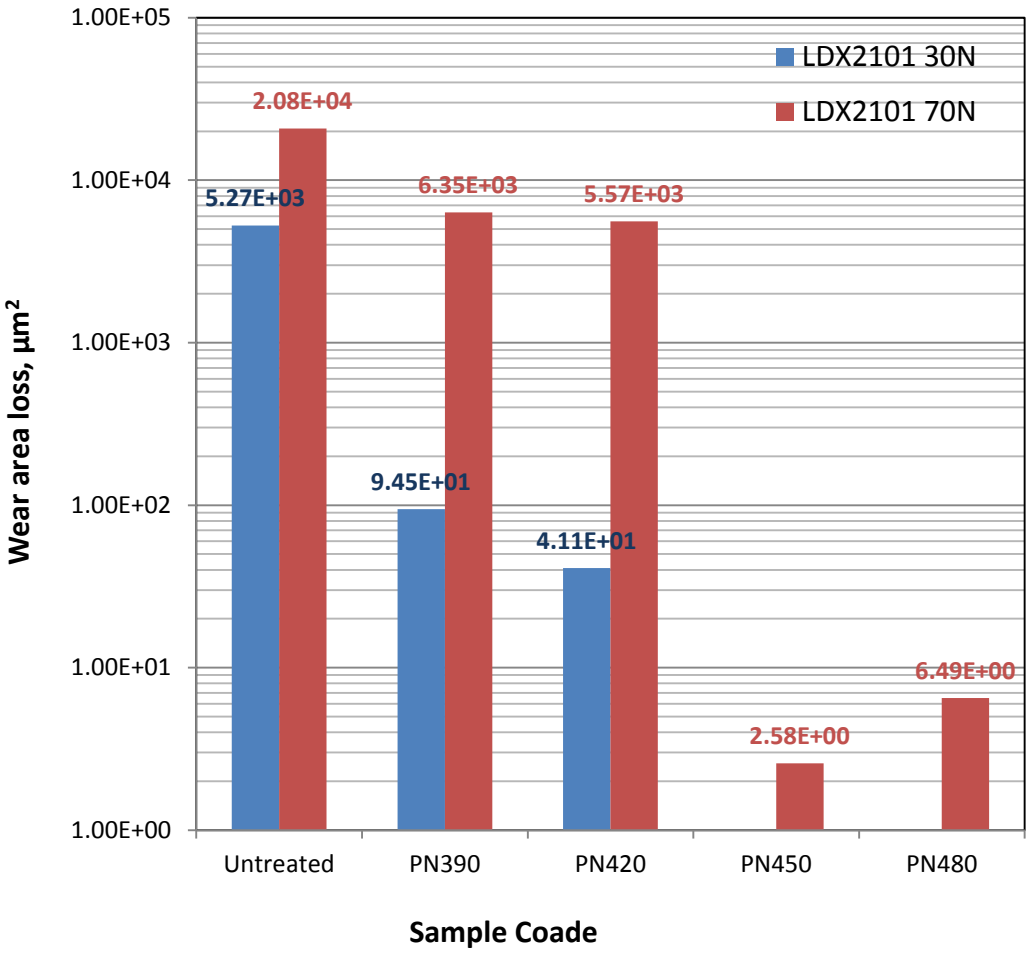

Figure 4.5.1-1 Dry wear area loss of untreated and plasma nitrided samples for LDX 2101steel under 30 and 70N; counterpart: WC ball, Ø=8mm.

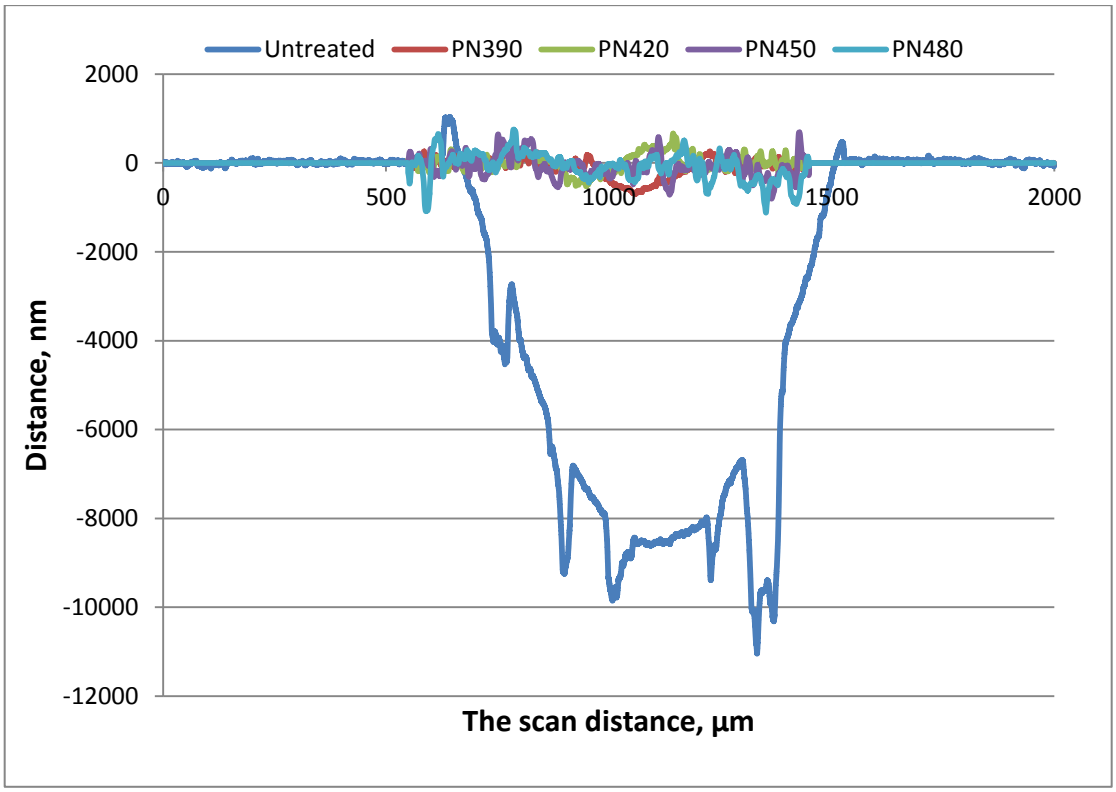

(a)

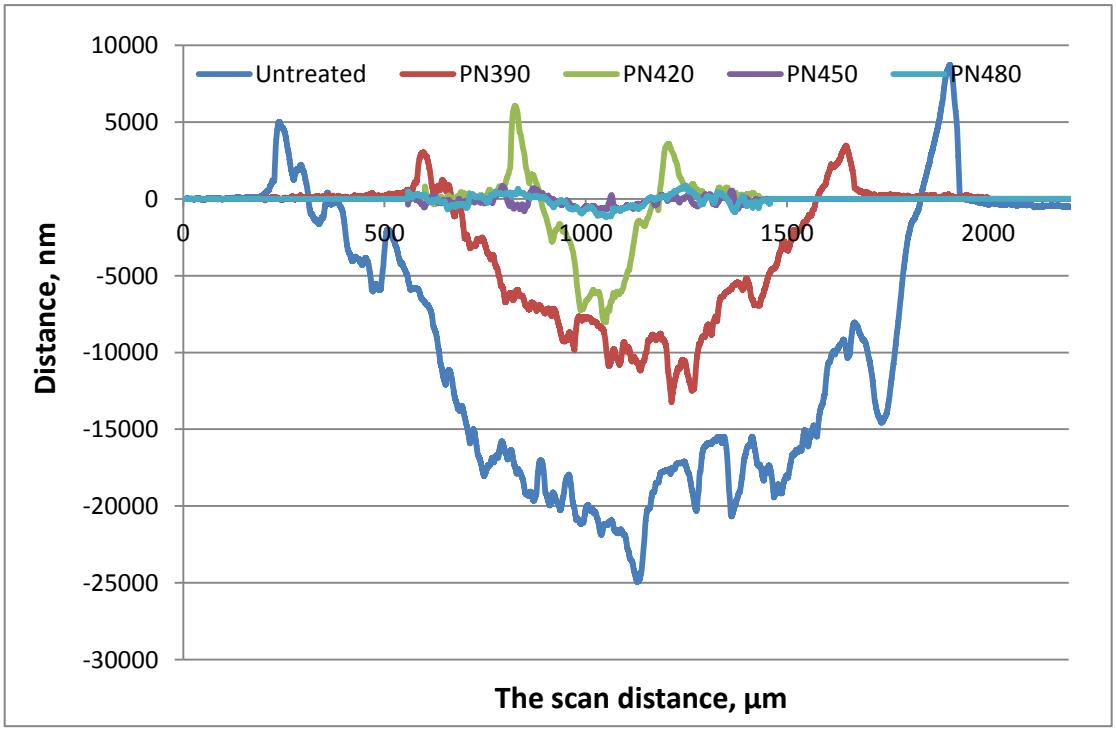

(b)

Figure 4.5.1-2 The cross-sectional wear area loss under a loading condition of (a) 30N and (b) 70N for plasma nitriding samples of LDX 2101

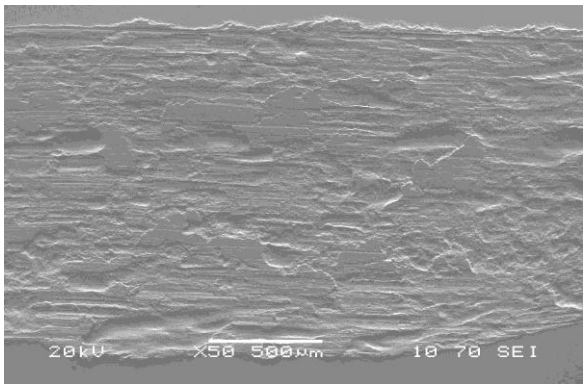

(a)

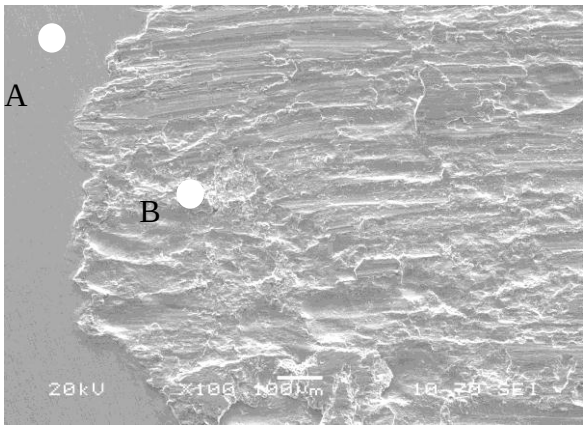

(b)

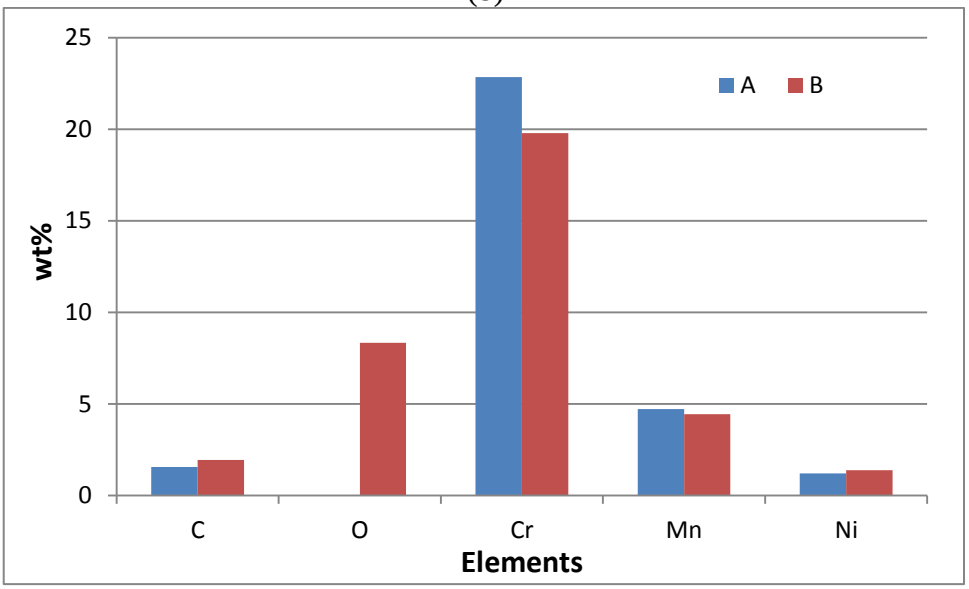

	C	O	Cr	Mn	Ni
A	1.55	0	22.84	4.71	1.2
B	1.93	8.34	19.79	4.44	1.38

(c)

Figure 4.5.1-3 Wear morphologies of untreated sample of LDX 2101 under 70N load with (a) low resolution and (b) high resolution images and (c) EDX results.

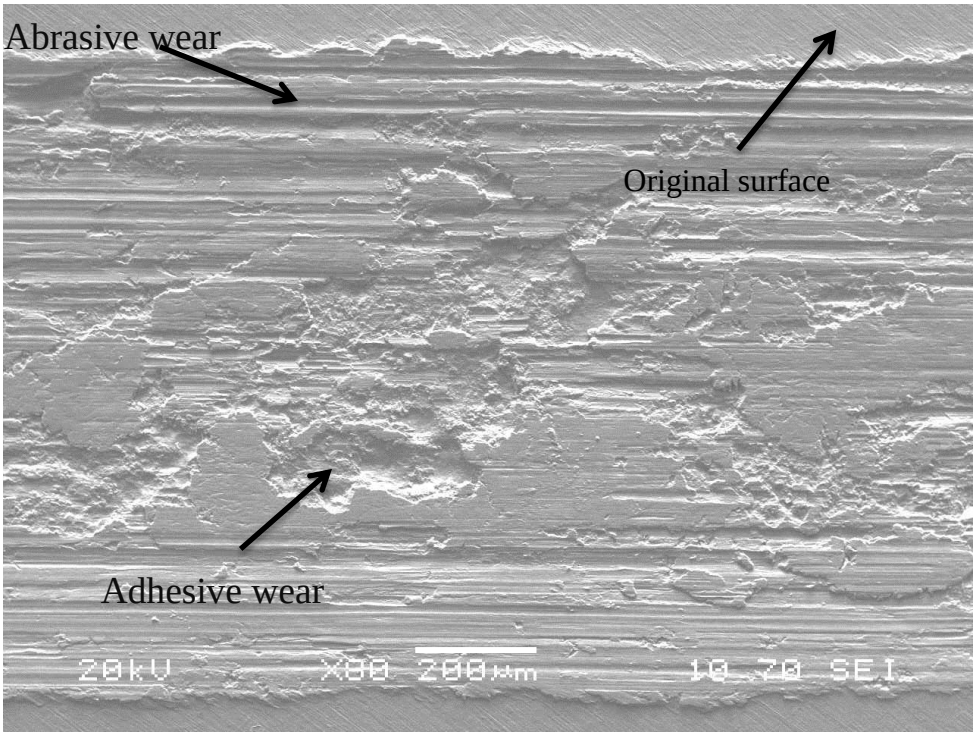
Abrasive wear
Original surface
Adhesive wear
20kV X80 200μm 10 70 SEI

(a)

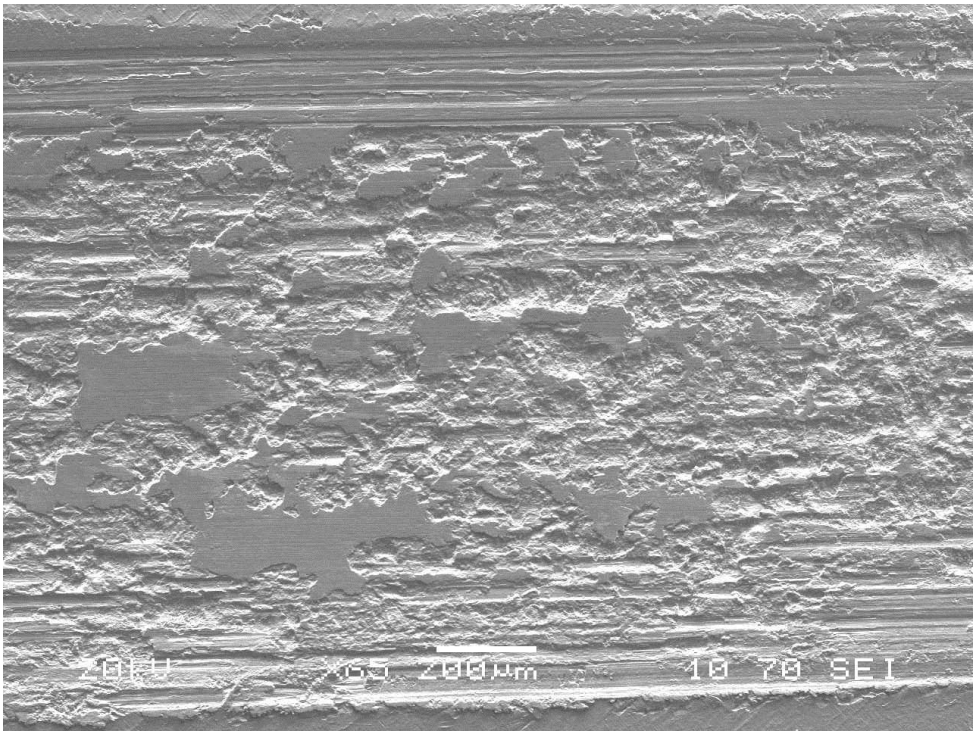
20kV X65 200μm 10 70 SEI

(b)

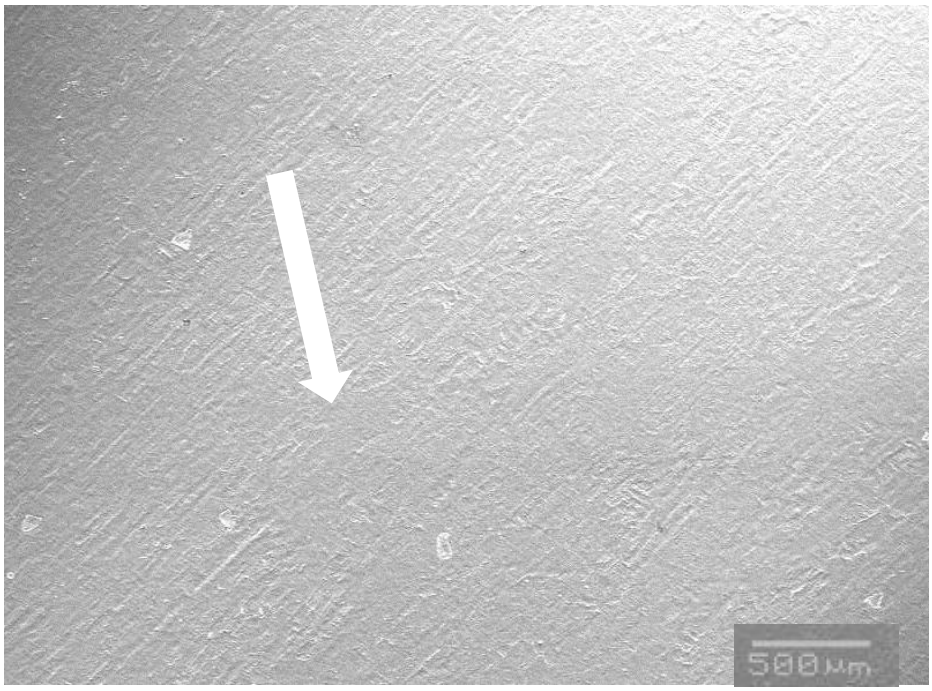

(c)

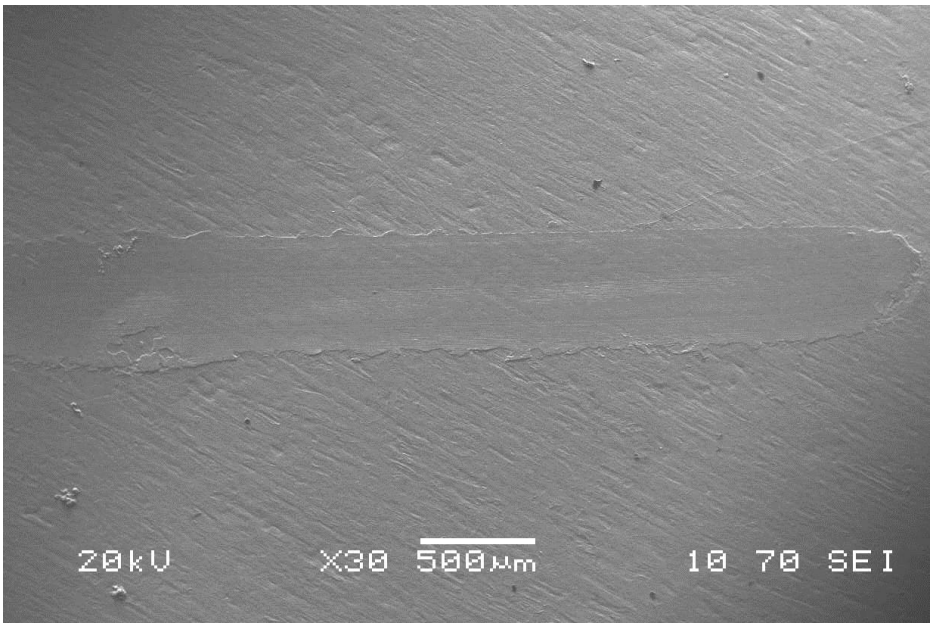

(d)

Figure 4.5.1-4 Wear track morphologies of plasma nitrided LDX 2101 samples of (a) PN390, (b) PN420, (c) PN450 and (d) PN480 after wear test under 70N load.

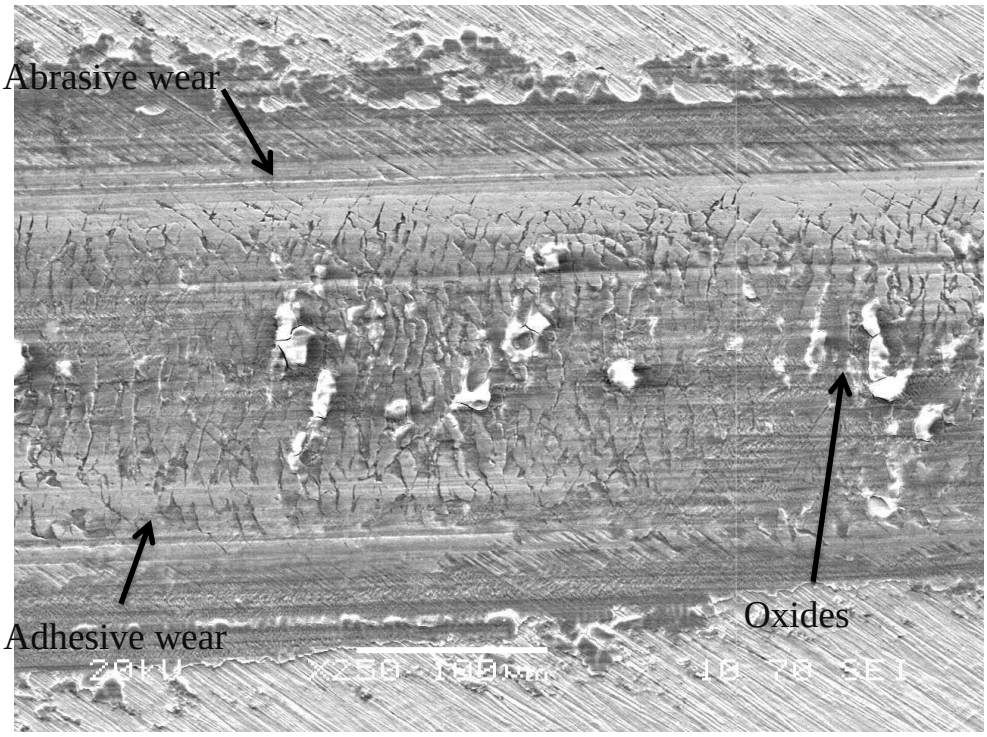
Abrasive wear
Adhesive wear
Oxides
20kV X250 100µm 10 70 SEI

(a)

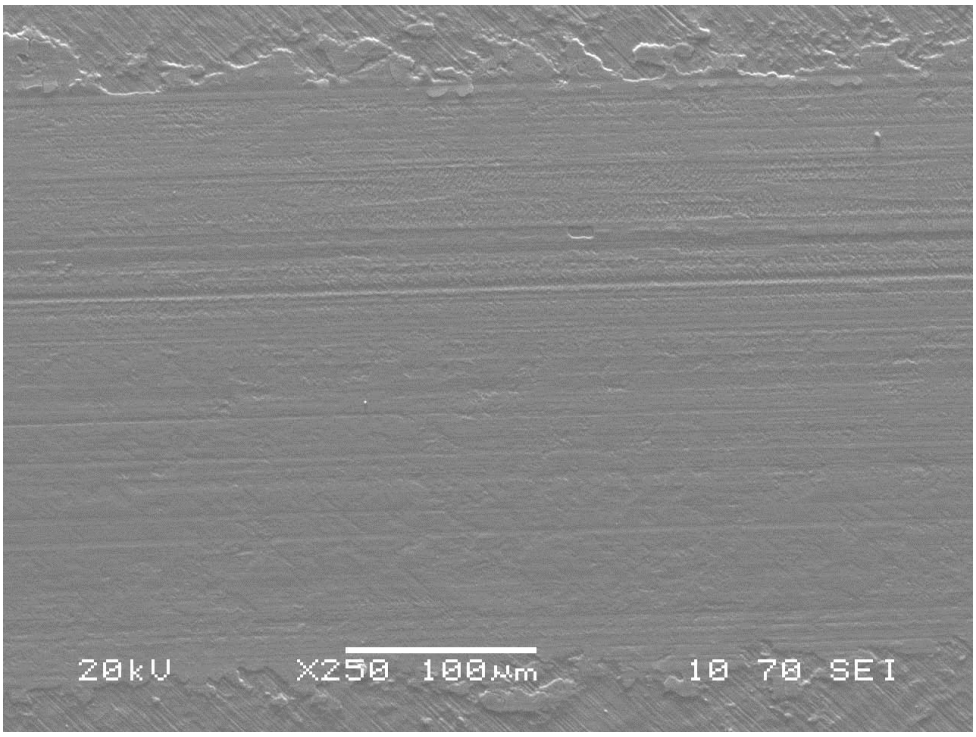
20kV X250 100µm 10 70 SEI

(b)

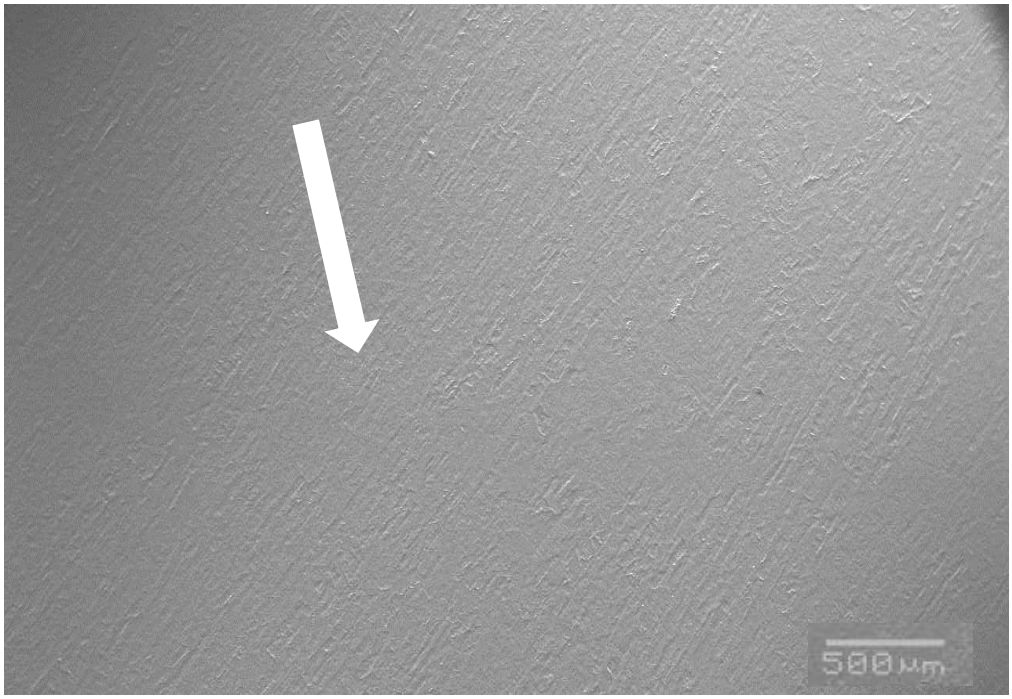

(c)

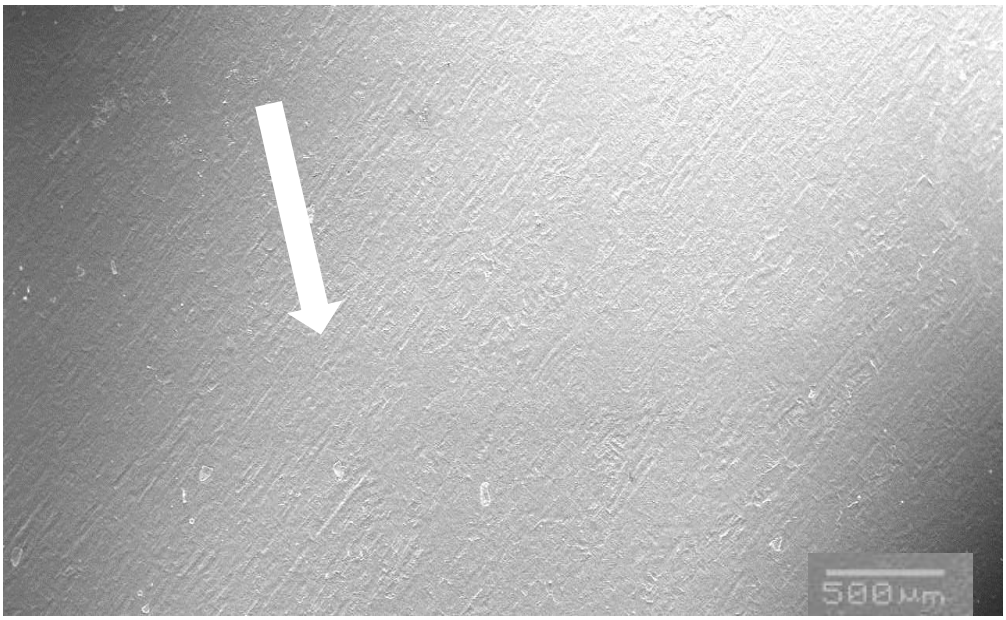

(d)

Figure 4.5.1-5 Wear track morphologies of plasma nitrided LDX 2101 samples of (a) PN390, (b) PN420, (c) PN450 and (d) PN480 after wear test under 30N load.

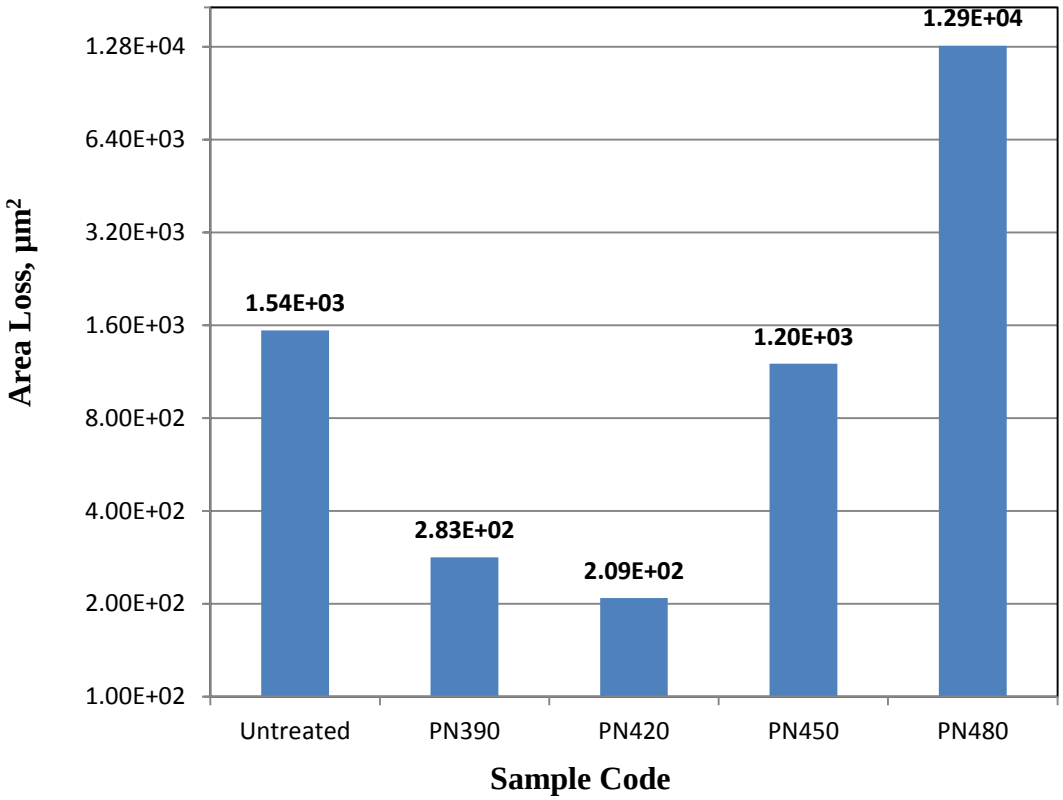

Figure 4.5.2-1 Corrosion wear results of untreated and plasma nitrided samples for LDX 2101 steel under 70N; counterpart: WC ball, Ø=8mm.

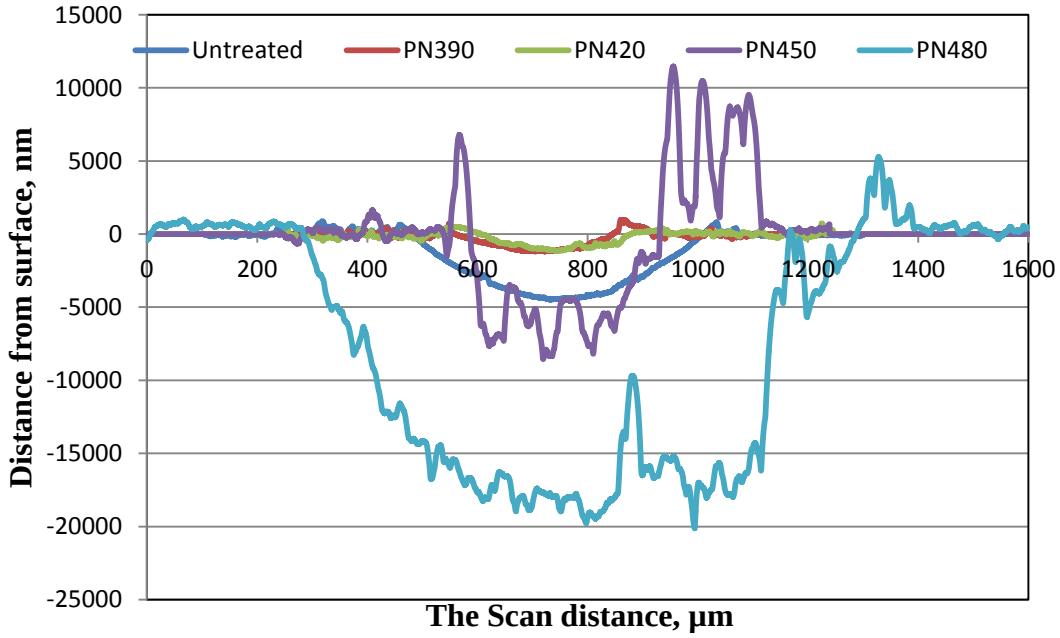

Figure 4.5.2-2 The cross-sectional corrosion wear area loss under a loading condition of 70N for plasma nitriding samples of LDX 2101

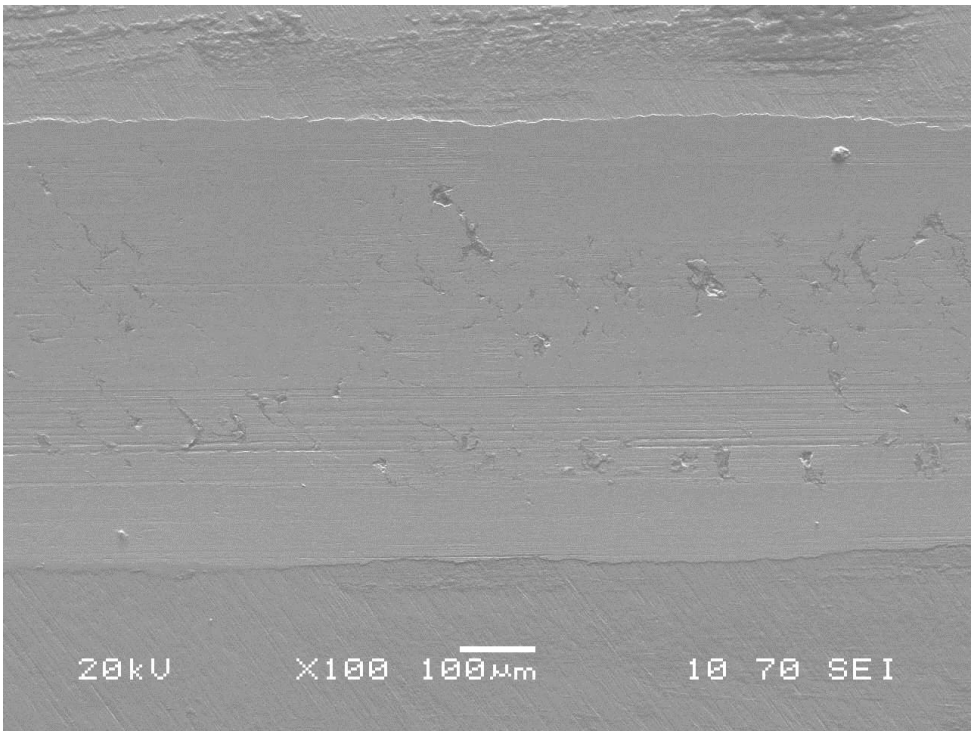

(a)

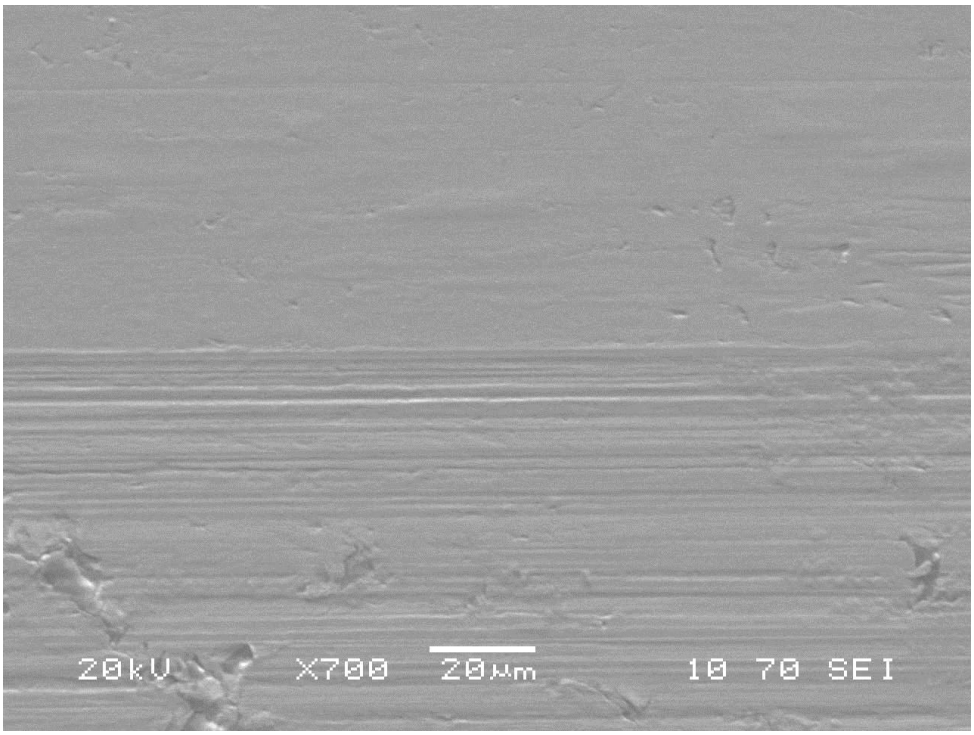

(b)

Figure 4.5.2-3 Corrosion wear morphologies of untreated sample of LDX 2101 under 70N load with (a) low and (b) high magnification pictures

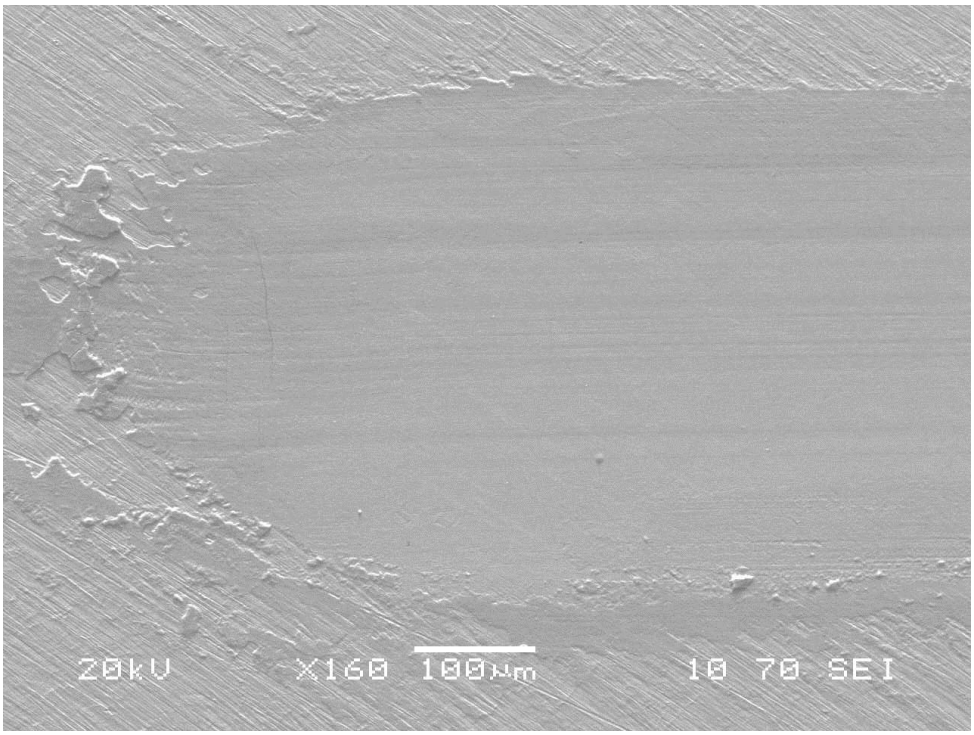

(a)

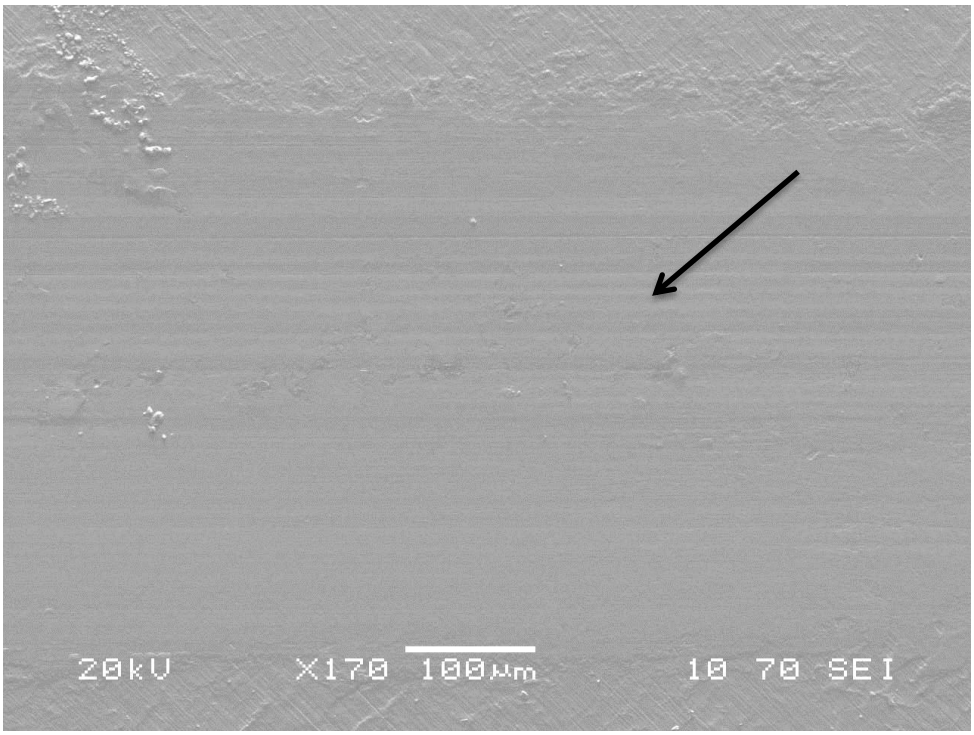

(b)

Figure 4.5.2-4 Corrosion wear morphologies of (a) PN390 and (b) PN420 of LDX 2101 under 70N load.

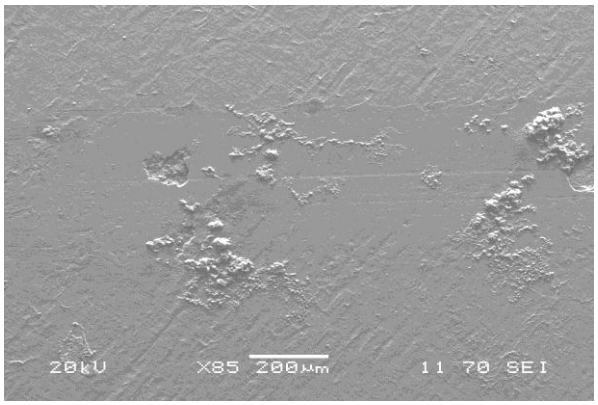

(a)

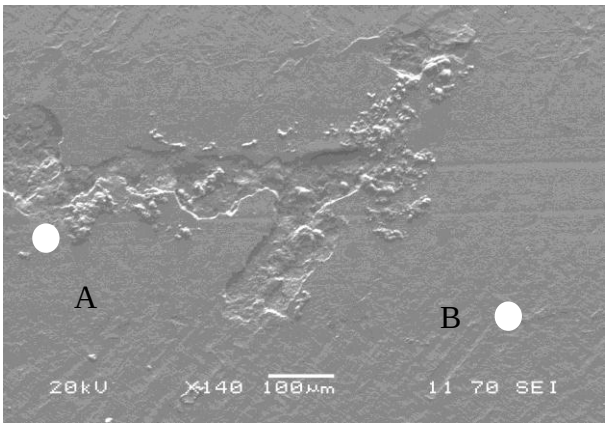

(b)

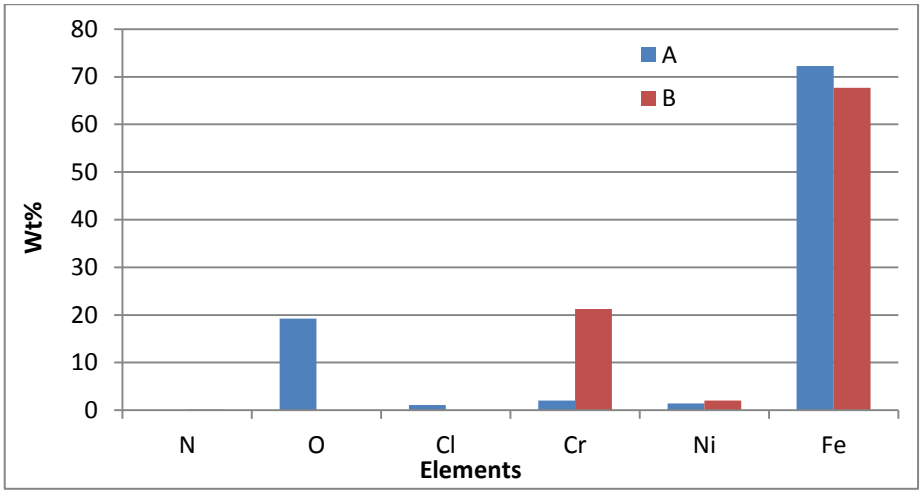

	N	O	Cl	Cr	Ni	Fe
A	0	19.23	1.11	2.01	1.42	72.25
B	0.13	0	0	21.27	1.99	67.68

(c)

Figure 4.5.2-5 Corrosion wear morphology of PN450 sample: (a) overview, (b) higher magnification of part of (a) and (c) EDX analysis of 'A' and 'B' in (b).

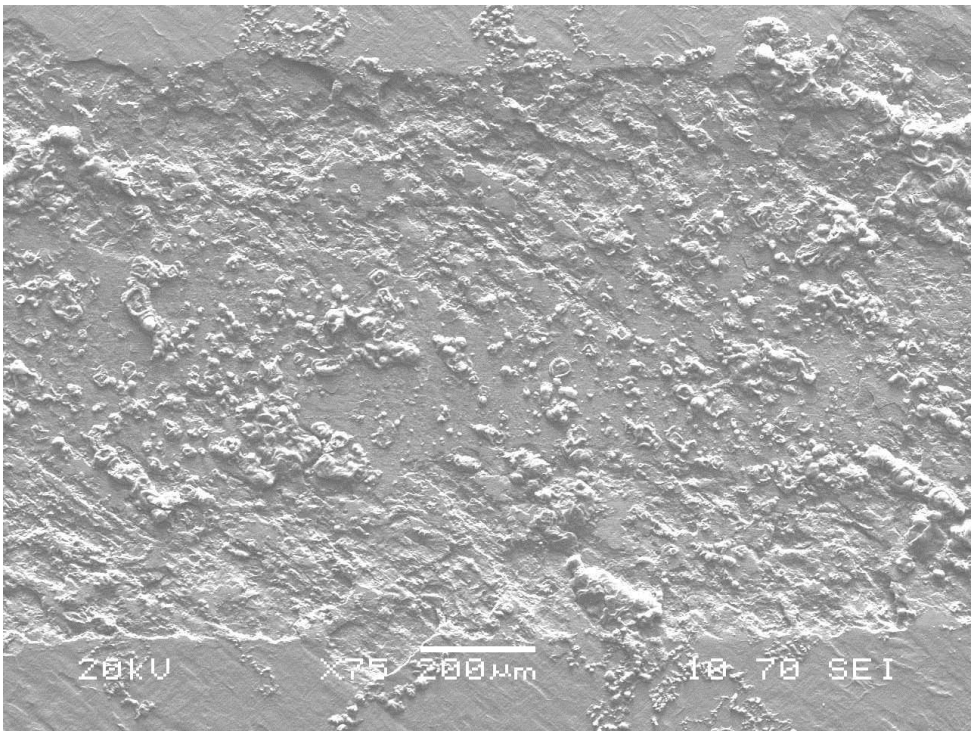

(a)

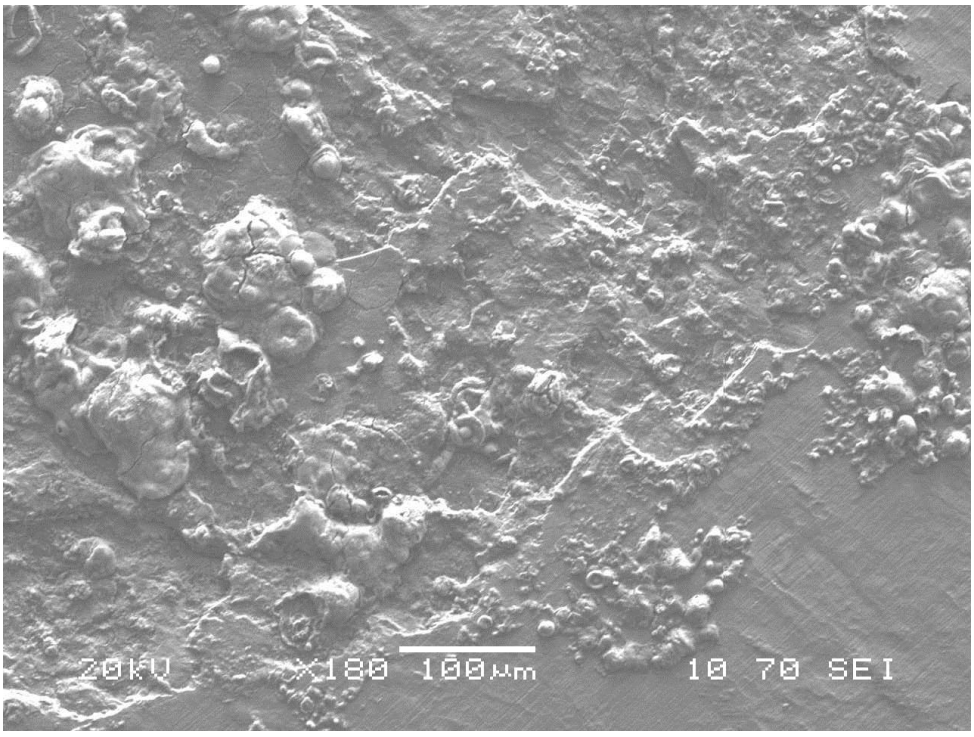

(b)

Figure 4.5.2-6 Corrosion wear morphology of PN480 sample: (a) overview and (b) higher magnification.

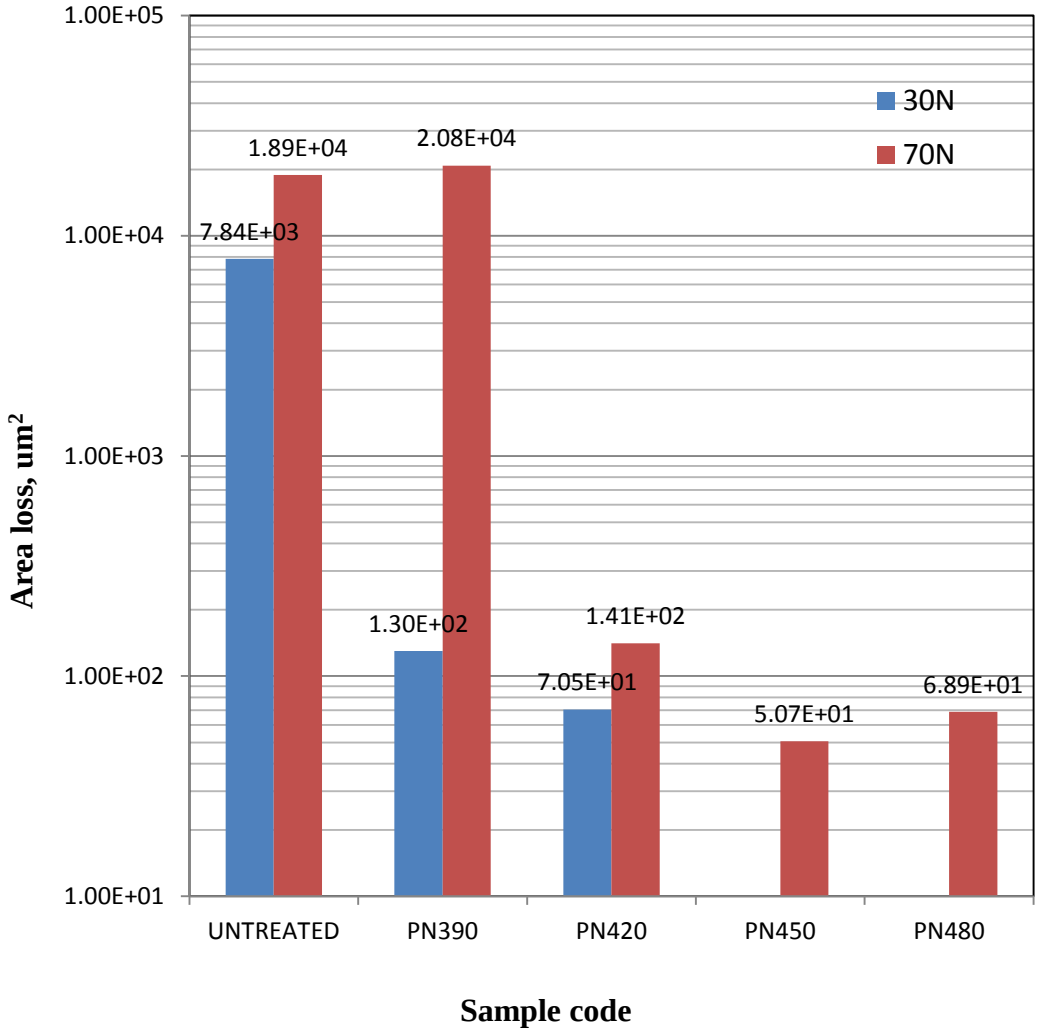

Figure 4.5.3-1 Dry wear area loss of untreated and plasma nitrided samples for LDX 2404 steel under 30 and 70N; counterpart: WC ball, Ø=8mm.

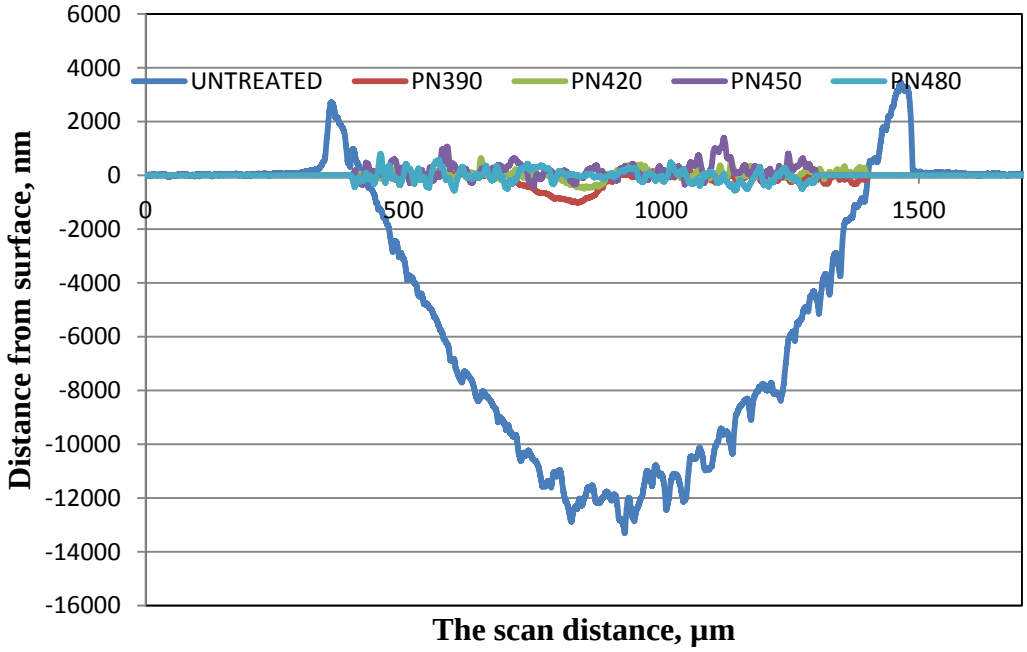

(a)

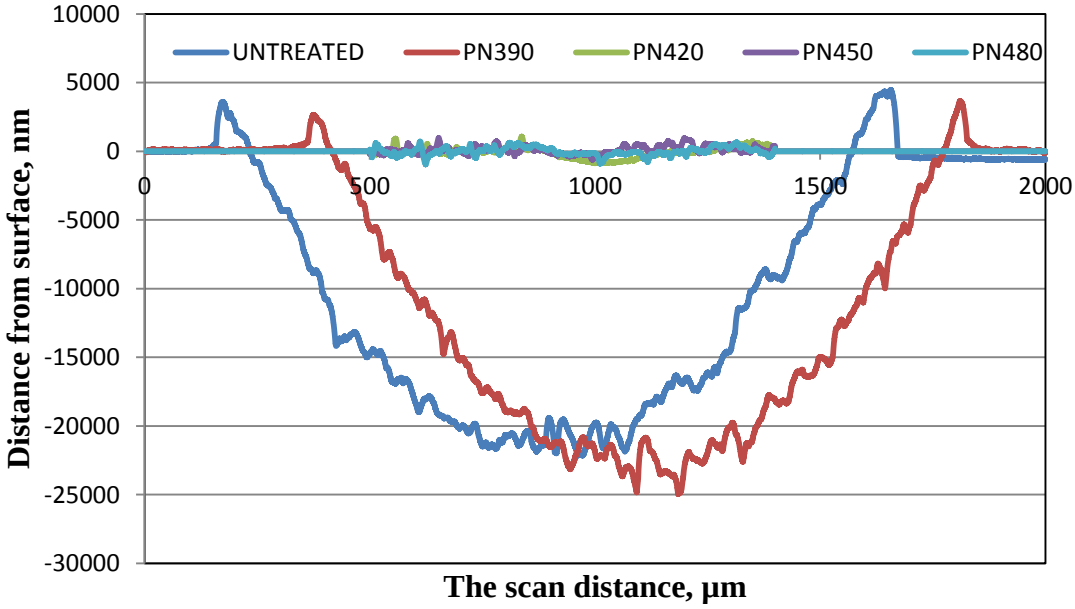

(b)

Figure 4.5.3-2 The cross-sectional wear area loss under a loading condition of (a) 30N and (b) 70N for plasma nitriding samples of LDX 2404

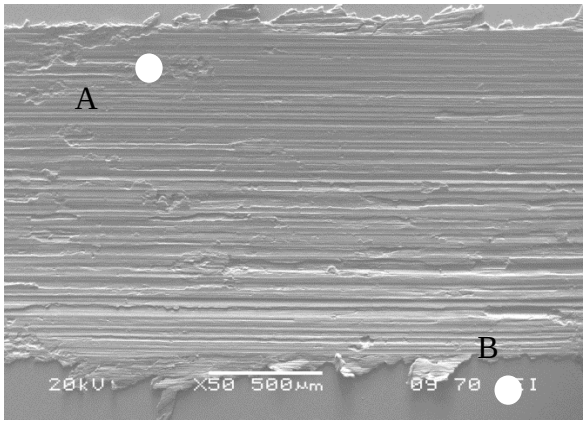

(a)

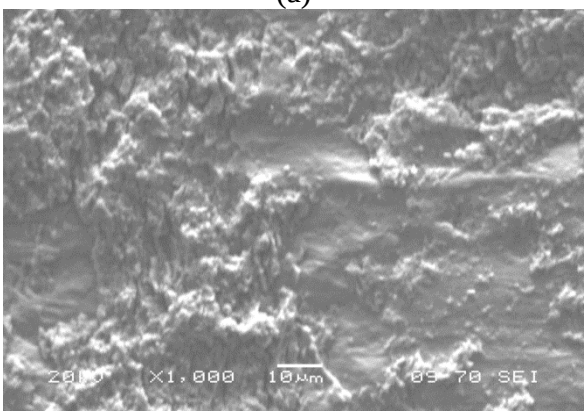

(b)

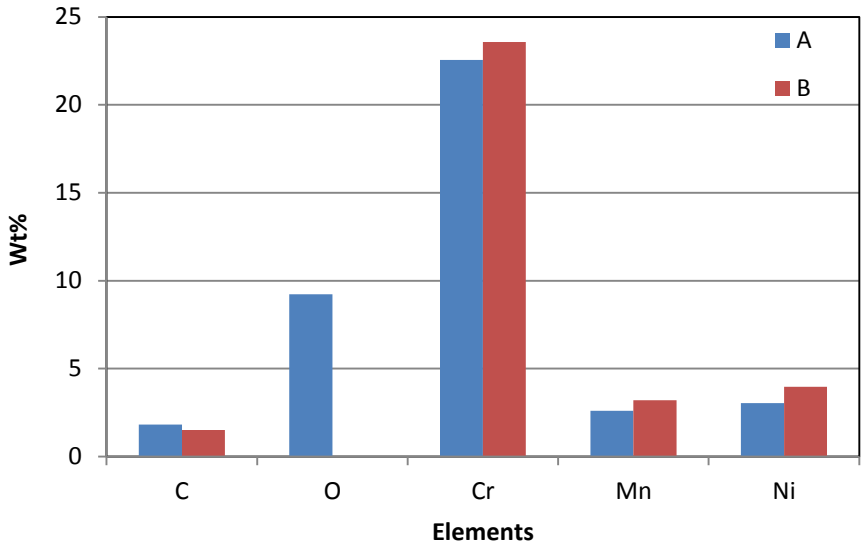

	C	O	Cr	Mn	Ni
A	1.82	9.24	22.56	2.61	3.04
B	1.52	0	23.57	3.21	3.97

(c)

Figure 4.5.3-3 Wear morphologies of untreated sample of LDX 2404 under 70N load with (a) low resolution and (b) high resolution images and (c) EDX results.

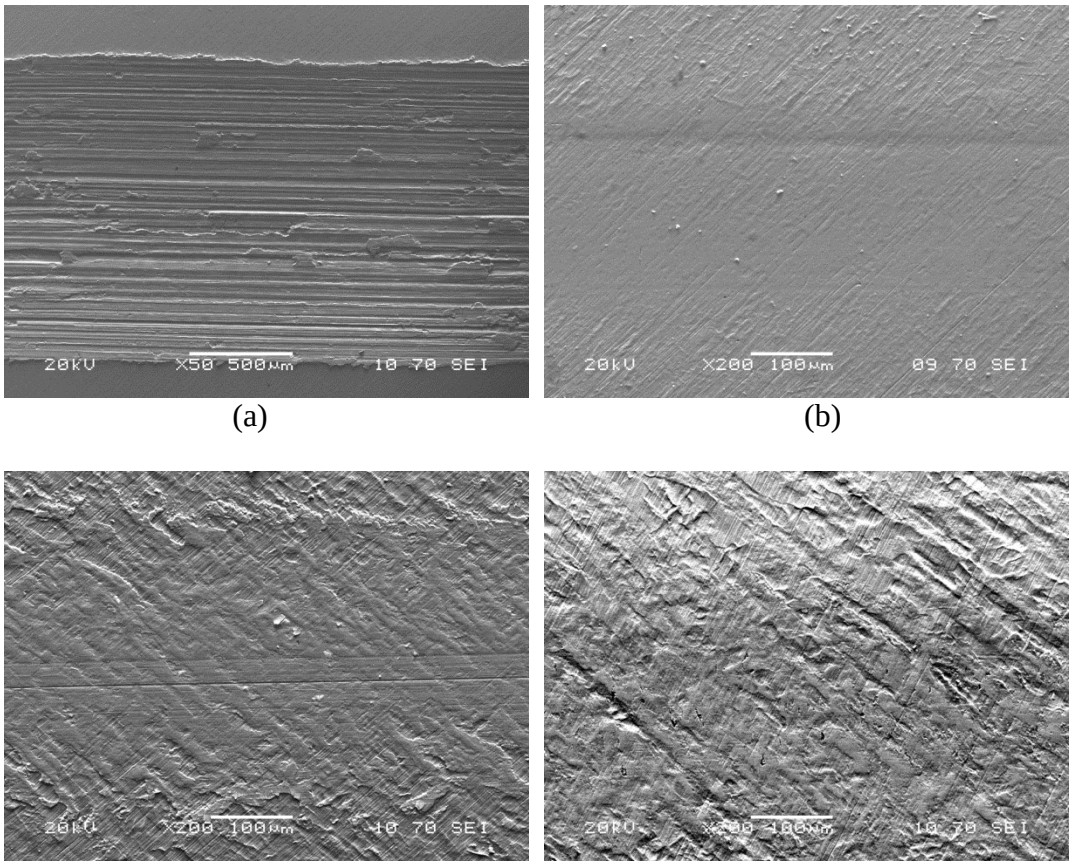

(a) (b)

(c) (d)

Figure 4.5.3-4 Wear morphologies of plasma nitriding samples of (a) PN390, (b) PN420, (c) PN450 and (d) PN480 for LDX 2404 under 70N load.

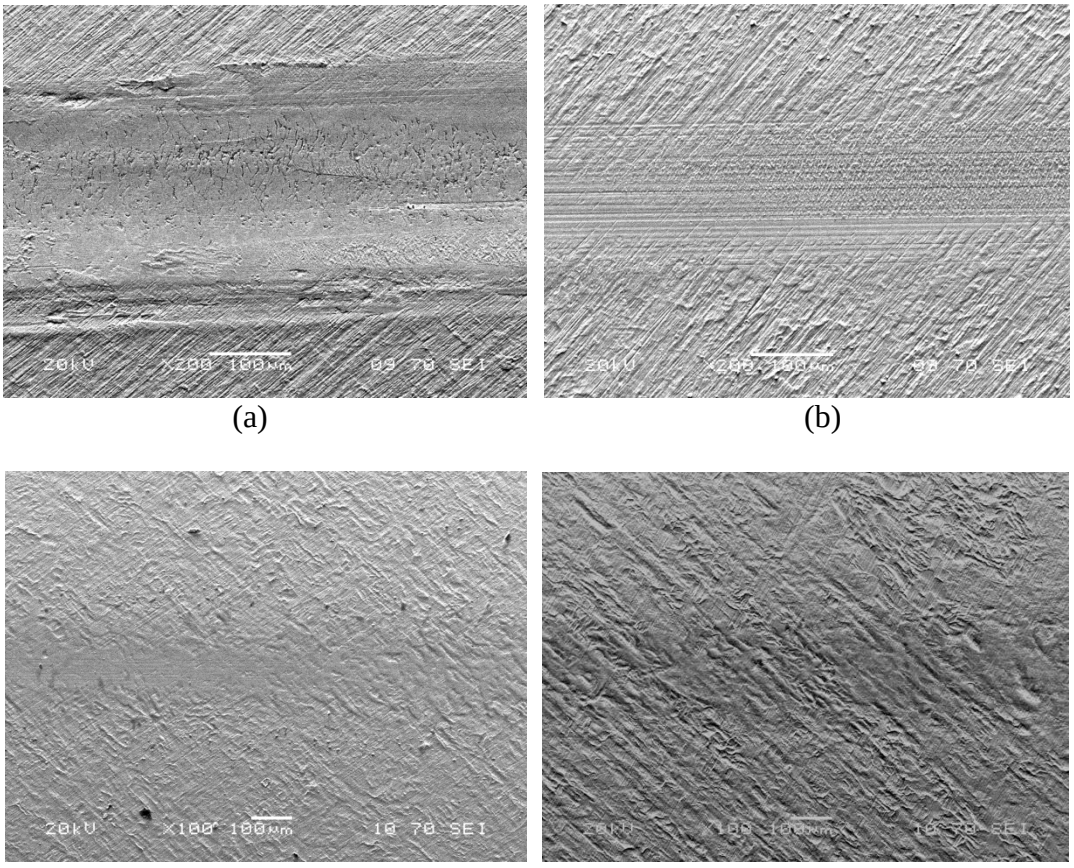

(a) (b)

(c) (d)

Figure 4.5.3-5 Wear morphologies of plasma nitriding samples of (a) PN390, (b) PN420, (c) PN450 and (d) PN480 for LDX 2404 under 30N load.

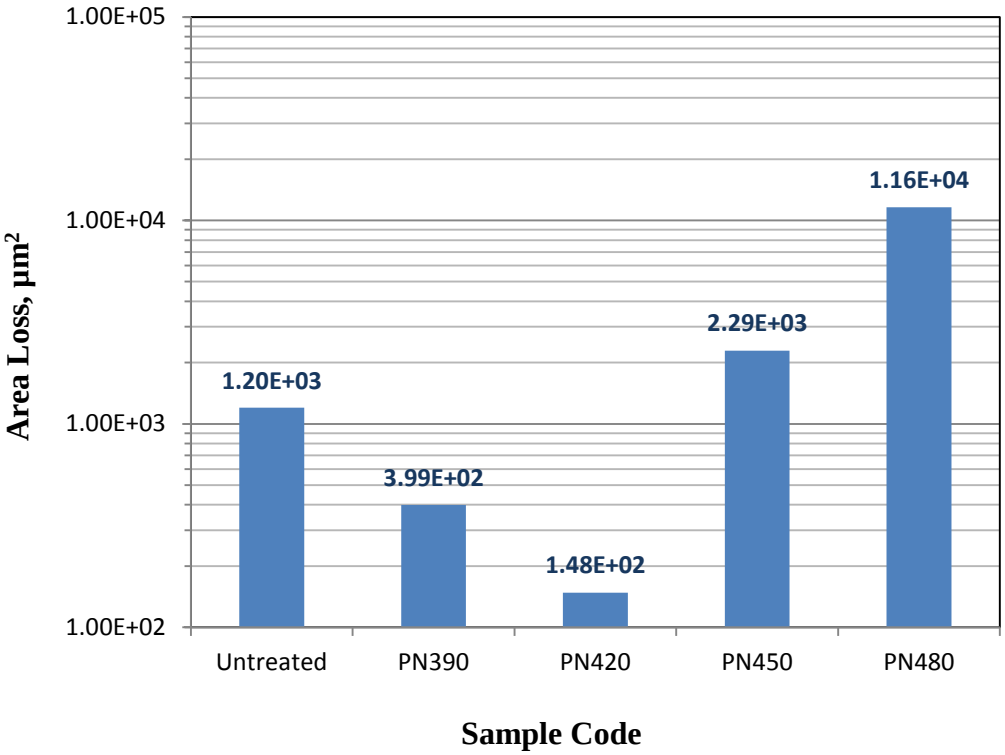

Figure 4.5.4-1 Corrosion wear area loss of untreated and plasma nitrided samples for LDX 2404 steel under 70N

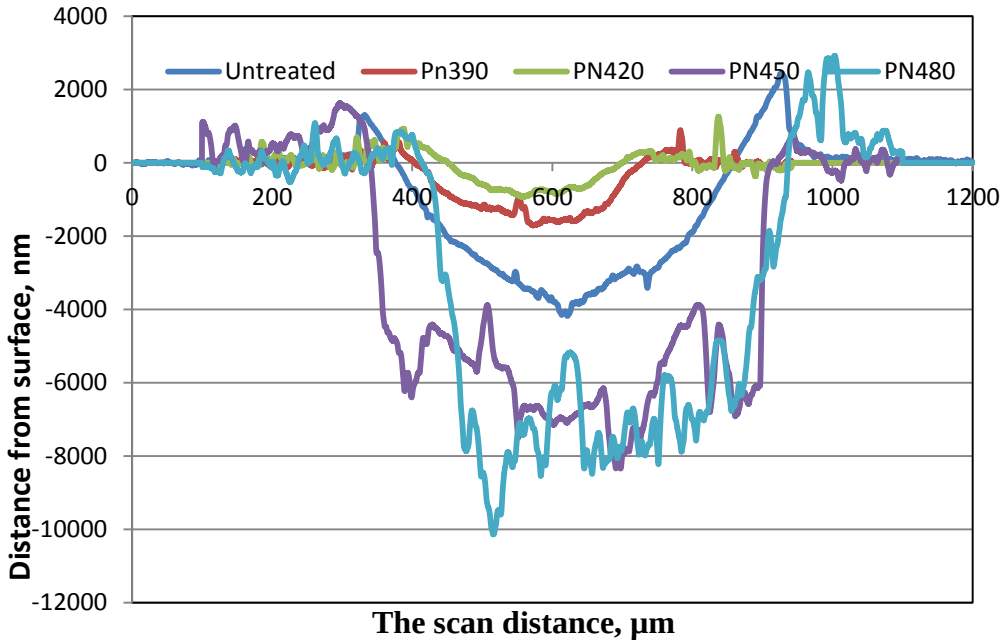

Figure 4.5.4-2 The cross-sectional corrosion wear area loss under a loading condition of 70N for plasma nitride and untreated samples of LDX 2404

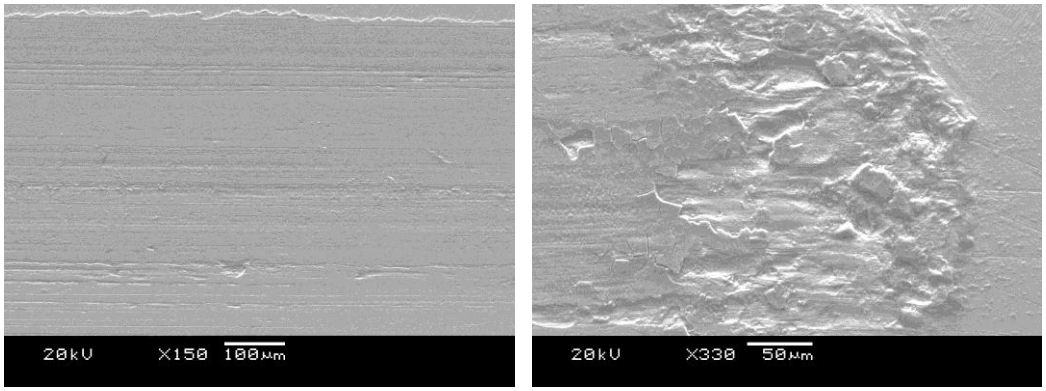

(a) (b)

Figure 4.5.4-3 Corrosion wear morphologies of untreated sample of LDX 2404 under 70N load with (a) low and (b) high magnification pictures

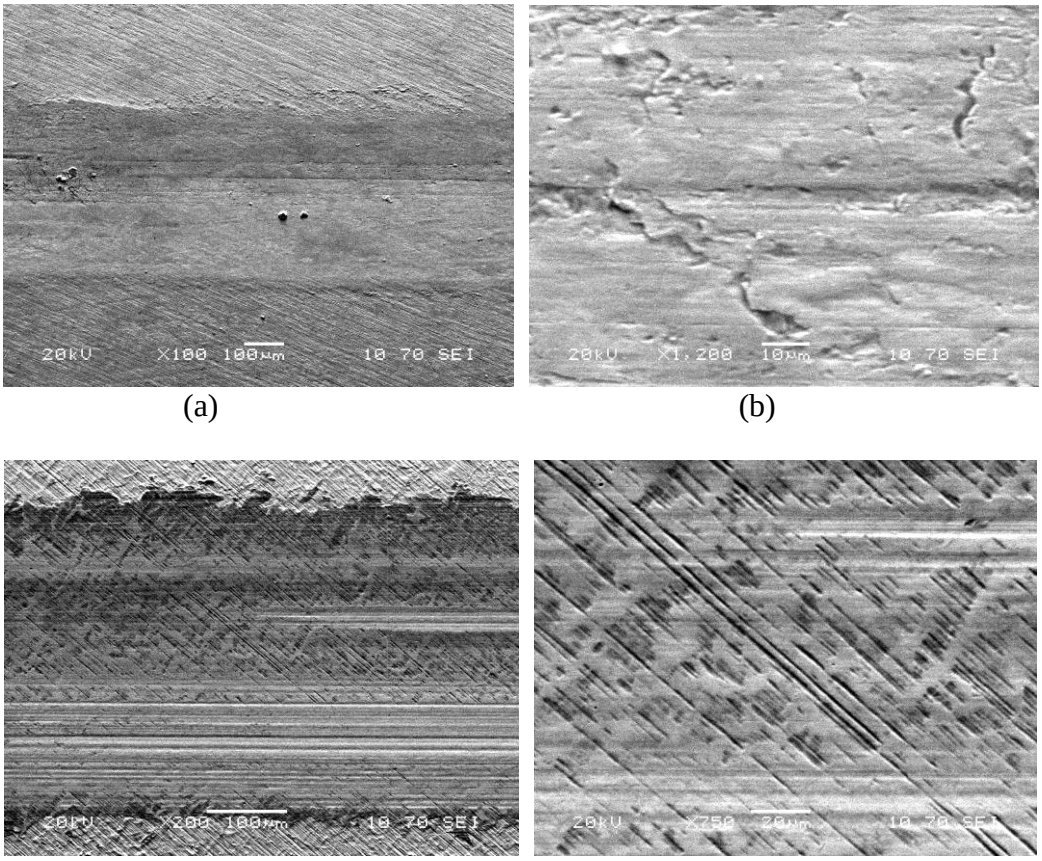

(a) (b)

(c) (d)

Figure 4.5.4-4 Corrosion wear morphologies of PN390 (a) overview and (b) higher magnification and PN420 (c) overview and (d) higher magnification under 70N.

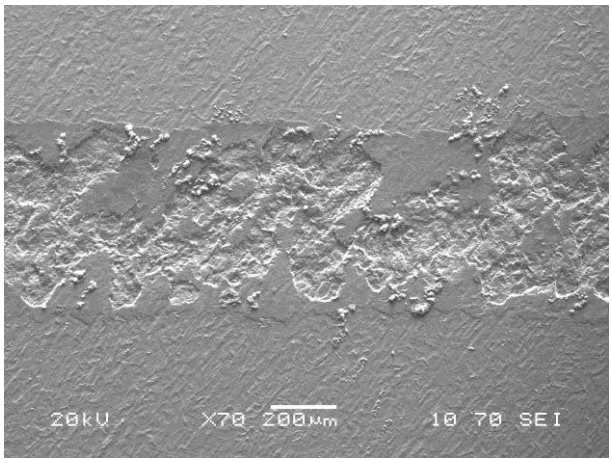

(a)

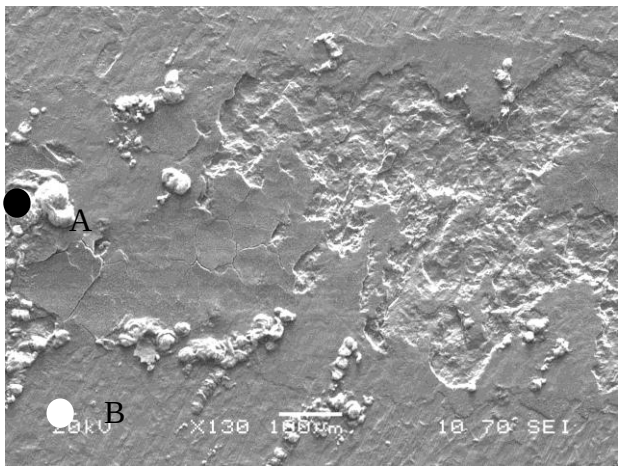

(b)

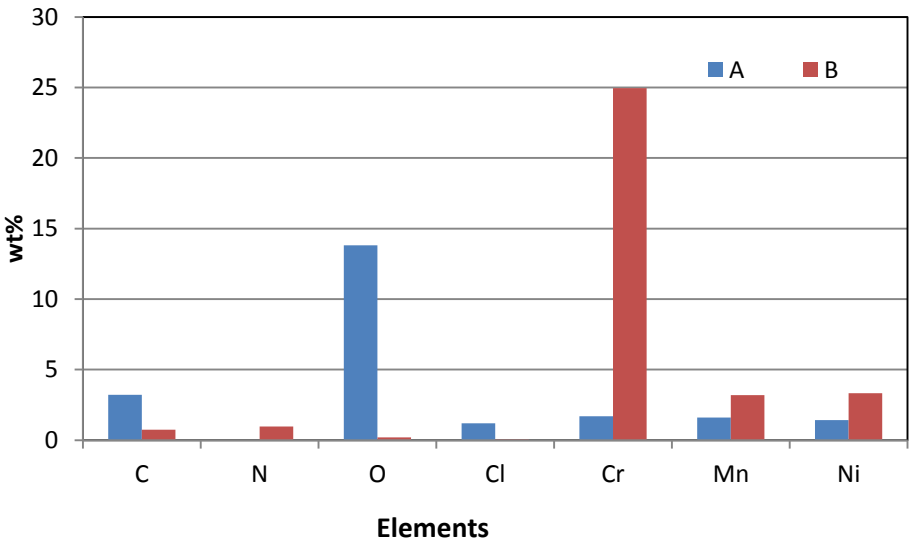

(c)

Figure 4.5.4-5 Corrosion wear morphology of PN450/10 (a) overview, (b) higher magnification, (c) EDX results

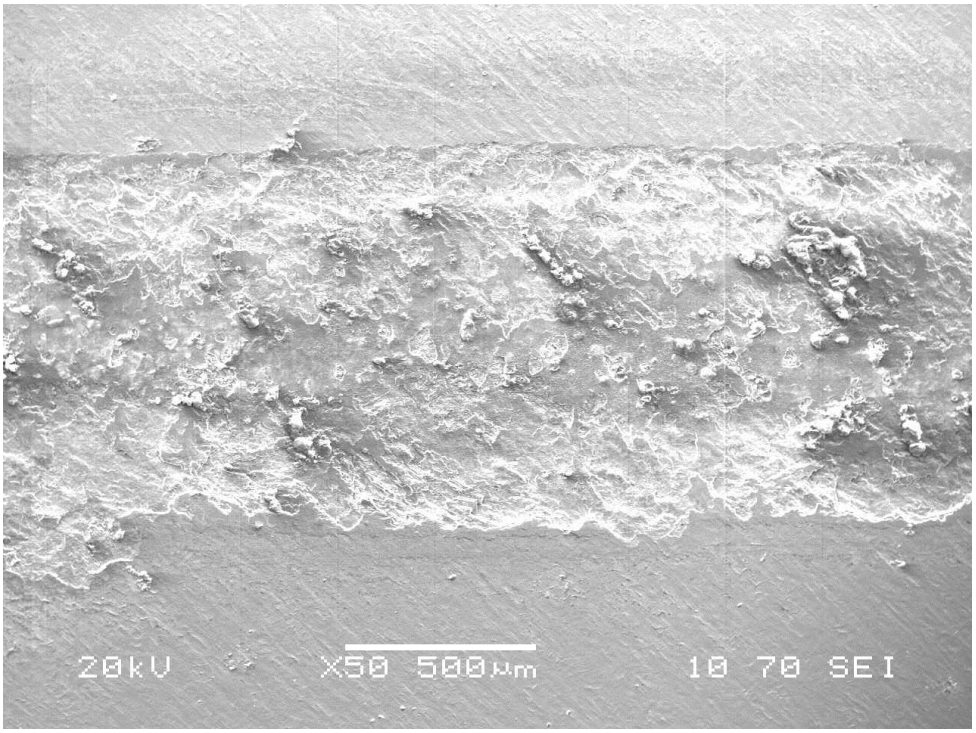

(a)

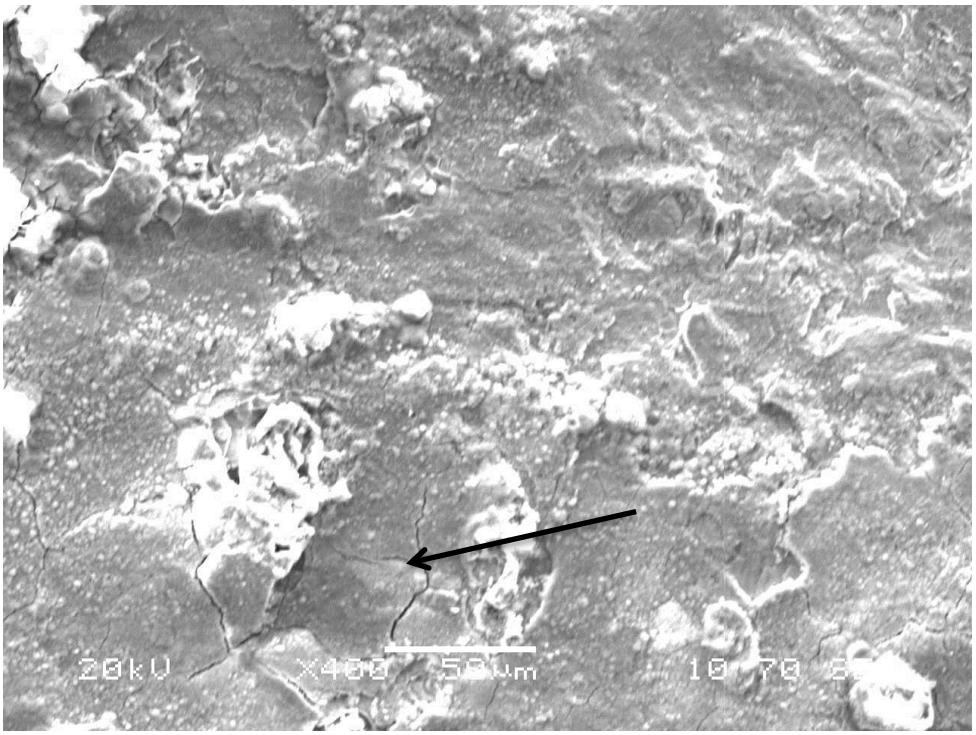

(b)

Figure 4.5.4-6 SEM corrosion wear morphology of sample LAX2404 PN480 (a) overview and (b) higher magnification of part of (a).

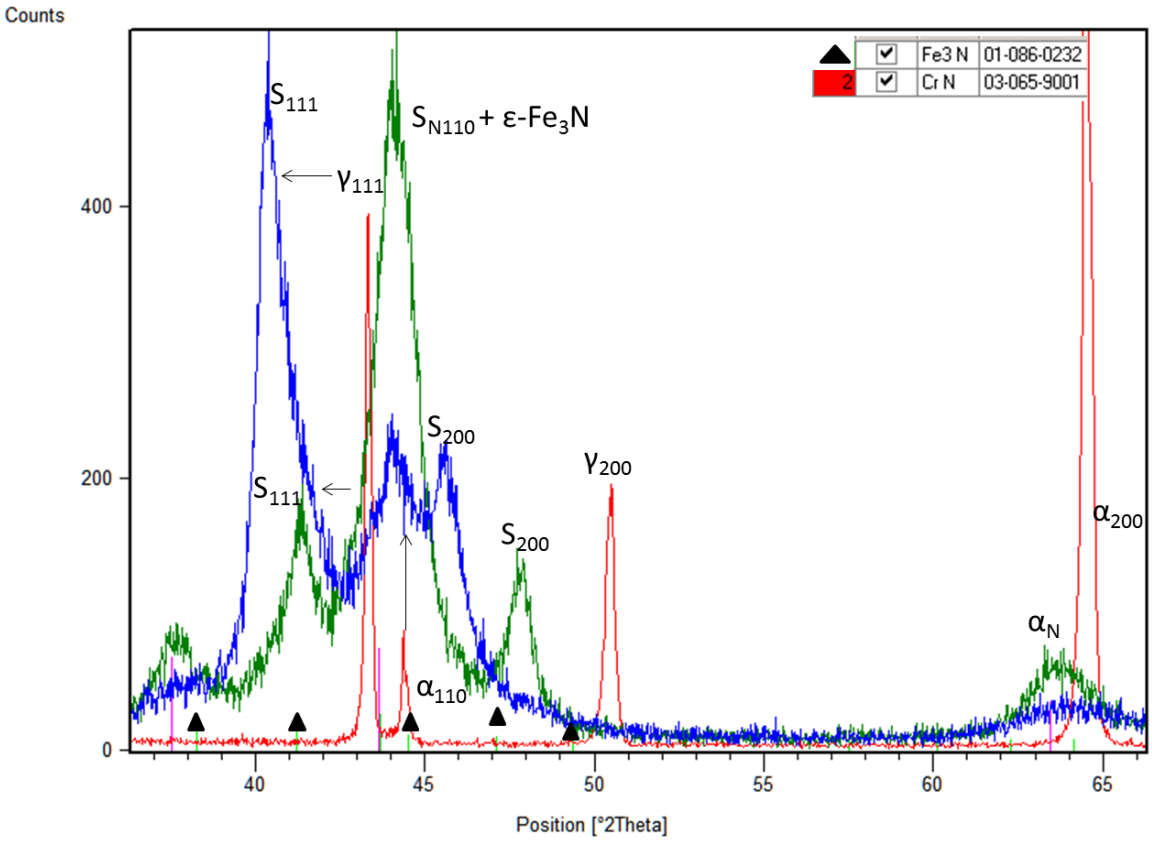

Figure 5.1 XRD patterns taken from as-received LDX2101 (red), longitudinal section view surface (green) and transvers sectional view surface of LDX2101PN450 samples.